Journal of the National Academy of Forensic Engineers®

Vol. 32 No. 2 December 2015

National Academy of Forensic Engineers®

Journal Staff

Technical Review Process

The Technical Review Committee Chair chooses the reviewers for each Journal manuscript from amongst the members and affiliates of the NAFE according to their competence and the subject of the paper, and then arbitrates as necessary during the review process. This confidential process concludes with the acceptance of the finished paper for publication or its rejection or withdrawal. The name(s) of authors are included with their published works. However, unpublished drafts together with the names and comments of reviewers are entirely confidential during the review process and are excised upon publication of the finished paper.

National Academy of Forensic Engineers®

Board of Directors

President
Jeffrey D. Armstrong, P.E.
Fellow

President-Elect
John P. Leffler, P.E.
Senior Member

Senior Vice President
William C. Bracken, P.E.
Fellow

Vice President
Michael D. Leshner, P.E.
Fellow

Treasurer
Jerry S. Ogden, P.E.
Fellow

Secretary
Paul Swanson, P.E.
Member

Past Presidents
E. Ross Curtis, P.E.
Senior Member

Paul R. Stephens, P.E.
Fellow

Richard M. Ziernicki, Ph.D, P.E.
Fellow

Directors at Large

Martin Gordon, P.E.
Member

Marvin M. Specter, P.E., L.S.
Fellow

Executive Director
Arthur E. Schwartz, Esq.

Submitting Proposed Papers to NAFE for Consideration

A concise abstract of approximately 100 words shall be sent to the Journal Editor for initial consideration. Upon approval of the abstract, the author will be scheduled to present their work at one of the semi-yearly NAFE Technical Conferences. A 90% complete draft copy of the manuscript shall be submitted to the Journal Editor for review and approval no later than 30 days before the conference.

For complete details about requirements for authors, visit:
www.nafe.org/assets/docs/journalcontents.pdf

For the NAFE Bylaws content "Responsibilities of, Obligations of and Guidelines for Authors, the Journal Editor, Technical Review Committee Chair, and Technical Reviewers," visit:
www.nafe.org/assets/docs/journalguidelines.pdf

Copies of the Journal

The Journal of the National Academy of Forensic Engineers® contains papers that have been accepted by NAFE. In most cases, papers have been presented at NAFE seminars. Members and affiliates receive a copy of the Journal as part of their annual dues. To obtain additional copies, the costs are as follows: $15.00 for members and correspondents of the NAFE; $30.00 for members of the NSPE not included in NAFE membership; $45.00 for all others. Requests should be sent to Arthur Schwartz, Executive Director, NAFE, 1420 King St., Alexandria, VA 22314-2794. Individual Journal papers may also be purchased and downloaded from the NAFE website at www.nafe.org.

Editor's Note

Some graphics reproduced in this black and white print edition are more clearly represented in the electronic version, which displays graphics in full color.

Comments by Readers

Comments by readers are invited, and, if deemed appropriate, will be published.
Send to: Arthur Schwartz, Esq., Executive Director, 1420 King St., Alexandria, VA 22314-2794.
Comments can also be sent via email to journal@nafe.org.

Material published in this Journal, including all interpretations and conclusions contained in papers, articles, and speeches, are those of the specific author or authors and do not necessarily represent the view of the National Academy of Forensic Engineers® (NAFE) or its members.

Table of Contents

All papers in this edition were presented at the NAFE seminar held 7/18/15 in Seattle, WA.

Forensic Engineering Analysis of Vehicle-Pedestrian Impact Using EDR Data and Reconstruction Software

By Michael Kravitz, P.E. (NAFE 451F)

Abstract

This paper will analyze a pedestrian impact with a 2012 vehicle in a criminal matter. The driver of the vehicle struck the pedestrian before crashing into a chain-link fence and tree. The driver was arrested and charged with vehicular homicide and driving while intoxicated (DWI). The question was: Where was the pedestrian standing when she was struck? The airbag control module was downloaded by the prosecution expert. The speed, steering angle, and longitudinal/ lateral accelerations were recorded for a period of 5 seconds prior to algorithm wake-up as a result of a fence side-swipe and then algorithm enable (AE) for the deployment of the vehicle-side airbags after impacting a tree. The recorded data was input into Virtual Crash and PC-Crash (accident reconstruction software that uses Newton's laws of motions in analysis). The software allowed the time-distance-speed path of the vehicle to be visualized. The prosecution expert opined that the pedestrian was struck on the sidewalk a short distance from where she came to rest. This author was retained by the defense to determine the pedestrian's position — either in the roadway or on the sidewalk.

Keywords

Pedestrian, Crash Data Retrieval, CDR, computer simulation software, accident reconstruction, criminal, DWI

Case Description

The defendant driver was driving westbound on a service road between 1 a.m. and 2 a.m. on a Saturday morning after leaving a local bar. The accident description (per the police report) was as follows:

> *At the point of occurrence, motor vehicle one was traveling westbound on a parkway service road at an unsafe speed. Rear left tire was a spare. Motor vehicle lost control, mounted sidewalk on northwest corner, striking above stationary pedestrian. Motor vehicle then struck chain-link fence, a tree and did then re-strike the fence. Pedestrian was pronounced "dead" on scene by EMS. Operator of motor vehicle was removed to hospital and arrested for DWI by police officer.*

Based on the initial police report and diagram as shown in **Figure 1**, the driver was arrested on a DWI and was charged with vehicular homicide with a blood alcohol value of 0.17. The police accident reconstructionist took color photographs and rendered a sketch of how the event occurred.

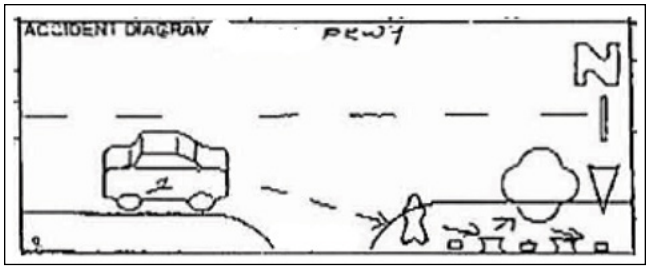

Figure 1

Police report diagram shows the vehicle traveling west. Then it veers to the north to strike the pedestrian standing on the sidewalk, strikes the fence, strikes the tree, and comes to rest west of the tree.

Michael Kravitz, P.E., 484 West 43rd Street, Suite 32s, New York, NY 10036; (212) 244-3890; mckravitz@gmail.com

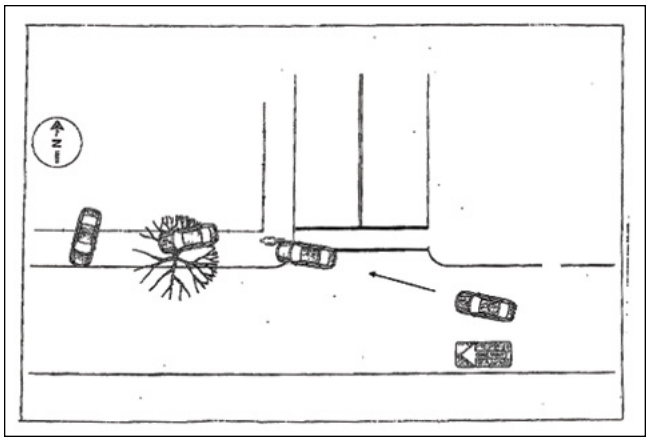

Figure 2
The sketch prepared by the prosecution accident reconstructionist is similar to the sketch in the police report in that it shows the deceased pedestrian being struck while standing on the sidewalk.

Portions of the grand jury hearing were acquired by the defendant's attorney, which described the prosecutor's expert witness opinion. He had been a police officer for 25 years, with 19 years as a highway accident investigation technician, 12 years as a trained accident reconstructionist from the Institute of Police Technology and Management (IPTM), and with recent yearly accident reconstruction training from Northwestern University. The court qualified him as an expert witness in vehicular collision reconstruction. The witness testified to the following:

a. Weather was clear and dry.
b. Vehicle was traveling west.
c. Driver lost control of vehicle and veered to right.
d. Vehicle drove up onto the northwest curb of the service road.
e. There were scrape marks on sidewalk from vehicle undercarriage.
f. After mounting curb, vehicle struck pedestrian, who was standing on the corner sidewalk.
g. Pedestrian was found lying prone on sidewalk.
h. One of pedestrian's sneakers was found under second parked car from corner.
i. Vehicle passenger-side view mirror found near stop sign pole.
j. After striking pedestrian, vehicle continued west and struck the chain-link fence.
k. Vehicle continued west and struck a tree.
l. After striking the tree, vehicle rotated counterclockwise and came to final rest beyond the tree with the rear of vehicle against the fence and the front on the sidewalk.
m. There was vehicle damage on the upper portion of passenger-side windshield.
n. The vehicle was traveling in excess of the 30-mph speed limit.
o. The pedestrian had injuries to her face.

The accident reconstructionist performed no measurements or calculations, nor did he use any reconstruction software to arrive at his opinion that the pedestrian was standing on the northwest corner of the sidewalk (as shown in **Figure 2**).

The pedestrian's head came in contact with the windshield, as observed by the spider pattern (see **Figure 3**), which appears to be bowing outward, on the passenger side of the defendant's vehicle. This bowing was probably caused by contact with the tree on the driver's side as the vehicle rotated into the tree.

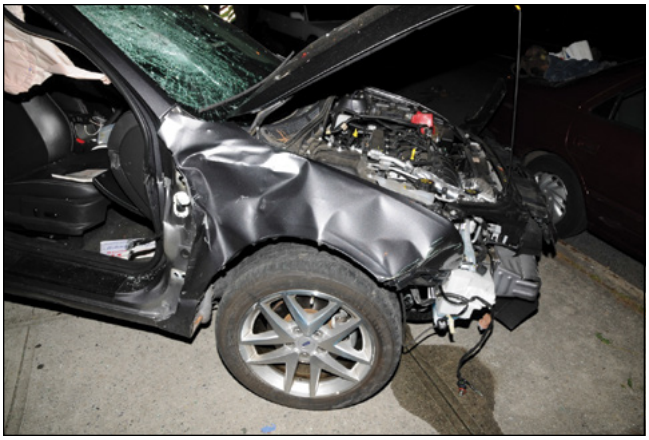

Figure 3
Defendant's vehicle in rest position on sidewalk. Notice the spider pattern on the windshield, which is a classic indication (as noted in the medical examiner's report) that the pedestrian's head struck the windshield at that point.

The medical examiner's report stated that the pedestrian had blunt trauma to the head, trunk, and extremities. According to this document, the left side of the victim's face, eyelid, nose, and upper/lower lips were contused. The scalp, left temporal, and all the bones of the anterior, middle, and posterior cranial fossa were fractured. The blunt trauma to the head and spider windshield pattern are consistent with the head striking the windshield. The Office of the Medical Examiner also reported that the pedestrian was last treated at a local hospital for psychiatric illness 10 days prior to her death and had a history of mental illness.

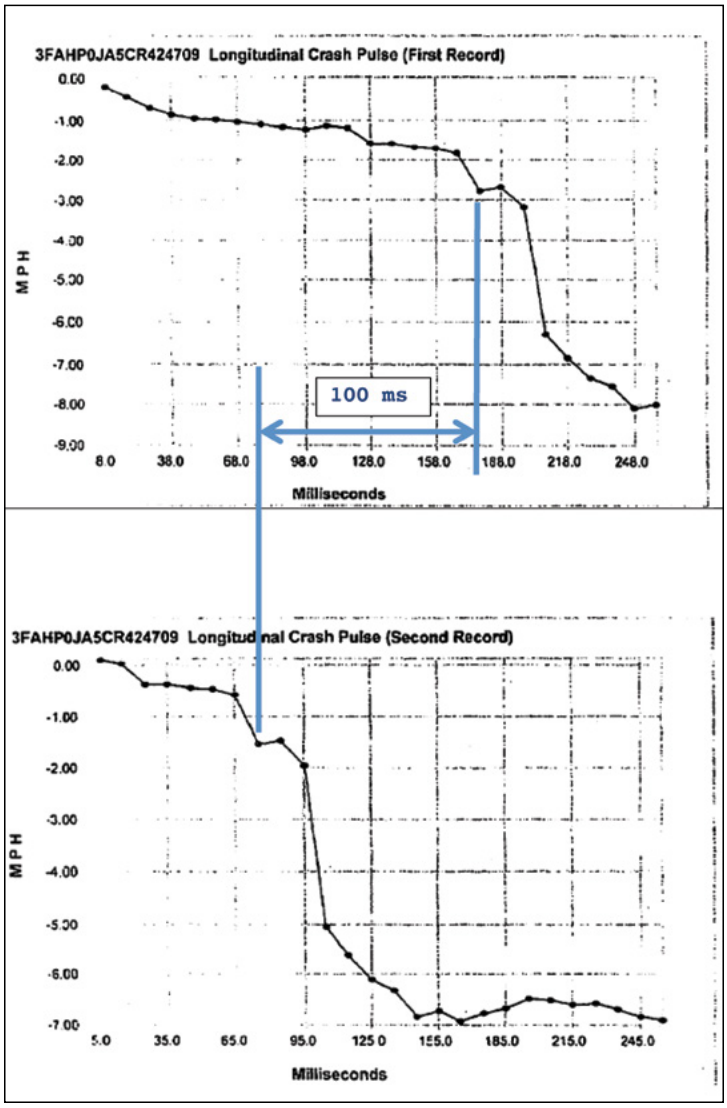

Figure 4 and 5
The above graphs show the longitudinal crash pulse for the first and second records. The horizontal arrow shows the overlap of 100 milliseconds of the two records.

The airbag control module, which was downloaded 10 days after the accident, showed there were two events[1]. The first was a non-deployment (ND) event because there was no airbag deployment, and the data was not locked. The second was a locked airbag deployment event of the side airbags. The two events were separated by approximately 100 milliseconds and were confirmed using the graphs in the Crash Data Retrieval[2] (CDR) report as shown in **Figures 4** and **5**. The graphs depict the change in velocity in miles per hour and time in milliseconds at the start of airbag deployment. This indicated that the first event was probably the sideswipe with the fence when the vehicle made contact with the corner and along the fence. The second event deployed the side airbags, which coincides with the rear driver side impact when the vehicle rotated into the tree.

The stability control telltale would have been flashing at 2 Hz, indicating that the vehicle was losing traction 2 seconds prior to AE. The accelerator pedal was at 100% throttle, and the brake was not applied. The driver's steering inputs showed that he performed a hard steer to the left at approximately 2 seconds prior to AE. The steering also showed that the driver steered to the right between -5 seconds and -3 seconds and then to the left; however, stability was maintained. This could be attributed to the emergency spare tire on the rear right, which had a 15-inch radius while the standard tires had a 16-inch radius.

Pre-Crash Data -5 to 0 sec [2 samples/sec] (First Record)

Times (sec)	Speed vehicle indicated MPH [km/h]	Accelerator pedal, % full	Service brake, on/off	Engine RPM	ABS activity (engaged, non-engaged)	Stability control (engaged, non-engaged)	Traction Control via Brakes (engaged, non-engaged)	Traction Control via Engine (engaged, non-engaged)
-5.0	47.6 [77.0]	73	Off	5,600	non-engaged	non-engaged	non-engaged	non-engaged
-4.5	48.5 [78.0]	75	Off	4,100	non-engaged	non-engaged	non-engaged	non-engaged
-4.0	51.0 [82.0]	86	Off	4,200	non-engaged	non-engaged	non-engaged	non-engaged
-3.5	52.6 [85.0]	87	Off	4,400	non-engaged	non-engaged	non-engaged	non-engaged
-3.0	55.3 [89.0]	87	Off	4,400	non-engaged	non-engaged	non-engaged	non-engaged
-2.5	57.2 [92.0]	89	Off	4,600	non-engaged	non-engaged	non-engaged	non-engaged
-2.0	59.7 [96.0]	99	Off	4,700	non-engaged	engaged	non-engaged	non-engaged
-1.5	60.3 [97.0]	100	Off	4,800	non-engaged	engaged	non-engaged	non-engaged
-1.0	64.0 [103.0]	0	Off	5,100	non-engaged	engaged	non-engaged	non-engaged
-0.5	58.4 [94.0]	0	Off	4,600	non-engaged	engaged	non-engaged	non-engaged
0.0	57.8 [93.0]	0	Off	3,700	non-engaged	engaged	non-engaged	non-engaged

Figure 6
Five seconds of pre-crash data for the first event show that approximately 1 second prior to AE the defendant took his foot off of the accelerator. It also shows that his vehicle reached the speed of 64 mph 1 second prior to AE.

Pre-Crash Data -5 to 0 sec [2 samples/sec] (Second Record)

Times (sec)	Speed vehicle indicated MPH [km/h]	Accelerator pedal, % full	Service brake, on/off	Engine RPM	ABS activity (engaged, non-engaged)	Stability control (engaged, non-engaged)	Traction Control via Brakes (engaged, non-engaged)	Traction Control via Engine (engaged, non-engaged)
- 5.0	47.8 [77.0]	73	Off	5,600	non-engaged	non-engaged	non-engaged	non-engaged
- 4.5	48.5 [78.0]	75	Off	4,100	non-engaged	non-engaged	non-engaged	non-engaged
- 4.0	51.0 [82.0]	86	Off	4,200	non-engaged	non-engaged	non-engaged	non-engaged
- 3.5	52.8 [85.0]	87	Off	4,400	non-engaged	non-engaged	non-engaged	non-engaged
- 3.0	55.3 [89.0]	87	Off	4,400	non-engaged	non-engaged	non-engaged	non-engaged
- 2.5	57.2 [92.0]	89	Off	4,600	non-engaged	non-engaged	non-engaged	non-engaged
- 2.0	59.7 [96.0]	99	Off	4,700	non-engaged	engaged	non-engaged	non-engaged
- 1.5	60.3 [97.0]	100	Off	4,800	non-engaged	engaged	non-engaged	non-engaged
- 1.0	64.0 [103.0]	0	Off	5,100	non-engaged	engaged	non-engaged	non-engaged
- 0.5	58.4 [94.0]	0	Off	4,600	non-engaged	engaged	non-engaged	non-engaged

Figure 7
Five seconds of pre-crash data for the second event show that approximately 1 second prior to AE the defendant took his foot off of the accelerator, which is identical to the first event.

Prosecutor's Argument

Referencing the CDR download (as shown in **Figures 6 & 7**), which put the defendant's vehicle speed as high as 64 mph (103 kmh) in a 30-mph zone — and given the fact that the defendant had a blood alcohol level of 0.17 — he was charged with DWI. The defendant was arrested, removed from the scene, and taken to the hospital (where he was in a coma for the first three days and then stayed for several weeks). He was unable to recall events leading up to the crash.

Based on the opinion of the prosecutor's expert witness and the evidence presented by him to the grand jury, the prosecutor charged the driver with vehicular homicide and DWI with the maximum prison time of 25 years.

Case Material Reviewed

The author reviewed 84 photographs taken by the police of the vehicle at the scene as well as photographs taken when the vehicle was in the police impound. Also reviewed were the CDR report, pages from the grand jury testimony of the prosecutor's expert witness, and portions of the medical examiner's report. The author also visited the location and took measurements and photographs.

Defendant's Argument

The author was engaged by the defendant's attorney, and used the data from the CDR download to analyze the case. The 5 seconds of pre-crash data, prior to AE, was input into the accident reconstruction software Virtual Crash (V-Crash)[3] and PC-Crash[4]. The computer software calculations for PC-Crash and Virtual Crash are based on Newtonian physics, linear and rotational energy, and momentum principles. The results are plotted, and the vehicle is shown in motion and rest position. The data used included the speed, steering angle, and longitudinal acceleration. This data was recorded every 100 milliseconds, beginning with the velocity of the defendant's vehicle of 48 mph (77 kmh).

Using Internet satellite maps to gather an aerial view of the location, the path of the vehicle was plotted along the parkway service road. Note that there was a discrepancy between the CDR data recorded regarding speed and the speed calculated using the input values of longitudinal acceleration. The maximum speed calculated using Virtual Crash and PC-Crash software was approximately 60 mph versus the CDR-recorded speed of 64 mph. This could be attributed to the asynchronous writing of the data in the airbag control module and/or the frequency of data recording: the airbag control

Figure 8
This shows the path of the vehicle as it moves from the roadway onto the sidewalk and into the fence and tree. The motion depicted was created by inputting the CDR longitudinal accelerations, steering angles, and speeds into PC-Crash sequences.

CLICK ON PHOTO TO ACTIVATE VIDEO.

FLASH PLAYER MUST BE INSTALLED TO RUN THE VIDEOS.
IT CAN BE DOWNLOADED AT: HTTPS://GET.ADOBE.COM/FLASHPLAYER/

module catching the maximum speed but not at the appropriate data writing time. Some studies have also shown that the accuracy of pre-crash data in EDRs vary from 1% to 4%. This could also account for the difference. The EDR is using engine RPM and tire size ratios to calculate the reported speeds, but it cannot account for worn tires.

Virtual Crash was selected over PC-Crash for the reconstruction because the Virtual Crash pedestrian model remained in the standing position until vehicle contact, whereas the PC-Crash multibody began to sag due to gravity immediately upon starting the software. The time between the start of the software and the subsequent pedestrian impact was approximately 3 seconds — hence the sagging of the PC-Crash multibody.

At the corner, the software allowed the placement of a model tree and model fencing into which the defendant's vehicle crashed (see **Figure 8**). Somewhere along the vehicle's path the pedestrian was struck. Through iteration, the pedestrian's rest position was determined and agreed with the location of the body rest position as represented by police photographs. The software showed the pedestrian's head impacted the windshield as indicated by the scene photographs. After impact with the vehicle, the pedestrian was projected into the chain-link fence of the adjacent ball field and fell onto the sidewalk in the rest position. Using Virtual Crash software, iterations were performed of the vehicle-pedestrian impact.

When placing the pedestrian on the northwest corner of the street, the pedestrian was projected along the service road and came to rest in this road. The author also determined that the pedestrian could not have been struck while on the sidewalk because the carry distance of the pedestrian was greater than the width of the sidewalk. The vehicle would have thrown the pedestrian along the service road and not into the chain-link fence. Therefore, the pedestrian must have been struck east of the northwest corner of the service road somewhere within the path of the vehicle.

Various placements of the pedestrian — from the crosswalk east along the vehicle path to approximately in front of the bus stop — would have thrown her into the chain-link fence, striking her head on the passenger-side windshield as the evidence showed (see **Figures 9** through **12**). The closer the pedestrian strike was to the northwest corner of the street, the greater the probability

Figure 9
Pedestrian rest position. Notice the indentation of the chain-link fence where pedestrian struck as a result of her trajectory from the vehicle into the fence. The arrow shows the indentation into the chain-link fence.

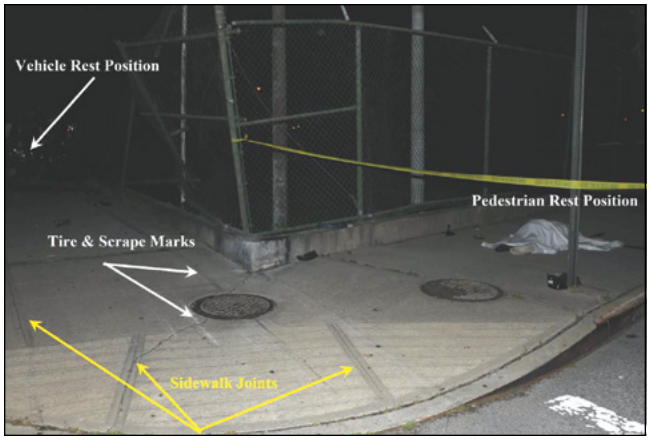

Figure 10
The photograph shows tire marks and scrapes (white arrows) where the vehicle mounted the sidewalk and sideswiped the fence. The yellow arrows depict the sidewalk joints. At this point in time, the vehicle was yawing; the fence sideswipe caused AE but no airbag deployment (ND).

Figure 11
The spider pattern of the passenger side of the windshield shows where the pedestrian's head struck the glass. Also shown are the deployed side airbags.

Figure 12
The interior of the vehicle shows that the front airbags were not deployed.

of the pedestrian being thrown over the chain-link fence. Therefore, the most probable strike of the pedestrian was in the street adjacent to the corner bus stop.

Analysis Methods

The author reviewed the CDR report, took the 5 seconds of pre-crash data (which included the longitudinal acceleration, steering angle, and speed before the crash), and input the data into Virtual Crash and PC-Crash software to get the time/distance path of the vehicle (see **Figures 13** through **15**). The purpose was to place a model pedestrian in the path of the vehicle to determine the throw distance and location of where she was struck and landed in the final rest position (see **Figures 16** through **20**).

The author used the speed of the vehicle at the time of AE as 57.8 mph (93.0 kmh) to arrive at the distance the vehicle traveled between the first and second record enable events. The time lapse of 100 milliseconds and speed of the vehicle in "record one" AE yields that the distance the vehicle traveled between the two records was approximately 8 feet. This distance approximately coincides with the distance between when the first and second records were enabled,

Pre-Crash Data -5 to 0 sec [2 samples/sec] (First Record)

Times (sec)	Speed vehicle indicated MPH [km/h]	Accelerator pedal, % full	Service brake, on/off	Engine RPM	ABS activity (engaged, non-engaged)	Stability control (engaged, non-engaged)	Traction Control via Brakes (engaged, non-engaged)	Traction Control via Engine (engaged, non-engaged)
-5.0	47.8 [77.0]	73	Off	5,600	non-engaged	non-engaged	non-engaged	non-engaged
-4.5	48.5 [78.0]	75	Off	4,100	non-engaged	non-engaged	non-engaged	non-engaged
-4.0	51.0 [82.0]	86	Off	4,200	non-engaged	non-engaged	non-engaged	non-engaged
-3.5	52.6 [85.0]	87	Off	4,400	non-engaged	non-engaged	non-engaged	non-engaged
-3.0	55.3 [89.0]	87	Off	4,400	non-engaged	non-engaged	non-engaged	non-engaged
-2.5	57.2 [92.0]	89	Off	4,600	non-engaged	non-engaged	non-engaged	non-engaged
-2.0	59.7 [96.0]	99	Off	4,700	non-engaged	engaged	non-engaged	non-engaged
-1.5	60.3 [97.0]	100	Off	4,800	non-engaged	engaged	non-engaged	non-engaged
-1.0	64.0 [103.0]	0	Off	5,100	non-engaged	engaged	non-engaged	non-engaged
-0.5	58.4 [94.0]	0	Off	4,600	non-engaged	engaged	non-engaged	non-engaged
0.0	57.8 [93.0]	0	Off	3,700	non-engaged	engaged	non-engaged	non-engaged

Figure 13
First record of pre-crash data from the non-deployment event.

Pre-Crash Data -5 to 0 sec [2 samples/sec] (Second Record)

Times (sec)	Speed vehicle indicated MPH [km/h]	Accelerator pedal, % full	Service brake, on/off	Engine RPM	ABS activity (engaged, non-engaged)	Stability control (engaged, non-engaged)	Traction Control via Brakes (engaged, non-engaged)	Traction Control via Engine (engaged, non-engaged)
-5.0	47.8 [77.0]	73	Off	5,600	non-engaged	non-engaged	non-engaged	non-engaged
-4.5	48.5 [78.0]	75	Off	4,100	non-engaged	non-engaged	non-engaged	non-engaged
-4.0	51.0 [82.0]	86	Off	4,200	non-engaged	non-engaged	non-engaged	non-engaged
-3.5	52.8 [85.0]	87	Off	4,400	non-engaged	non-engaged	non-engaged	non-engaged
-3.0	55.3 [89.0]	87	Off	4,400	non-engaged	non-engaged	non-engaged	non-engaged
-2.5	57.2 [92.0]	89	Off	4,600	non-engaged	non-engaged	non-engaged	non-engaged
-2.0	59.7 [96.0]	99	Off	4,700	non-engaged	engaged	non-engaged	non-engaged
-1.5	60.3 [97.0]	100	Off	4,800	non-engaged	engaged	non-engaged	non-engaged
-1.0	64.0 [103.0]	0	Off	5,100	non-engaged	engaged	non-engaged	non-engaged
-0.5	58.4 [94.0]	0	Off	4,600	non-engaged	engaged	non-engaged	non-engaged

Figure 14
Stability control telltale flashing light at 2 Hz signaled at 2 seconds prior to AE, which coincided with a hard steer to the left, as shown in Figure 15.

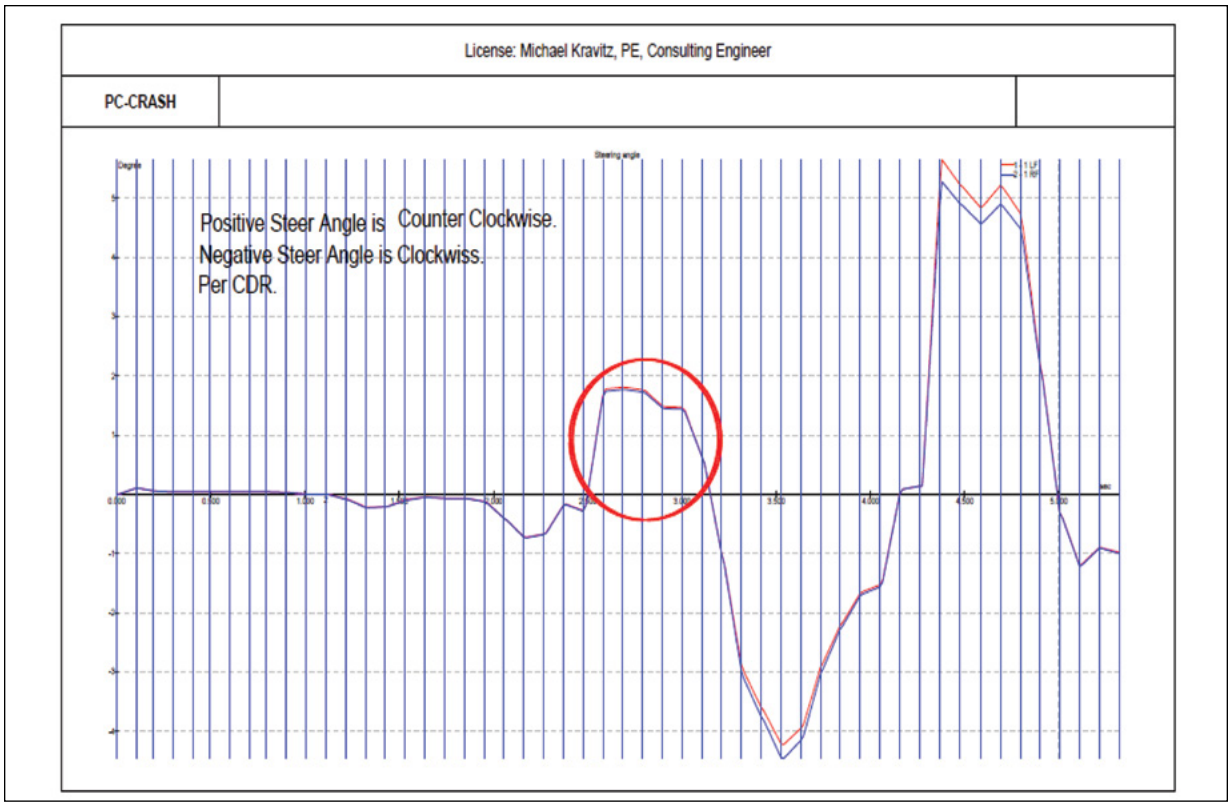

Figure 15
Steering diagram shows a hard steer to the left (counter-clockwise) at approximately 2.3 seconds prior to AE. The hard steer to the left is what the author opines is an evasive action by the driver to avoid the pedestrian or a reflex action after striking the pedestrian. Vehicle travels left to right.

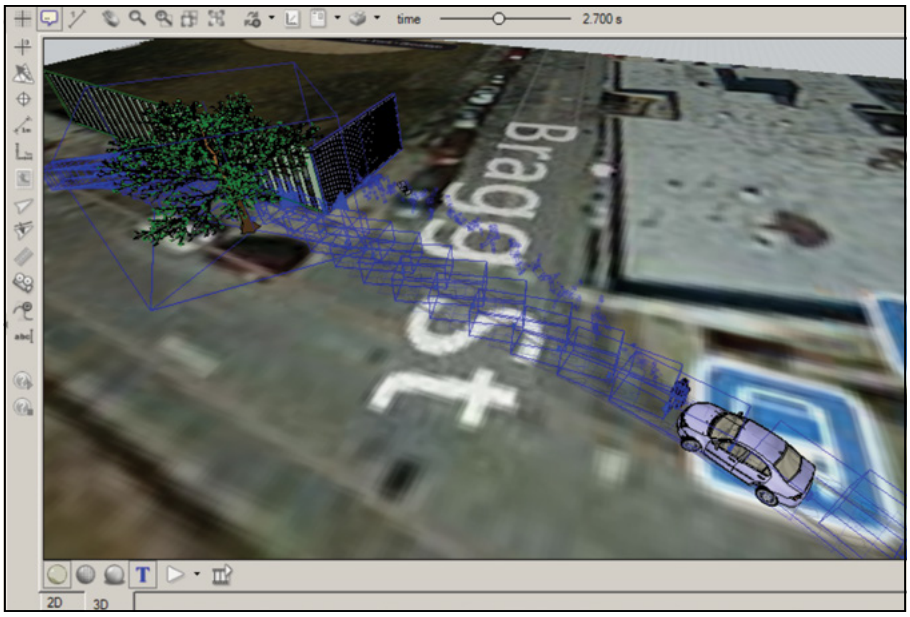

Figure 16
2.7 seconds into simulation corresponds to -2.3 seconds CDR. Pedestrian is in the roadway in front of bus stop. The image is taken from Virtual Crash simulation.

CDR Timing	Virtual Crash Timing
-5	0
-4	1
-3	2
-2	3
-1	4
0	5

Figure 17
Timings comparing the CDR with Virtual Crash data.

which is the estimated distance between the vehicle striking the fence and the tree. This was important because it validated the opinion of the author that the pedestrian was not struck on the sidewalk. Therefore, record one AE was caused by the vehicle striking or side-swiping the fence — not the pedestrian.

Additionally, the pedestrian was not standing on the sidewalk when struck by the vehicle because there was not enough distance for her to be carried by the vehicle and strike the fence, as shown in **Figure 9**. The carry time of the pedestrian is approximately 200 milliseconds, which was estimated from the video. In order for the pedestrian to strike the fence, she would have to be projected from the windshield within approximately 110 milliseconds to 175 milliseconds over a distance of between 10 feet and 15 feet at a speed of 58.7 mph and still strike the fence at the angle to create the depression in the chain-link fence, as evidenced in **Figure 9**. The opinion of the prosecution expert that the pedestrian was struck while standing on the sidewalk could not have happened based on the speed of the vehicle, the distance to the fence, and the carry distance of the pedestrian on the hood of the vehicle.

Pre-Crash Data -5 to 0 sec [10 samples/sec] (Second Record)

Times (sec)	Steering Wheel Angle (degrees)	Stability Control Lateral Acceleration (g)	Stability Control Longitudinal Acceleration (g)	Stability Control Yaw Rate (deg/sec)
-5.0	1.0	0.031	0.164	0.25
-4.9	0.8	0.008	0.151	0.12
-4.8	0.7	0.038	0.143	0.12
-4.7	0.8	0.029	0.122	0.0
-4.6	0.8	0.008	0.132	0.0
-4.5	0.8	0.008	0.145	0.62
-4.4	0.8	0.048	0.203	0.37
-4.3	0.5	0.043	0.148	0.5
-4.2	0.3	0.05	0.169	1.0
-4.1	0.1	0.068	0.155	0.62
-4.0	-1.7	0.051	0.232	0.12
-3.9	-4.5	0.02	0.19	-0.5
-3.8	-4.2	-0.026	0.167	-1.25
-3.7	-1.9	-0.018	0.172	-1.0
-3.6	-0.9	-0.008	0.115	-1.0
-3.5	-1.4	-0.026	0.164	-0.5
-3.4	-1.4	-0.017	0.151	-0.25
-3.3	-2.5	0.008	0.165	-0.37
-3.2	-5.3	-0.124	0.164	-0.75
-3.1	-14.7	-0.159	0.141	-2.5
-3.0	-13.5	-0.216	0.126	-5.37
-2.9	-3.3	-0.173	0.174	-6.5
-2.8	15.7	0.018	0.161	-2.87
-2.7	34.8	0.253	0.146	4.87
-2.6	35.5	0.337	0.172	12.37
-2.5	26.9	0.39	0.147	15.37
-2.4	29.1	0.477	0.148	14.75
-2.3	26.7	0.669	0.081	18.37
-2.2	1.9	0.644	0.013	19.62
-2.1	21.5	0.465	0.075	14.5
-2.0	59.5	0.127	0.133	4.0
-1.9	-72.5	0.043	0.116	-11.87
-1.8	-94.9	-0.525	0.104	-27.62
-1.7	-78.8	-0.788	0.002	-36.62
-1.6	-57.4	-0.936	-0.146	-37.0
-1.5	-43.5	-0.817	-0.041	-30.0
-1.4	-33.1	-0.998	-0.083	-27.62
-1.3	-7.9	-1.123	-0.304	-26.62
-1.2	1.9	-0.849	-0.532	-20.0
-1.1	4.0	-0.969	-0.235	-15.87
-1.0	57.8	-0.823	-0.25	-13.12
-0.9	105.6	-0.022	-0.27	-1.37
-0.8	97.9	-0.105	-0.26	20.0
-0.7	91.4	0.169	-0.129	32.5
-0.6	98.0	0.699	-0.288	38.87
-0.5	99.7	1.267	-0.257	41.62
-0.4	43.1	0.445	-0.09	41.75
-0.3	-6.3	0.252	-0.274	35.37
-0.2	-24.0	0.271	-0.028	28.5
-0.1	-17.9	0.513	-0.241	25.37
0.0	-19.7	2.0	-1.069	29.75

Figure 18
CDR report shows that the hard steering to the left begins at approximately -2 seconds prior to AE. This can be attributed to either an evasive steer or reaction steer after striking the pedestrian.

-2.2	1.9	0.644	0.013	19.62
-2.1	21.5	0.465	0.075	14.5
-2.0	59.5	0.127	0.133	4.0
-1.9	-72.5	0.043	0.116	-11.87
-1.8	-94.9	-0.525	0.104	-27.62
-1.7	-78.8	-0.788	0.002	-36.62
-1.6	-57.4	-0.936	-0.146	-37.0
-1.5	-43.5	-0.817	-0.041	-30.0
-1.4	-33.1	-0.998	-0.083	-27.62
-1.3	-7.9	-1.123	-0.304	-26.62

Figure 19
Close-up of the timing from approximately 2 seconds prior to AE.

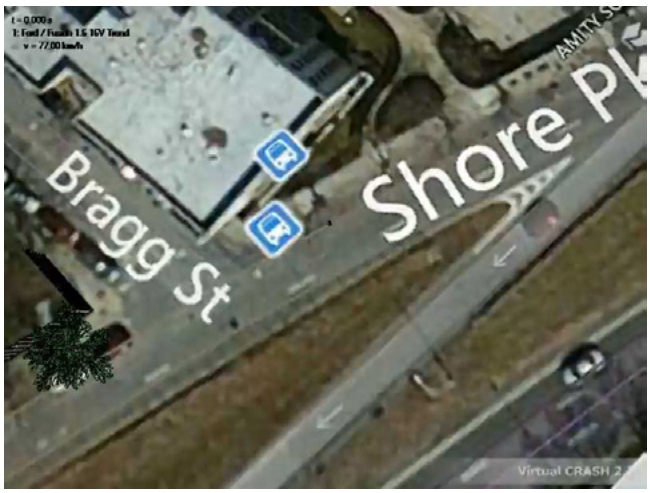

Figure 20
Above is the overview of the path of the vehicle along the service road. The vehicle strikes the pedestrian in the roadway near the bus stop. The pedestrian is projected into the chain-link fence and falls to the sidewalk. The vehicle continues into the tree and comes to rest at approximately its rest position as depicted in the photographs.

CLICK ON PHOTO TO ACTIVATE VIDEO.

Figure 21
Closer view of the pedestrian being struck by the vehicle.

CLICK ON PHOTO TO ACTIVATE VIDEO.

Below is a series of consecutive images taken from the prepared video depiction of the position of the pedestrian head strike on the windshield. **Figure 22** through **Figure 25** are images taken from Virtual Crash simulation software that show where the pedestrian was struck relative to the vehicle. Similarly, **Figure 26** through **Figure 29** show where the pedestrian would have been struck relative to the vehicle if she was struck on the sidewalk, if she were standing on the northwest corner sidewalk. **Figures 22** through **29** are identical with the head striking the windshield at the same location. This shows that had the pedestrian been struck while standing on the sidewalk, the windshield pattern would have been the same, but the pedestrian would have come to rest along the service road instead of where she came to rest on the sidewalk (as indicated in **Figures 20, 21, 30,** and **31**).

Figure 22
Stop motion of pedestrian struck by vehicle.

Figure 23
Stop motion of pedestrian struck by vehicle.

Figure 24
Stop motion of pedestrian struck by vehicle.

Figure 25
Stop motion of pedestrian struck by vehicle.

Figure 26
Stop motion of pedestrian struck by vehicle.

Figure 27
Stop motion of pedestrian struck by vehicle.

Figure 28
Stop motion of pedestrian struck by vehicle.

Figure 29
Stop motion of pedestrian struck by vehicle.

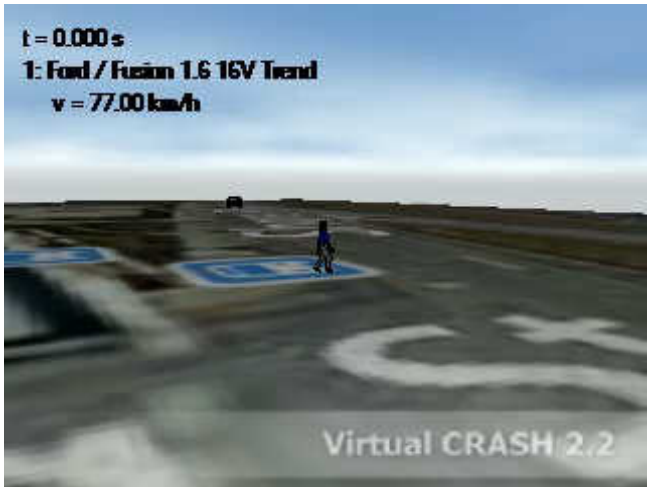

Figure 30
Video of pedestrian being struck in street near bus stop and projected into the fence.

CLICK ON PHOTO TO ACTIVATE VIDEO.

Figure 31
Video of pedestrian being struck on the northwest corner sidewalk as opined by the prosecution expert.

CLICK ON PHOTO TO ACTIVATE VIDEO.

Other Considerations and Discrepancies

The problem with the author's analysis is that the graph below, which is taken directly from the CDR data, shows a small change in velocity at 2.3 seconds — the estimated point of pedestrian impact (see **Figure 32**). The graph below, which is from the Virtual Crash pedestrian impact data, shows a distinct change in velocity at the same time.

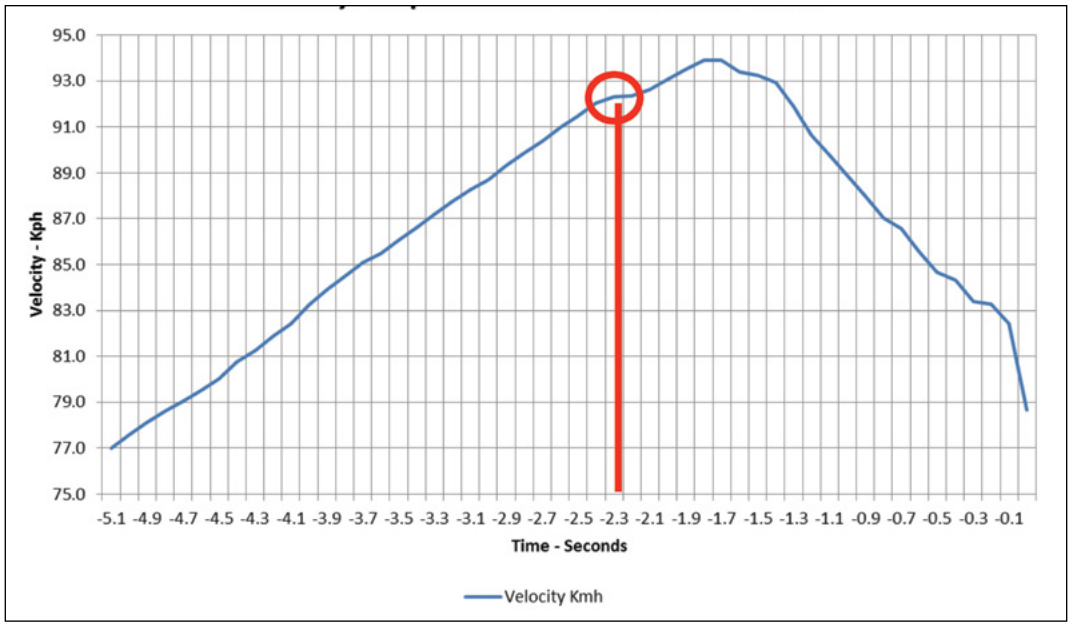

Figure 32
The velocity of the vehicle (in kph) from the CDR download where the probable pedestrian hit coincides with the simulation by Virtual Crash as shown. Vehicle travels from left to right.

The probable cause of error is because the vehicle is at 100% throttle, which has a small effect on the change in velocity of the vehicle but a large effect on impacting the pedestrian.

The CDR graph shows flattening of the velocity curve where the pedestrian probably struck.

The Virtual Crash graph with the pedestrian hit shows a vertical drop in velocity (see **Figure 33**).

Conclusion

The conclusion of the author was that the pedestrian was struck by the vehicle in the roadway of the service road opposite the bus stop where there is no crosswalk. The pedestrian was not struck while standing on the northwest sidewalk of the street and service road as the prosecution expert opined because there was not enough time or distance for the pedestrian to strike the chain-link fence at the angle evidenced in the photographs.

The defendant negotiated a plea to DWI/speeding and was sentenced to three years in prison.

The use of computer software enabled the author to examine this case based on the data captured in the airbag control module, which led to an analysis based on physics and Newton's laws of motion and not to *ipse dixit* opinion.

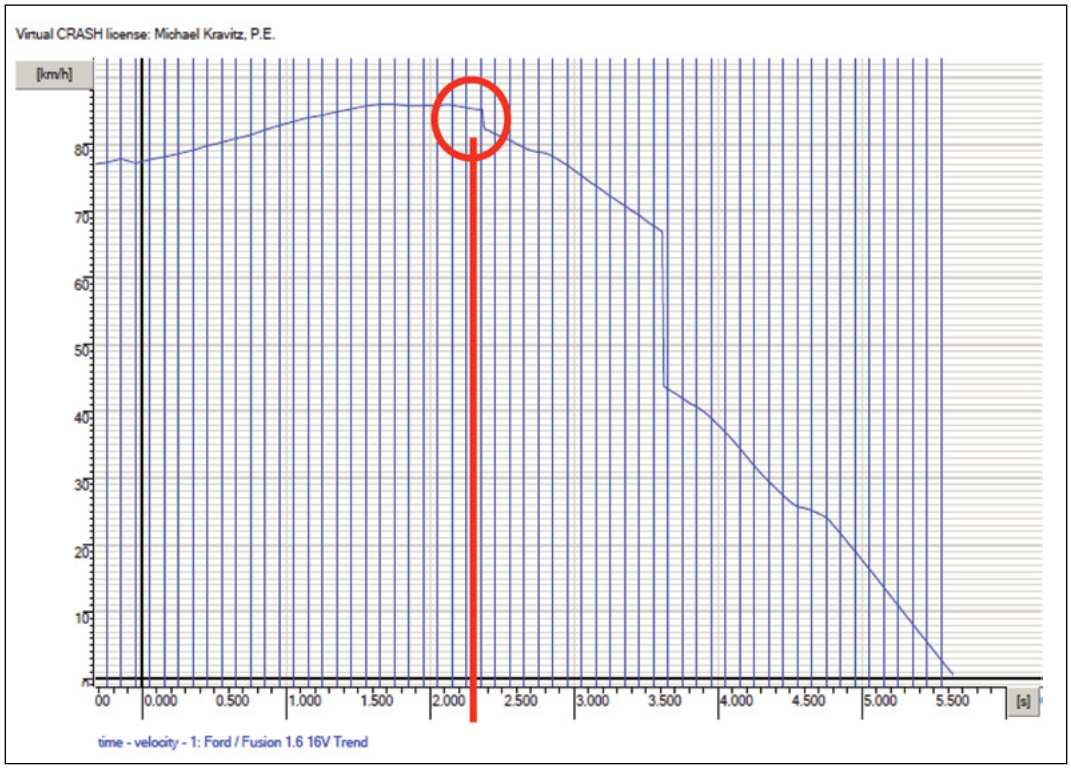

Figure 33
The graph above shows the pedestrian hit at about 2.3 seconds from the simulation of Virtual Crash. Notice the vertical drop indicated, which shows a change in velocity of the vehicle (traveling left to right).

Epilogue

After sentencing, the author was informed of the negotiation between the prosecutor and defendant's attorney that resulted in the DWI plea. The defendant's attorney discovered that the pedestrian had a psychological illness, and it was noted in her records by her doctor that she wished to commit suicide by walking in front of a vehicle. She gave this statement to her psychiatrist 10 days prior to the accident. It was surmised by the defendant's attorney that she wanted to walk onto the service road that night. The on-ramp entrance to the parkway was a short distance from where she was struck, as indicated by the arrow (see **Figure 34**).

Figure 34
Image of pedestrian being struck in street near bus stop.

References

1. 49 CFR 563.8 – data format. National Highway Traffic Safety Administration, Department of Transportation (event data recorders). Code of Federal Regulations, United States Government Printing Office. http://www.gpo.gov/fdsys/granule/CFR-2011-title49-vol6/CFR-2011-title49-vol6-sec563-8

2. Bosch Crash Data Retrieval software system, version 10.2 (Bosch Diagnostics, www.boschdiagnostics.com/cdr)

3. Virtual Crash (V-Crash) accident reconstruction software, 2.3 (www.vcrash3.com)

4. PC-Crash accident reconstruction software, version 10.0 (MEA Forensic, www.pc-crash.com)

Forensic Engineering Evaluation of Utility Compressor Truck Explosion/Fire

By Christopher B. Shiver, P.E. (NAFE 661S)

Abstract

A compressed air system installed as a package on a utility company truck experienced a pressure boundary rupture in service, resulting in burning lubricant discharge onto an employee. Numerous design and component defects were alleged, and a series of expert group examinations of the truck, compressor system, and components occurred over the course of approximately three years. The author was retained by one of more than 20 component suppliers involved in this evaluation. Key issues included design of the compressor system and individual components in the pressure boundary, control system, and cooling system. Based on inspection and analysis, there were several causes for this incident that involved individual component and system design deficiencies, installation deficiencies, and operator training inadequacies.

Keywords

Forensic engineering, truck, air compressor, fire, explosion, safety system, controls

Introduction

A severe injury involving a utility company work truck occurred when the operators attempted to restart a power take off (PTO) driven air compressor after it shut down due to high temperature during heavy use and in hot weather conditions. During the restart attempt, while the operator was at the compressor control position, a pressure boundary component ruptured, resulting in discharge and ignition of hot oil onto that person. Reports that the injured operator restrained the system reset push button at the reset (in) position during the restart attempt (overriding the automatic high temperature shutdown) proved to be important in this case. The evaluation of the compressor system — and its numerous components from various sources — included focus on system pressure and temperature control/limitation, integrity of pressure boundary components, overall system design for safety and human factors, original assembly and maintenance of the truck and compressor system, and operational and maintenance information/instructions provided to persons responsible for those activities.

Background

The truck involved in the incident was used frequently by utility work crews for accessing and maintaining underground facilities. The truck included an air compressor system (mounted under the truck rear body) that was intended mostly for powering pneumatic excavation and other heavy tools (**Figure 1**). The compressor was driven by the truck engine through an electrically engaged PTO unit, and was rated for approximately 185 standard cubic feet/minute (scfm) output at 110 pounds/square inch – gage (psig). The compressor system maximum operating pressure and temperature were 175 psig and 250°F, respectively. The compressor system included provisions for separating the screw-type compressor lubricating oil from the output air in two stages prior to discharge to the working tools (by means of a sump/receiver tank and oil coalescer/separator), and recirculation of that oil back to the compressor after passing through a filter and forced draft air flow oil cooler.

Compressor control features included operator-adjustable automatic regulation of output air pressure in response to tool demand and automatic blowdown of the system, whenever a manual or automatic shutdown of the compressor occurred. The oil cooler fan was designed to be cycled by a temperature sensor to maintain the oil between 160°F to 200°F. Safety control features included separate high pressure (150 psig) and temperature (240°F) shutdowns and a pressure relief valve set to discharge at 175 psig. The system included a manual reset push button switch for restart after an automatic shutdown.

Christopher Shiver, P.E., 1200 Trailmore Drive, Roswell, GA 30076; (770) 587-5054; chrisshiverpe@bellsouth.net

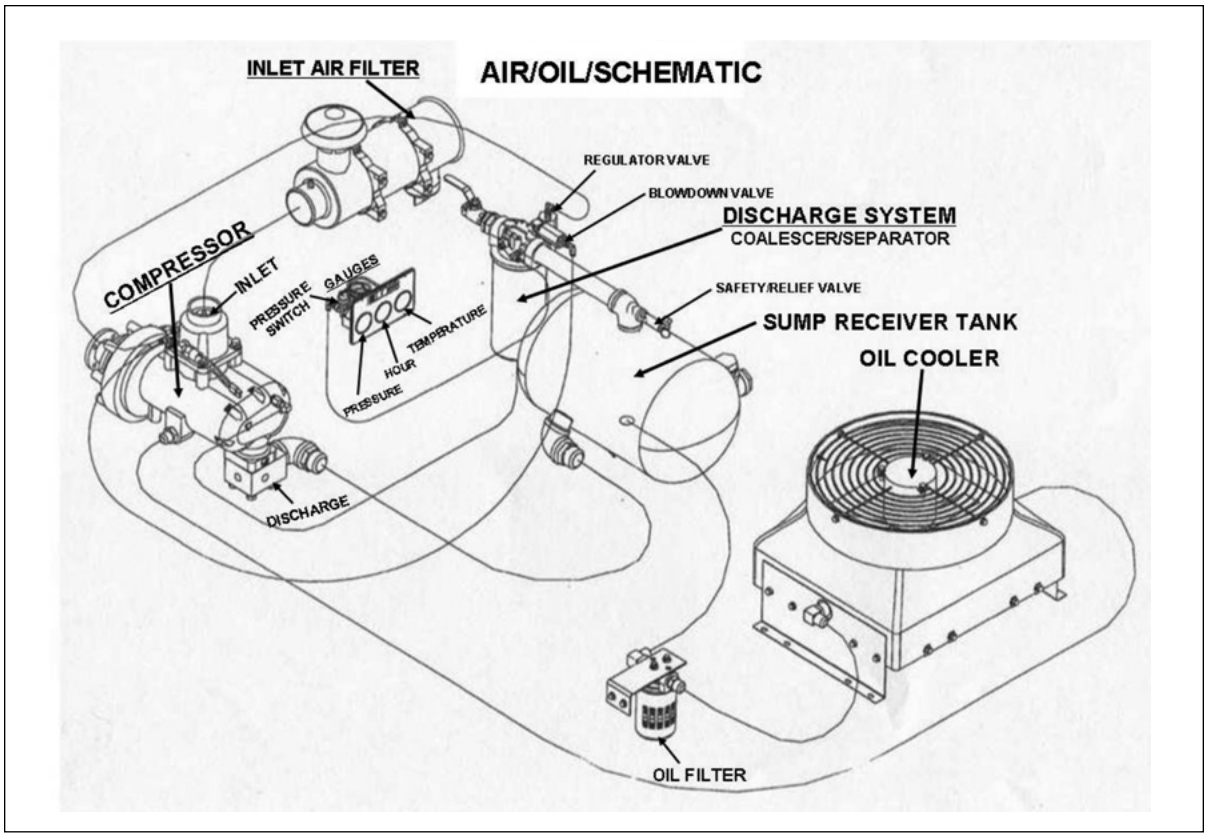

Figure 1
Air/oil schematic for compressor system.

Information and documentation provided by the manufacturer of the compressor system (operations, installation, and parts manual for the subject system as well as competitors' compressor systems, system drawings, component lists, and sworn depositions of manufacturer management personnel) indicated that the model of system installed on this truck was not actually "designed" by this particular manufacturer. Rather, the manufacturer sold a rough copy of other similar systems that had been manufactured by possible competitors. There was no record of any independent design analysis or review of the system design having been conducted by the subject compressor system manufacturer. Instead, the component selection decisions were based on what had been done at other companies that key managers (at the compressor manufacturer) had worked with in the past. There was no apparent evidence of a Failure Modes and Effects Analysis (FMEA) or some other type of safety evaluation of the system operation (including possible abnormal or adverse situations) by the compressor system manufacturer. In addition, the testimony of those same managers revealed that the installation, operation, and maintenance manual contents, instructions, and warnings were also mostly based on literature produced by other competitor manufacturers rather than being an original document written to specifically encompass the subject system, including some of its unique features.

Truck & Compressor System Inspection

Over a three-year period, approximately two dozen parties involved in the evaluation conducted at least eight inspections of the truck, compressor system, individual system components, and exemplars for this equipment. The examinations started with inspection of the truck and compressor in the post-incident condition and then systematic removal of the complete compressor system for further laboratory examination and testing. During this process, examination and testing of exemplars occurred, including a similar complete truck and compressor system assembly used by the same utility company as well as various exemplar assemblies and components for the subject model compressor system.

Initial examination indicated that the compressor system was installed under the truck with the screw-type compressor installed behind the engine and transmission with the compressor drive shaft connected to the PTO on the transmission (**Figure 2**). The air inlet filter, air/

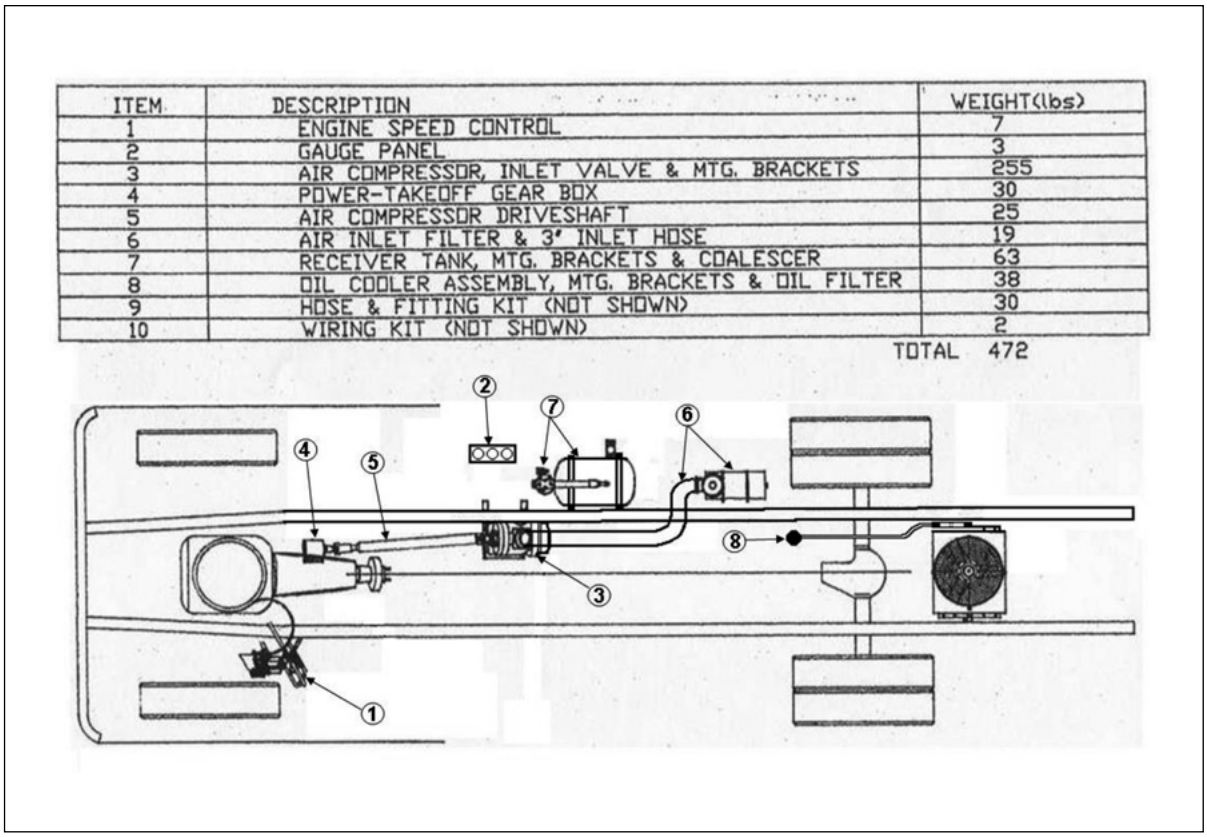

ITEM	DESCRIPTION	WEIGHT(lbs)
1	ENGINE SPEED CONTROL	7
2	GAUGE PANEL	3
3	AIR COMPRESSOR, INLET VALVE & MTG. BRACKETS	255
4	POWER-TAKEOFF GEAR BOX	30
5	AIR COMPRESSOR DRIVESHAFT	25
6	AIR INLET FILTER & 3' INLET HOSE	19
7	RECEIVER TANK, MTG. BRACKETS & COALESCER	63
8	OIL COOLER ASSEMBLY, MTG. BRACKETS & OIL FILTER	38
9	HOSE & FITTING KIT (NOT SHOWN)	30
10	WIRING KIT (NOT SHOWN)	2
	TOTAL	472

Figure 2
Compressor system component locations diagram on truck frame.

oil sump/receiver tank, and oil coalescer/separator were all installed from back to front, respectively, on the vehicle passenger side frame outboard side behind the cab access steps. Installed in a hole cut into the kick plate portion of those steps, just forward of the oil coalescer/separator, was the instrument cluster, which included the pressure/temperature gauges, limit controls, and manual reset switch (**Figure 3**). A separate hole with no apparent purpose was also present in the kick plate aft of the controls locations. The oil cooler was installed between the truck frame rails aft of the rear axle. It is important to note that after the subject incident occurred, the utility company modified similar work trucks that had this compressor system, relocating the instrument cluster from the cab passenger side steps to the rear bumper area (as noted on an inspected exemplar truck).

Figure 3
Damage to passenger side steps and control gauges.
Note unused extra hole in steps.

The burn damage to the truck and compressor system indicated that a limited explosion and fire had initiated between the truck passenger side frame rail and cab step in the vicinity of the oil coalescer/separator, which uses gravitational and inertial effects to separate the compressed air and oil. The cylindrical coalescer/separator's thin-walled metal casing evidenced a rupture due to internal overpressure on the side toward the vehicle front (**Figure 4**). Burning oil discharge toward the vehicle front and passenger side step was evident, which caused destructive fire/heat damage to the instrument cluster and passed outward through the cluster hole cut in the step's kick plate as well as the other nearby similar hole. Beyond the instrument cluster and coalescer/separator — and their hose and wiring connections — the compressor system was generally intact with limited or negligible fire effects.

Figure 4
Damage to oil coalescer/separator, including rupture.

Inspection and testing of compressor system components also revealed that the mounting loops for the steel wire grill (located under the oil cooler fan) had fractured in three of four locations, causing the grill to sag downward (**Figure 5**). The center of the fan grill directly supported the fan motor such that this sagging was causing the fan blade tips to make contact with the fan shroud under the oil cooler. The blade tips and shroud evidenced abrasion damage from this contact. Detailed metallurgical examination of the failed mounting loops indicated fatigue fracture over time with possible initiating damage from road debris impacts.

Figure 5
Fan grill support fracture (one of three).

Detailed inspection and testing indicated that the following other compressor system components were in acceptable condition or functioning properly, based on the original manufacturer's specifications and maintenance requirements (both the subject compressor system manufacturers' literature, and literature provided by component suppliers/manufacturers where available):

- Compressor modulating control valve and air inlet valve
- Timer, relays, and switches that control truck engine speed during compressor operation
- Cooling fan temperature switch and relay
- Solenoid-actuated PTO
- Inlet air filter
- Oil filter
- Blowdown valve
- Pressure relief valve
- Electrical control system circuit breaker
- Electrical push button reset switch/relay

Where practical, the proper working condition of each of the items listed above was confirmed by functional testing — both individually and when connected to other interactive components.

Metallurgical analysis of the ruptured oil coalescer/separator cylindrical shell was performed, including computerized tomography x-ray scanning and scanning electron microscope viewing of the failure region with energy dispersive analysis for materials characterization (**Figure 6**). The findings of this analysis revealed that the material had been overheated from within, resulting in rupture by normal operating pressure forces. In addition to the rupture location, the shell had also bulged outward in several other locations due to overheating while at or below system design pressure. It was determined that the system was below the design pressure based on no evidence of relief valve or high pressure shutdown control actuation prior to the coalescer rupture.

Compressor system temperatures and pressures were sensed and limited by pressure and temperature gauges with integral switch contacts that were reportedly set to the design shutdown limits by the compressor system manufacturer. Both of these gauge and switch assemblies were severely disrupted by the fire damage — such that their functional conditions and settings prior to the incident could not be determined. Both of the gauge and switch assemblies were found wired to the control system reset switch/relay — such

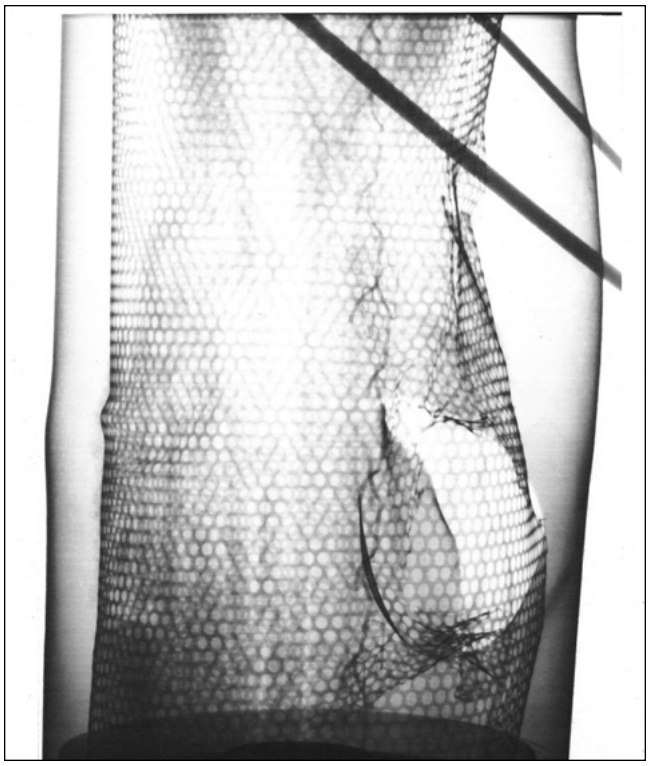

Figure 6
Oil coalescer/separator x-ray image in rupture zone.

that the opening of either set of switch contacts on high pressure or temperature would have shut down the compressor. The compressor could be restarted after a shutdown by momentarily pressing the button on the reset switch/relay. However, if an excessive pressure or temperature condition had still been present, shutdown would recur upon release of the button. Testing of this control system using the same model of exemplar components in place of the damaged components indicated that holding down the reset button would allow continued compressor operation — even if one or both of the gauge switch contacts had opened in response to an excessive pressure or temperature condition. It was observed that the reset switch/relay installation on the subject truck included a still-legible compressor system manufacturer's label at the button stating: "Push Button to Restart Engine or Compressor" with no other instructions or warnings.

Functional testing of the oil cooler fan assembly was performed, including the shroud and grill with three out of four supports fractured. The testing demonstrated that the fan rotation was significantly impeded by the contact between the blade tips and shroud, with intermittent stoppage occurring. This contact and rotation interference was found to be affected by the changing vibration as the fan speed varied due to this abnormal condition. It was also observed that with the fan motor connected to a DC power supply (in the same manner as found on the truck) the curved fan blades were rotating in reverse from the component manufacturer's design intent. Comparison of the air flow in reverse rotation to intended normal rotation indicated overall flow reduction was approximately one-third below normal in the reverse direction. Calculations for axial fan air flow based on established fan engineering principles[1] further confirmed these findings.

Analysis was also performed on residual oil remaining within the compressor system oil filter casing, the air/oil sump/receiver tank, and the oil coalescer/separator casing. The oil quantity recovered was approximately 15 percent of the compressor system manufacturer specified operating quantity, though some oil was still left on system component internal surfaces. This oil was still liquid, evidencing moderate usage conditions and normal viscosity. This analysis was important because some documentation provided by the compressor system manufacturer indicated that, in some instances, oil usage beyond the recommended replacement intervals (based on engine hours and time) in high ambient temperature and humidity conditions could result in severe thickening and color change (to a pink tone) of the compressor oil. This severe oil deterioration was reportedly determined to have been a cause for some previous pressure boundary failures involving compressor systems manufactured by the subject company.

Exemplar Truck & Compressor System Studies

Inspection and testing were performed on the same model compressor system mounted on a similar model truck owned by the same utility company as the subject truck. More-involved testing was also performed on a separate similar model truck and compressor system that had been purchased in a used condition solely for testing purposes. Tests were primarily oriented toward evaluating the potential for compressor system overheating in hot weather conditions similar to those documented at the time of the incident. The tests included normal operation with the compressor discharge air driving the tool reported in use at the time of the incident and also with abnormal operation of the oil cooler fan, including impeded rotation and reverse flow. The tests results indicated that with normal function of the oil cooler, the compressor system did not reach the high temperature shutdown level, but it did shut down in several instances where the oil cooler fan operation was impaired.

One of the parties in this evaluation proposed a modification to the electrical control safety shutdown circuit for the compressor system, which was intended to prevent the system from restarting or running with the reset button held down by an operator, if the system pressure and/or temperature was above the high shutdown limit values (**Figure 7**). Based on input from the other parties involved, the proposed control circuit was assembled using new exemplar components (same model components as specified by the compressor system manufacturer) for comparative testing to the original control circuit. The modified circuit included addition of a single-pole/double-throw relay and two diodes as well some wiring connection modifications (**Figure 8**). The testing demonstrated that it was possible to have designed and installed an electrical control safety shutdown circuit on the compressor system that would have prevented the system from restarting or running with the reset button held down by an operator, if the system pressure and/or temperature was above the high shutdown limit values. The expense and effort required for this modification was determined to be negligible in comparison to the total system cost.

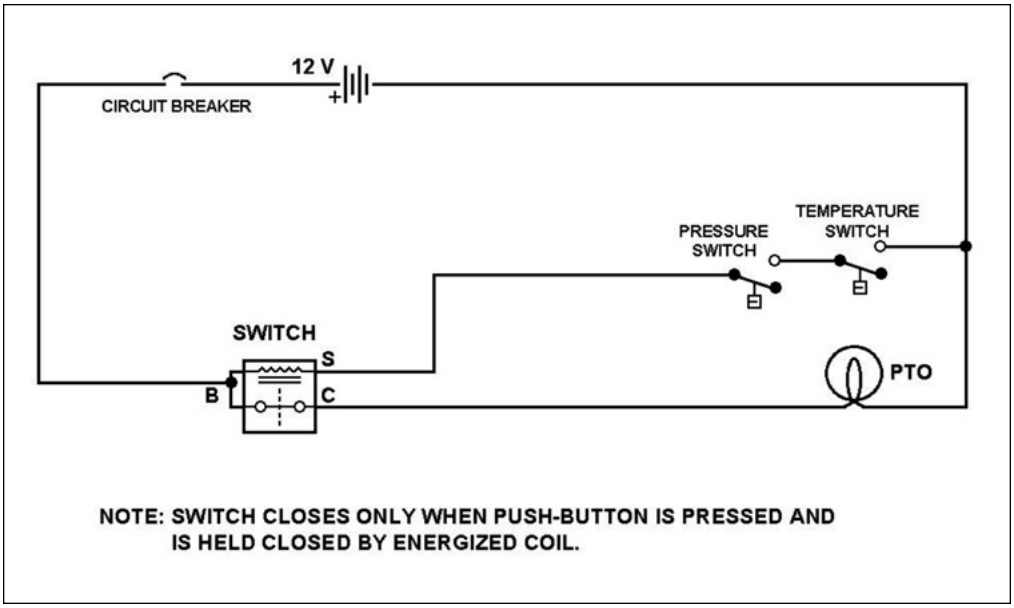

Figure 7
Original safety shutdown circuit.

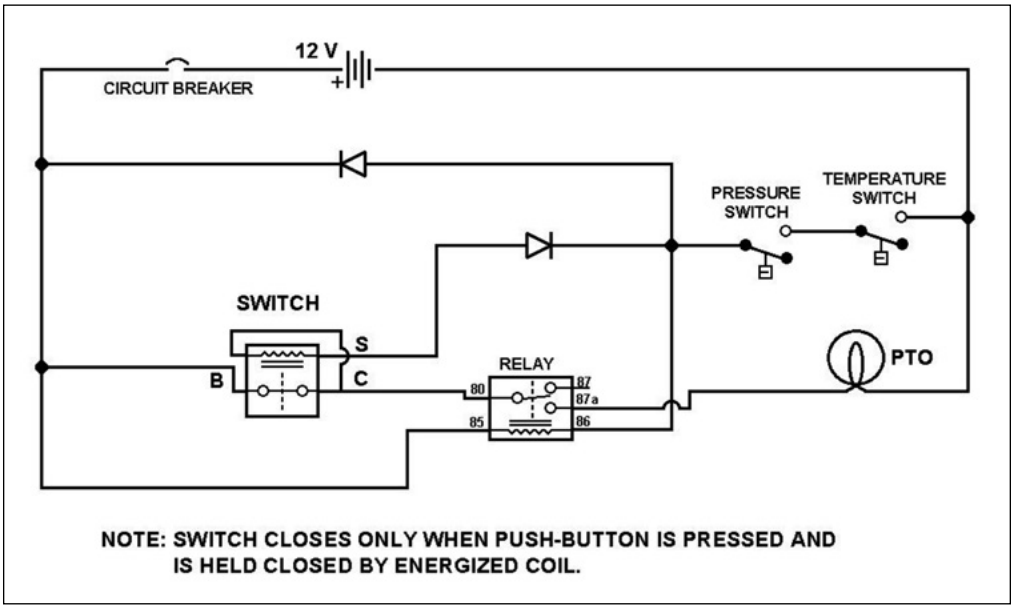

Figure 8
Modified safety shutdown circuit.

Research

Review of two American National Standards for compressor systems of the subject type[2,3,4] indicates that manual restart capability is permitted only if this does not create a hazard or cause damage to the equipment. The compressor system manufacturer must also provide the user with startup and shutdown procedures, where an improper procedure could create a hazard to personnel or cause damage to the equipment. In addition, the compressor system user had to maintain the equipment in accordance with the manufacturer's instructions to promote continuous operator safety.

Review of federal regulations applicable to worker safety during use of compressor systems[5,6] indicates that safety appliances, including control devices, shall be constructed, located, and installed so that they cannot be readily rendered inoperative by any means.

International Standards Organization publications[7,8] that generally applied to the design of the subject compressor system outlined general systematic methods for establishing appropriate levels of safety and hazard reduction in equipment designs. In particular, they indicate that such analysis should include an assessment of safety function and component reliabilities, the consequences of failure or defeat of a safety critical component/system (including control circuits), and the ability of critical safety components to function reliably in the intended usage environment/application. These principles were further covered in additional engineering papers presented at international design and safety conferences[9,10] and in an engineering society design guide[11].

Similar compressor systems from the subject manufacturer and other manufacturers that had been mounted on work trucks owned by other entities were also reviewed, as was installation literature provided by other manufacturers. It was found that control locations for truck-mounted compressor systems were typically well away from high-pressure components on these systems. In addition, many manufacturers specifically instructed or warned installers against locating the control components in a position that might expose an operator to hazards caused by either a failure in the high-pressure portions of the system or by possible discharge from the pressure relief valve.

Conclusion

Evaluation of the entire subject compressor system clearly indicated that a breach had occurred due to an over-temperature condition in the oil coalescer/separator. The damage observed to the compressor and truck further indicated that this breach had resulted in discharge of hot compressed air mixed with compressor oil into the area where the compressor controls had been located. The report that a system operator was manipulating those controls at that time is consistent with the reported severe burn injuries he reportedly sustained. The detailed examination performed on the ruptured oil coalescer/separator casing indicated that its rupture was due to normal internal pressurization in an overheated condition, and was not related to any material or fabrication defect in that component.

Inspection and testing of the subject compressor system oil cooler assembly indicated that several functional conditions likely impeded the cooler's performance. The cooler fan grill support fractures were resulting in probable intermittent slowing or stopping of the fan rotation. Analysis of these fractures indicated that thrown debris from the truck rear axle tires was a probable contributor — in combination with expected vehicle road vibration. Also noted in the installation manual for this system (provided by the manufacturer) was that the subject under-truck rear installation location for the cooler was one of several options for positioning it — with the other optional locations in areas less vulnerable to road hazards. In addition, during the cooler installation, incorrect wiring connections resulted in reverse rotation, which caused reduced air flow even when the fan was rotating unimpeded. Therefore, it was determined that installation deficiencies had resulted in compromise of the oil cooling system on the subject vehicle, which was the probable cause for the compressor system overheating, leading to the incident. In addition, the system design, which permitted installation in an area under the truck where damage due to road debris was an expected condition, was deficient and also contributed to the oil cooler conditions.

The subject compressor system design and installation included automatic shutdown controls in the event of either an air/oil over-temperature or over-pressure condition. However, the control system also included a manual reset push button, which would allow the operator to not only restart the system if an over-temperature or over-pressure condition existed, but would also override those automatic shutdown

features if the button were held in. During the evaluation, it was proven that with minimal additional design effort and expense, the control system could have been configured to prevent operator override of the automatic shutdown features. In addition, the manufacturer's labeling and instructions did not provide any specific directions on how to properly use that reset switch or identify possible hazards of pushing the button (or holding it in) during over-temperature or over-pressure conditions. These design deficiencies were not compliant with the governing national standards applicable to design and safety of air compressor systems of this type. They were also not in accordance with the "standard of care" for design of commercial/industrial equipment.

Also noted during the evaluation was that the truck passenger side cab access step assembly had been cut out in at least one location to accommodate the location of the compressor control components. The locating of the controls in this position was not in accordance with potential locations recommended by the system manufacturer's installation manual. Further, at least one additional cutout had been made for reasons the equipment installer could not explain. The presence of this extra cutout and the controls in close proximity to the oil coalescer/separator contributed to the operator suffering serious injury when that component ruptured.

Extensive documentation was provided by the utility company regarding regular maintenance and inspection of the subject truck compressor system, mostly by outside contractors. It was noted that none of these inspections identified the fan grill failure conditions, which had likely occurred over time because three separate supports had failed. On this basis, it was determined that a failure to perform proper inspections of the compressor system was a probable contributor to overheating of the system and the subject incident.

Review of the training procedures for the injured operator and other members of the same work crew indicated a lack of a systematic approach and an over-reliance on "on-the-job" learning methods by the utility. In particular, no means were documented for assuring that workers received complete operational and safety instruction on the equipment they were using. During sworn statements by these workers, it was apparent that many misunderstood how the subject compressor system functioned and should be operated. Of critical importance was the fact that many of the operators also did not understand the potential safety consequences of restarting the compressor system while it was in an overheated condition or holding down the reset switch to prevent an automatic shutdown. It also became clear that certain supervisory personnel (who did understand those safety consequences) had not taken the proper steps to assure that their subordinates understood those concepts or knew how to operate the equipment safely. As a result, improper and incomplete training of the injured operator was determined to be an important contributing factor to the incident. These training deficiencies were potentially compounded by the lack of safety guidance or instruction regarding operation of the reset control provided by the compressor system manufacturer.

References

1. Jorgensen R. Fan engineering – an engineers handbook. 6th edition. Buffalo NY: Buffalo Forge Co.; 1961.
2. ANSI/NFPA B93.114M-1987. Pneumatic fluid power – systems standard for industrial machinery. Milwaukee WI; National Fluid Power Association.
3. ANSI/NFPA T2.25.1M-1986. Pneumatic fluid power – systems standard for industrial machinery. Milwaukee WI; National Fluid Power Association.
4. ANSI/ASME B19.1-1995. Safety standard for air compressor systems. New York; American Society of Mechanical Engineers.
5. OSHA 29CFR1910.169-1996. Compressed gas and compressed air equipment – air receivers. Washington, DC; Occupational Safety & Health Administration.
6. OSHA 29CFR1926.306-1993. Safety and health regulations for construction – tools – hand and power – air receivers. Washington DC; Occupational Safety & Health Administration.
7. ISO 14121-2007. Safety of machinery – principles of risk assessment. Geneva Switzerland; International Standards Association.
8. ISO/TR 12100-1992. Safety of machinery – basic concepts, general principles for design. Geneva Switzerland; International Standards Association.
9. Hornbeck D. A holistic approach to safety automation. Paper presented at: XVIII World Congress on Safety and Health at Work. June 29 – July 2, 2008; Seoul Korea.

10. Smith CO. Design deficiencies? Devastation. Paper presented at Annual Winter Meeting, American Society of Mechanical Engineers. November 1981; Washington DC.
11. An instructional aid for occupational safety and health in mechanical engineering design, publication #100184. New York: American Society of Mechanical Engineers Safety Division; 1984.

Acknowledgement

Figures 1, 2, 7, and 8 were prepared with the valuable assistance of professional graphics specialist Monica Helms of Marietta, GA.

Forensic Engineering Investigation of Above-Ground Pool Submersion Accidents

By Richard Ziernicki, Ph.D., P.E. (NAFE 308F) and William H. Pierce, P.E. (NAFE 846C)

Abstract

In the United States, approximately 35 children under the age of five years old drown each year after accessing above-ground pools via pool ladders. Consumer Product Safety Commission (CPSC) data also shows that approximately 486 additional children sustain submersion-related injuries after accessing above-ground pools via pool ladders. In many cases, these events occurred during brief lapses of adult supervision. This paper focuses on potential product defect issues related to child submersion accidents, including the role of user manuals, alternative designs, warnings, instructions, and child behavior testing. The authors examine the issues related to the investigation of above-ground swimming pool submersion accidents. In addition, procedures and steps are outlined that may be useful in analyzing whether the swimming pool is defective and unreasonably dangerous.

Keywords

Swimming pool, above-ground pool, submersion, drowning, defective product, unreasonable dangerous product, pool ladder, guarding

Introduction

Young children have been known to drown while using pool ladders to gain unauthorized access to above-ground pools; evidence of this dates back to the 1960s when the hazard was specifically mentioned in several patents. For example, a patent issued in 1966 discusses the hazard[1] as follows:

> *"However, a problem is presented with the use of regular stepladders for such purposes because young children have climbed up the ladder when no adults were present and have fallen into such pools and have drowned."*

Using the combination of data published by the CPSC[2] and a pediatrics journal article[3], it is estimated that there are 35 submersion-related deaths and an additional 486 submersion-related injuries associated with children under the age of five gaining unauthorized access to above-ground pools using pool ladders.

In general, safety is a combined effort of a designer, manufacturer, user (operator), and employer (if involved). However, if something goes wrong, the highest price (injury or death) is paid by the user/operator. Therefore, it is essential to design and manufacture the product as safely as practical.

In many cases, an equipment designer and manufacturer heavily rely on instruction manuals, warnings, and proper training of potential users. They downplay the importance of the hazard and risk analyses that may detect safety issues. Some reasons for this type of approach, which (if unsuccessful) may result in serious injury or death, include a lack of safety knowledge, an aversion to including more costly safety features, or simple recklessness.

Occasionally, when serious injury or death occurs, the injured party or his/her estate brings a lawsuit against the designer, manufacturer, and/or distributor under the claim of a "defective and unreasonably dangerous product." After analyzing the accident, an expert witness is asked whether a product is defective and if the designer, manufacturer, distributor, or operator contributed to the incident causation.

In simple terms, a product may be defective and unreasonably dangerous if it can cause an injury or death, and it is technologically and economically feasible to design the hazard out of the machine or to guard against that hazard. Technologically feasible means that before the product was manufactured, there was technology available to make the product safer and to eliminate (or guard against) the hazard. Economically feasible means that a safer design can be achieved at a reasonable cost.

Richard Ziernicki, P.E., 7185 South Tucson Way, Englewood, CO 80112-3987; (303) 925-1900; rziernicki@knottlab.com

A product can be unreasonably dangerous if it is defectively designed, manufactured, or maintained — or if it has defective warnings and instructions.

Background

The parents of a two-year-old child purchased an above-ground pool package from a store, which included both a pool and ladder (**Figure 1**). They installed the pool with the ladder in the backyard of the residence.

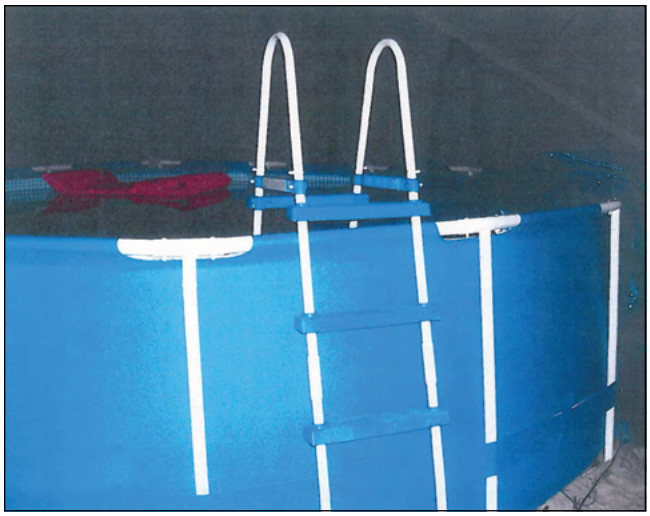

Figure 1
Above-ground swimming pool involved in the accident.

According to the police report, the accident occurred when the mother got out of the pool and briefly went inside the residence while the child was playing in the sandbox in the backyard. After spending three to five minutes inside, the mother went outside to check on the child and found the child floating in the pool. The mother yelled for the child's father, and the father performed CPR on the child. As a result of the accident, the child sustained permanent brain injuries. Apparently, the child climbed the A-frame ladder and fell into the pool.

Manufacturer Literature

The manual for the metal-frame above-ground pools and ladders provided with the manufacturer's pool packages had some warnings pertaining to parental supervision and removal of the ladder from the pool. For example, one warning stated:

> "NEVER LEAVE CHILDREN UNATTENDED WHILE IN OR NEAR THE POOL."

The warning is an indication of a hazard recognized by the manufacturer as having the potential for serious injury or death. In this case, the hazard is the need for constant supervision. Another warning example in the ladder manual stated:

> *"Remove and secure ladder away from the pool when the pool is not in use to prevent unauthorized, unintentional, or unsupervised pool entry."*

The warning is a further indication of a recognized hazard requiring users to take the ladder out of the pool after each use.

According to the manufacturer's director of risk assessment (in his deposition), "the A-frame ladder is lightweight. It's easy to remove from the pool."

Anthropometric Testing

Anthropometric testing was performed on an exemplar ladder to determine the forces and mechanics involved with lifting the ladder out of the pool. The anthropometric study was used to determine whether requiring users to lift the ladder out of the pool after each use was acceptably safe.

The lifting mechanics of an actor shown in the safety DVD provided with the exemplar pool purchased were analyzed. The ladder shown in the safety DVD was much shorter than the subject ladder.

A female and male test subject lifted an exemplar ladder above the barrier height of the pool with similar lifting mechanics as the actor in the safety DVD. Photographs were taken of the test subjects lifting the ladder above the barrier. The lifting mechanics involved with lifting the ladder above the barrier were compared to safe lifting weight limits published by the Health and Safety Executive (U.K.)[4].

In this testing, the minimum lifting force required to lift the ladder out of the pool was 84 percent more than the acceptable lifting limit for females and 22 percent more than the acceptable lifting limit for males. Therefore, the lifting force required to lift the ladder out of the pool was unreasonably heavy, according to the Health and Safety Executive guidelines.

The authors of this paper concluded that lifting the ladder out of the pool is a cumbersome process that, by industry standards, requires an unreasonable amount of lifting force. According to a safety engineering textbook[5],

"It is known that a person will generally tend to follow those procedures, which involve minimal physical and mental effort, discomfort, or time. Any procedure contravening this basic principle is certain to be modified or ignored by the persons supposed to carry it out."

Therefore, the burdensome process of removing the ladder from the pool after each use has the potential to be ignored by users. When the process of removing the ladder is ignored by users, young children may be needlessly exposed to the pool accessibility hazard.

It was apparent that instead of mitigating the hazard, the manufacturer showed disregard for engineering safety and human life by dismissing the pool-access hazard associated with the A-frame ladder. In addition to simply dismissing the hazard, the manufacturer has attributed the cause of above-ground pool child drowning and near-drowning to improper adult supervision.

Published Literature

A detailed analysis of publically available sources[3,6] and CPSC data shows that, in many cases, child drowning and near-drowning events occurred due to a lapse of adult supervision of under 10 minutes.

For example, SafeKids International safety literature[6] states that in the time it takes for a parent to take his or her eyes off a child to perform a mundane yet quick task, such as sign for a package at the front door, "*a child can become submerged and sustain permanent brain damage or die*":

"*Drowning is quick and silent. In the time it takes to… cross the room for a towel (10 seconds), a child in the bathtub can become submerged.*

Answer the phone (2 minutes), and that child can lose consciousness.

Sign for a package at your front door (4-6 minutes), and a child submerged in a bathtub or pool can sustain permanent brain damage and die."

A pediatrics journal article published in 2010 further shows that 32 percent of children involved in portable pool-related submersion events had been left unattended for less than 5 minutes, and a majority of children (56 percent) had been left unattended for less than 10 minutes[3]. Therefore, the study (which used data readily available to the manufacturer) along with the SafeKids safety literature both show that a brief lapse in parental supervision is not only foreseeable, but it is also a frequently occurring hazard associated with above-ground pools.

The authors of the pediatrics journal article also analyzed the method of access to portable pools. The study found that a majority of children who drowned in above-ground pools (67.5 percent) accessed the pool by means of a ladder[3]. The above statistical data clearly shows that the ladder accessibility hazard is a highly probable event. Other entry methods included climbing on objects placed near the pool, accessing the pool by stairs, climbing over the edge of the pool, and being placed in the pool by another person.

It is apparent that removing the ladder completely from the pool is a cumbersome process, requiring an unreasonable amount of lifting force. Therefore, alternative safer ladders (as discussed below) were researched and inspected. The alternative safer ladders required less physical or mental effort and did not involve awkwardly lifting the ladder out of the pool.

Alternative Ladder Designs

The authors inspected a commercially available flip-up ladder in 2008 (alternative 1). This ladder (as designed) includes a moveable ingress ladder section that pivots about the top platform of the A-frame ladder. The moveable ingress ladder section may be positioned in the down position when the pool is in use and in the up position when it is not. Furthermore, when the ingress ladder section is in the up position, it can be secured into place by means of a padlock included with the product (**Figure 2**).

An updated version of the ladder (**Figure 3**) is currently commercially available (alternative 2). The presence of the ladder on the market in the United States for several years indicates that it is not only a commercially viable product, but also that the manufacturer is providing engineering updates to the ladder to improve its design.

The authors also inspected another model by the same manufacturer of alternative 1 and 2 (alternative 3), which has a built-in ladder shield (**Figure 4**). The ladder shield is designed to slide over the steps when the pool is not in use, thus blocking entry to the pool. A padlock is provided as an additional means to lock the shield into place.

Figure 2
Alternative ladder 1 inspected by the authors in 2008.

Figure 3
Alternative ladder 2 inspected by the authors in 2014.

Figure 4
Alternative ladder 3 inspected by the authors in 2014.

Figure 5
Alternative ladder 4 inspected by the authors in 2014.

Another commercially available safety ladder (alternative 4) has a door assembly that encloses the ladder steps (**Figure 5**). The ladder door is hinged on one side, allowing the door to open and shut. The hinged side of the door is spring-loaded so that the ladder door biases into the closed position when it is not in use. In addition, a spring-loaded latch secures the door into the closed position when not in use. In order to open the door, the user has to release the latch by engaging the handle located near the top of the door while simultaneously opening it.

The ladder's self-closing and self-latching door is a passive safety guard because it is automatically activated without intervention of the user. Passive safety guards, such as the self-closing and self-latching ladder door, are preferable over active safety guards from a safety engineering perspective because they most nearly eliminate the risk of human error.

The manufacturer of the pool package involved in the subject incident also makes a "deluxe" A-frame ladder, but continues to sell A-frame ladders similar to the one involved in the submersion accident. Both ladders are depicted side by side in **Figure 6**.

Figure 6
Comparison between A-Frame ladder included with pool (left) and "deluxe" manufacturer ladder (right).

The "deluxe" ladder is intended to be used in two positions — the down position when the pool is in use and the up position when it is not. When the ingress ladder section is in the down position, the bottom of the legs of the ingress section fit into slots near the base of the ladder, and the top of the legs snap into grooves near the top of the platform. Two clips add additional securement to the top of the legs of the ingress section.

In order to detach the ingress ladder section, the user releases the clips that secure the top of the ladder legs and then depresses two buttons that release the top of the ladder legs from the grooves. The ladder can then be removed, and two slots located on the ladder's top platform allow the ingress ladder to be stored in the up position.

The "deluxe" design in the United States is currently sold by the manufacturer as part of standard packages in France. Therefore, the design is both technologically and economically feasible. However, the manufacturer consciously chose to continue distributing the cheaper (and more cumbersome) A-frame ladder in the United States.

Testing of Children Behavior

The authors tested the safety features of several commercially available alternative ladders with guards. During the testing, young children between two and three years old were incentivized with candy or other objects to access an exemplar pool using the alternative ladders with guards. For example, a 35-month-old boy is depicted attempting to bypass the ladder guard in **Figure** 7. None of the children involved with the testing were able to access the pool with any of the commercially available alternative ladders with guards.

Figure 7
A 35-month-old boy attempting to access exemplar pool using alternative ladder 2.

Industry Codes and Regulations

During analysis, industry standards and local building codes regarding ladder, barrier, and pool safety were reviewed. The purpose of reviewing the standards and building codes was to determine whether the subject ladder and exemplar ladders were compliant.

The permitting process in place in the county where the pool was installed requires homeowners to submit "manufacturer's specifications on how to erect the pool and specifications on self-locking ladders."

The requirement of homeowners to send specifications on self-locking ladders indicates that officials in the county believed self-locking ladders were the standard of care, which is consistent with the engineers' opinion.

Further research shows that other counties within the United States establish that a removable ladder does not constitute an acceptable alternative to barrier requirements for an above-ground pool. For example, the Douglas County, Nebraska Requirements for Private, Residential, or Family Swimming Pools state:

> *The pool structure may be acceptable as a barrier, provided the 48-inch minimum height requirement is met, or if the barrier is mounted and sturdy on top of the pool structure. A removable ladder shall not constitute an acceptable alternative to barrier requirements. When the pool structure qualifies as the barrier, the ladder access area shall be enclosed with an approved minimum 48-inch-high fence with self-closing and self-latching gate or door. The self-latching device shall be located at least 45 inches above grade level for keeping the gate or door securely closed at all times*[7].

As another example, the Township of Wall, New Jersey Pool Fence Requirement states that (bold and underlined text written within requirement):

> *Barriers are required for above-ground pools;* ***a removable ladder is not an acceptable barrier*** *for the above-ground pool*[8].

In addition to building codes in the United States, there were various other resources that discuss whether a removable ladder is an acceptable barrier. Three examples are shown below:

Canadian Residential Swimming Pool Safety Regulation states:

> *6. An above-ground pool with a wall height of at least 1.2m from the ground at any point or a portable pool with a wall height of 1.4m or more is not required to be surrounded by an enclosure if access to the pool is by (1) a ladder equipped with a self-closing and self-latching safety gate, preventing its use by children. (2) A ladder or a platform access to which is protected by an enclosure having the features described in Section 4 & 5. (3) A patio attached to the residence and laid out so that the part giving access to the swimming pool is protected by an enclosure having features described in Section 4 & 5*[9].

The Australian Standard 1926 states:

> *The sides of above ground pool can be accepted as being part of a pool safety barrier, provided they comply with the Australian Standard 1926. However, a barrier must also be provided around the ladder. (It's not good enough to say the ladder will be removed when an adult is not present) as well as pipes, pumps, or anything else that can be climbed on*[10].

Therefore, it is clear that some local codes within the United States and international standards/regulations acknowledge that removable ladders are not safe and should not be used with above-ground pools. Further, the self-locking and self-latching ladder is an acceptable passive safety device that meets various local and international codes.

Summary

The authors' inspections, analysis, and testing show that several safer alternative designs were technologically feasible at the time the manufacturer made the subject pool and ladder.

Further, the authors concluded that the passive safety guard (self-closing and self-latching ladder guard) offered a higher level of protection of the alternative products commercially available.

Several local building codes in the United States and international standards/regulations acknowledge that general removable A-frame ladders (such as the ladder involved in the accident) are not safe, and certain regulations require passive safety devices, such as the self-closing and self-latching ladder guards.

As discussed above, the manufacturer relied on parental supervision to provide guarding against the hazard of drowning. As shown through the published literature, such reliance is not dependable and has led to many child drownings. It is more prudent for the manufacturer to follow proven safety methods and guard against the hazard of drowning by providing a proper ladder that prevents children from accessing the pool without parental assistance.

Conclusions

- Drowning and near-drowning events involving young children often occur during a brief lapse of adult supervision.
- Instead of mitigating the hazard through guarding or access prevention, the manufacturer supplied the unprotected A-frame ladder, easily climbable by children, with its above-ground pool packages.
- Accident statistics show reliance on parental supervision as guarding against the hazard of drowning is not effective.
- The self-closing and self-latching ladder guard is a passive safety device that offers a high level of protection for small children.
- The self-locking and self-latching ladder is an acceptable passive safety device that meets various local and international codes.
- Several safer alternative designs were technologically feasible at the time the A-frame ladder was manufactured.
- Relying on instructions and warnings may not be an effective procedure in preventing drowning accidents.

References

1. Gurian SD, Bernstein MM, inventors; Pool ladder. United States patent US 3,288,248. 1966 Nov 29.
2. Yang T. Pool and spa submersion: estimated injuries and reported fatalities. May 2013 [accessed July 29, 2105]: United States Consumer Product Safety Commission. https://www.cpsc.gov//Global/Research-and-Statistics/Injury-Statistics/Sports-and-Recreation/Pools/PoolSubmersions2013.pdf.
3. Shields B, Pollack-Nelson C, Smith G. Pediatric submersion events in portable above-ground pools in the United States, 2001-2009. Pediatrics. 2011;(128)(1):47-48.
4. Manual handling at work: A brief guide. Liverpool, England: Health and Safety Executive; [cited 2015 July 29]. http://www.hse.gov.uk/pubns/indg143.pdf.
5. Hammer W. Occupational safety management and engineering, 2nd Ed. Englewood Cliffs NJ: Prentice-Hall, Inc.; 1981.
6. Water safety tips. Safe Kids Tucson; [cited 2015 July 29]. https://www.tmcaz.com/files/Safe%20Kids%20-%20Water%20Safety.pdf.
7. Private, residential, or family swimming pools. Douglas County Environmental Services [cited 2015 July 30]. http://www.dceservices.org/images/stories/pdfs/pln_zn/priv_pools.pdf.
8. Pool fence requirements. Township of Wall NJ [cited 2015 July 30]. http://www.wallnj.com/DocumentCenter/Home/View/542.
9. Residential swimming pool safety regulation, CQLR c S-3.1.02, r 1. CanLII [cited 2015 July 30]. https://www.canlii.org/en/qc/laws/regu/cqlr-c-s-3.1.02-r-1/latest/cqlr-c-s-3.1.02-r-1.html.
10. Fencing frequently asked questions. Rose Park, South Australia: South Australian Swimming Pool & Spa Association; [cited 2015 July 30]. http://www.spasasa.com.au/fencing-frequently-asked-questions.

Forensic Evaluations of Built-Up Roofing Storm Damage Claims and the Appraisal Process

By Todd Springer, P.E. (NAFE 422C)

Abstract

Severe weather, which is a regular occurrence in the American Southwest, includes more than high temperatures and haboobs (dust storms). Severe thunderstorms, often accompanied by high winds and hail, are regularly experienced and have the potential to cause damage to roofing systems and other exterior building components. Insurance claims for storm damage — both legitimate and unwarranted — have come under increased scrutiny due to indistinct and altered dates of loss, the amending and broadening of damage causes, and the offering of technically unsupportable opinions by individuals who are less than qualified. Further, these claims often end in appraisal hearings that are decided by umpires for whom there are no minimum educational or experiential requirements.

Keywords

Forensic engineering, storm damage, roofing, appraisal, wind, hail, weather, advocacy, scientific basis, public adjuster

Introduction

Hail — and the effects of hailstone impacts to roofing materials — has become an increasingly controversial topic over the past decade, with the number of insurance claims for hail damage reported in the United States increasing by 84% from 2010 to 2012 (Fennig 2013). This rise in claims has been accompanied by an increase in disputes, promulgated by third-party intermediaries (i.e., public adjusters, roofing contractors, consultants, attorneys, etc.).

Built-up roofing (BUR) systems have been in use for more than 100 years, and have a history of good performance and durability. The system uses alternating layers of bitumen and reinforcing fabrics that compose plies. The initial ply is typically mechanically fastened to the roof deck. Additional layers are subsequently adhered via hot tar/asphalt or cold-applied adhesives and laid in an overlapping ("shingle") fashion. The top ply (referred to as the cap sheet) usually incorporates some form of ultraviolet radiation protection, such as a coating, gravel ballasting, or embedded roofing granules. Once assembled, the system is referred to as a "roofing membrane." **Figure 1** illustrates the overlapping installation as well as a photograph of a finished roof membrane system.

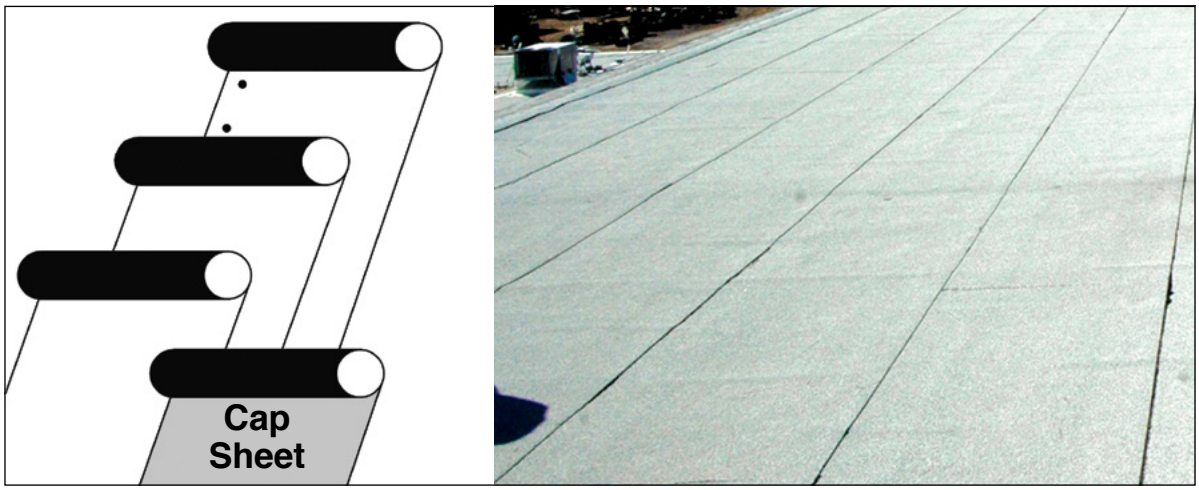

Figure 1
Built-up roofing.

Todd Springer, P.E., 3315 East Wier Avenue, Phoenix, AZ, 85040; (602) 443-1060; todd.springer@akeinc.com

Testing to evaluate the effect of hailstone impacts to BUR systems was first studied by the United States Department of Commerce (Greenfeld 1969). Additional testing has been conducted by independent organizations, including Haag Engineering in 1988 and 1993 (Marshall 2006). Testing was also conducted by this author to validate the results established by others and provide first-hand knowledge of the effects of hail stone impacts to roofing systems. The results of these tests consistently show that BUR has exceptional hailstone impact resistance, such that hailstones that are more than 2 inches in diameter are a typical "threshold" for functional damage. Examinations of BUR systems immediately following large hail events support the results of the aforementioned testing (Roofing Industry Committee on Weather Issues 2012).

The effects of wind on BUR systems have been well documented and are typically readily apparent (Roofing Industry Committee on Weather Issues 2007). Aside from damage resulting from wind-blown projectiles, wind damage will typically occur in the form of lifted, torn, and/or missing roofing material. Once compromised, wind is able to penetrate underneath the roofing membrane, rendering it more susceptible to additional wind damage.

In addition to third-party testing and field observations, manufacturers of BUR materials regularly test these systems to obtain wind and hail ratings. Although there is an abundance of test data published, including large-scale post-storm field inspection reports, this information is given varying degrees of credence by the ruling body in disputed matters. Disputed insurance claims can end up in litigation or what is referred to as an appraisal hearing. This paper will present two case studies that compare the differences in structure and handling of technical experts and opinions between insurance appraisal and litigation processes.

Litigation

In a typical litigation process, there are several criteria an expert must meet in order to have his/her testimony admitted.

> A witness who is qualified as an expert by knowledge, skill, experience, training, or education may testify in the form of an opinion or otherwise if:
>
> (a) the expert's scientific, technical, or other specialized knowledge will help the trier of fact to understand the evidence or to determine a fact in issue;
> (b) the testimony is based on sufficient facts or data;
> (c) the testimony is the product of reliable principles and methods; and
> (d) the expert has reliably applied the principles and methods to the facts of the case.

While the court allows an expert to rely upon his or her experience to formulate opinions, the court demands that those opinions be based on the facts of the case and supported by accepted scientific principles, methodologies, and studies. Litigation also follows a formal process that allows parties to request pertinent information through discovery or interrogatories and deposition testimony. This process includes the timely disclosure of expert opinions, and allows for a formal rebuttal of such opinions.

Appraisal Hearings

Most insurance policies contain what is referred to as an "appraisal clause." If it is determined that the claimed damage is covered — and the insured disagrees with the amount of money the carrier has offered — he or she can invoke the appraisal clause. In this process, both the carrier and insured will each hire an appraiser to independently evaluate the loss and determine the appropriate financial compensation. The appraisers must then select a third appraiser, termed an "umpire." The matter is resolved when any two appraisers (typically the umpire and one other) agree on an amount to be paid by the carrier.

Once an umpire is selected, both appraisers will submit paperwork in support of their determinations. Items submitted typically include technical reports, maintenance records, weather reports, and contractor estimates. The umpire will then review the material and hold an appraisal hearing. In this hearing, which is typically held in a conference room (or similar location), both appraisers will be allowed to present their arguments, based only on documents submitted prior to the hearing. In some instances, the hearing will also involve observations of the subject property. In the days, weeks, and sometimes months after the hearing, the umpire will make a decision. Sometimes, this process is more of a negotiation than the umpire simply assigning a monetary value to a loss.

There are no legal criteria that one must meet to become an umpire. Rather, insurance policies typically

dictate that an umpire must be "competent and disinterested" or independent. Therefore, umpires involved in these matters come from a variety of backgrounds, many of which do not involve dispute resolution (the essence of the matter). Additionally, there are no qualification requirements for technical opinions. It is not uncommon to see technical arguments presented without any basis in the established facts or recognized scientific data and literature.

Background in Arizona

On Oct. 5, 2010, several severe thunderstorms passed through the Phoenix metropolitan area. These storms produced large hailstones (up to 3 inches in diameter), which caused damage to thousands of roofing systems. While the majority of claims were filed in the months following the event, some continued to be filed several years after the event. Many of the later claims were initiated by roofing contractors, public adjusters, or attorneys and resulted in disputes as to the cause and extent of damages.

Case Study #1 – Large Commercial Strip Mall

This claim involved a large commercial strip mall covered with BUR systems of varying age and condition installed on a panelized roof structure. The insurance claim in this instance was filed more than a year after the reported date of loss, was accompanied by a report from an out-of-state firm comprised of public adjusters and roofing consultants, and was handled by a public adjuster with said firm (it should be noted that public adjusters are typically paid a percentage of the amount awarded by the carrier). The report (dated April 30, 2012) made the following claims:

- "Lot [*sic*] of the granules has been displaced, leaving the unprotected membrane and fibers."

- "The hail has impacted the roof membrane, separating the bitumen between the plies of felt, which, in turn, will allow for water intrusion… This is sometimes known as bruising…"

- "The modified built-up roof should be removed down to the decking and a new comparable roofs [sic] system installed."

On May 16, 2012, this author conducted a site inspection of the roofing systems at the subject location, which presented in varying conditions consistent with their respective ages. The 24-year-old roof, for example, had extensive granule loss, wrinkles in the membrane running perpendicular to the length of the plies, and repairs of varying styles throughout (some bituminous, some elastomeric, and additional layers of roofing). Spatter marks and condenser coil fin deformation on rooftop-mounted air conditioning equipment indicated that the largest hailstones in this location were approximately ¾ inches in diameter.

Spatter marks are most commonly created when hailstones impact surfaces with oxidized paint; the impact removes the oxidized paint, exposing the underlying darker paint. Measuring these marks provides insight into the size of hail experienced. The condenser coils of rooftop-mounted air conditioning units are covered with vertically aligned aluminum fins, which are relatively easy to deform, and are therefore readily affected by hail. Examination and measurements of the fin deformation also provide insight into the size of hail experienced. This data — combined with experience at locations where hail size was documented (typically via cell phone photos and video) and compared to spatter and fin deformation observed — allows an investigator to determine the size of hail experienced in an area.

A report was submitted by this author on May 22, 2012, offering the following:

- The maximum size of hail experienced at the subject location was approximately 1 inch in diameter.
  - Photographs of the observed spatter were provided in support of this statement. **Figure 2** presents a photograph of one of the largest spatter marks observed at this location.

- The widespread granule loss on the roofing systems was not a result of the subject storm.
  - Historical aerial images provided by Google Earth were presented, demonstrating similar amounts of granule loss before and after the storm.

- Areas of missing granules were not consistent with hailstone impacts.
  - References to simulated hailstone impact testing were provided in support of this conclusion.

- No bruising was observed or tactilely experienced.
  - Bruising has historically been defined as the fracture of the fibers within the mat of the roof

(Greenfeld 1969, Marshall 2006), and is considered the benchmark for functional damage.

- The roof had several patched areas of various ages. Most of the patchwork was inappropriately applied and would likely only have mitigated leaks — not stopped them.

- There were several "soft spots" in which the roof would sag noticeably when walked on, consistent with long-term water intrusion.

- The ultimate conclusion provided was that the roof did not sustain any functional damage as a result of hailstone impacts.

After this report was issued, several other reports were offered in support of the claim of hailstone impact damage to the roofing systems. The first of the additional reports was submitted by a licensed engineer, also from out-of-state, dated Oct. 14, 2012. Within his report, the engineer made the following claims:

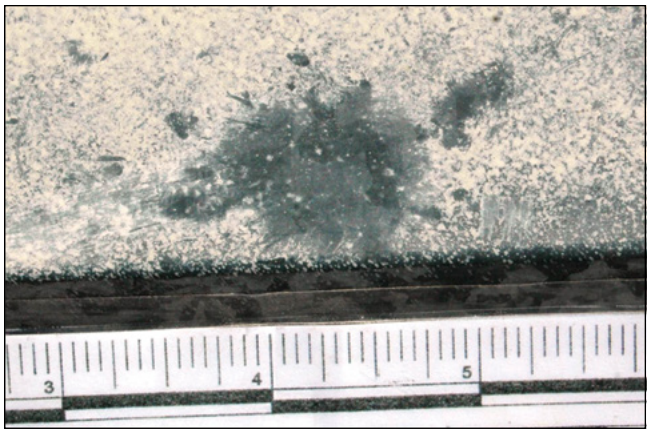

Figure 2
Spatter mark from hailstone impact (ruler demarcated in inches).

- "The velocity and size of the hail (½ to 1½ inches)…"

- "The size of hail impacts ranged from ½ inch to 1¾ inch."

- "According to the National Climate Data Center [*sic*], up to 2½-inch-sized hail was reported at the Scottsdale Airport, approximately 15.9 miles from the site."

- "Evidence shows penetration and/or damage to the membrane representative of these roofs. The roofs were functioning as intended prior to the storm damage. This damage creates water intrusion pathways through the top sheet."

Another report (dated Oct. 14, 2012) was submitted by an out-of-state civil and structural engineering firm. This report was sealed and submitted on two separate dates (12/3/12 and 12/10/12), offering the conclusion, "It is my professional opinion that the integrity of the bituminous membrane was compromised by the impact caused with what is consistent with hail." In this report, no determination was made with respect to the size of hail experienced other than it was consistent with what was reported during the storm.

A fourth report was submitted by an out-of-state architect (dated Oct. 17, 2012), who offered, "In my professional opinion, the roof … was damaged by hail. Impressions made to the roofing membrane are consistent with that of hail."

The basis provided in all four of the reports was photographs of areas of granule loss and statements that the authors had investigated hail damaged roofing systems in the past. Given that no scientific basis had been provided to support claims of hail damage, a request was made to collect roof samples from three of the roofing systems, have them desaturated, and examine the fiberglass mat microscopically for fractured fibers (i.e., bruising). The sample collection locations were determined by the parties alleging hail damage and were sent to a third-party laboratory for desaturation and examination.

Laboratory results revealed "no noted damage" to two of the samples. In the third sample, the laboratory noted a "soft spot in the glass where the binder used in the fabrication of the glass mat is missing; the glass fibers are continuous across this area." A second report was issued by this author on March 15, 2013, explaining the lab results, providing their correlation to previously cited testing, and reaffirming the original opinions offered.

Between March and December 2013, the original public adjuster unexpectedly died. In December, an appraiser (hired by the insured) submitted the previously mentioned reports, all alleging hail damage to the roofing systems. He also proposed that the roofs suffered from wind damage (an entirely new claim) in the form of ply separation from uplift forces. Seams were identified throughout the roof, with a focus on wrinkles in the

membrane as physical evidence of wind damage. Interestingly, the appraiser regularly worked as a public adjuster. After he was brought in, the amount of damages claimed nearly doubled, the type of claim changed, and he was the only person offering technical support of the alleged wind damage.

In lieu of this new assertion, another site inspection was conducted by this author to evaluate the roofing systems with regard to wind damage. In addition to the inspection, weather research was conducted to compare the subject storm with historical data. Finally, tenant interviews were performed to address claims that the roof had begun leaking only after the Oct. 5, 2010 event.

On Feb. 18, 2014, a third report was submitted by this author, addressing the recently introduced claim of wind damage. This report presented the following pertinent information:

- Several openings in the roof system were identified, none of which were related to wind damage:
  - Leak locations typically involved poor or missing flashing along parapets, around AC equipment and roof drains, as well as unsealed fastener penetrations.
  - The overwhelming majority of leaks identified from the interior of the building were identified near AC penetrations — associated with poor flashing.

- Tenant interviews (with tenants occupying suites before and after the subject storm event) confirmed that the roof had been leaking for more than 10 years "with any measurable amount of rain." Tenants also stated that the building maintenance person would periodically replace ceiling tiles but not fix the leaks.

- Historical weather data showed that the winds experienced during the Oct. 5, 2010 storms were consistent with those experienced in the area on a regular basis. Between the time of construction and the date of loss, 20 separate events were identified where equal or higher wind speeds were experienced.

- Ultimately, no wind damage was identified on the roofing systems.

- The wrinkles in the roofing system were related to expansion and contraction of the underlying roof structure. While the structure can expand and contract with temperature fluctuations, the roofing will not contract once stretched. Therefore, when the structure contracts, the roofing wrinkles to accommodate the change. These wrinkles were observed at 8 feet on center and corresponded with purlin locations.

- Several references were provided in support of these opinions (Roofing Industry Committee on Weather Issues 2007, Giffin 2009). In addition to these references, photographs of wind damage from previous investigations were provided as well as historical aerial images obtained through Google Earth, showing that conditions claimed as wind damage on the roof existed before the subject storm event.

The property did experience hail damage to the condenser coils of rooftop-mounted air conditioning units (fin deformation). Therefore, storm damage was identified and a monetary value assigned, allowing the insured to invoke the appraisal clause.

As part of his appraisal presentation (submitted on June 6, 2014), the appraiser for the insured authored a report that focused on wind damage, and did not identify any hail damage. The physical evidence of wind damage identified in the report included wrinkles in the system, which he argued were the result of wind uplift forces that created openings for roof leaks. In support of his argument, he provided invoices for building maintenance, documenting the purchase of replacement ceiling tiles, a letter from the property maintenance company stating that the roof had only started leaking after the storm, and information obtained from tenant interviews stating that the roof had only started leaking after the storm. He also provided two documents from the Proceedings of the Fourth International Symposium on Roofing Technology. The following noteworthy observations were made with respect to this report and supporting documentation:

- Maintenance records showed the purchase of 27 ceiling tiles four months prior to the subject storm and $2,000 of roof repair/ceiling tile replacement two months before the subject storm. No invoices were provided for roofing repairs after the storm.
  - The statement from the management company that the roof did not leak prior to the storm directly contradicts the invoices provided.

- The references provided from the symposium contained photographs and statements regarding wind damage that contradicted the photographs and statements in the report.

An example of wind damage, as identified by the public adjuster, is shown in **Figure 3**.

Figure 3
Area identified as wind damaged.

The appraisal hearing (conducted on June 18, 2014) was attended by both appraisers, the umpire, this author, a roofer hired by the public adjuster/appraiser for the insured, and a roofer hired by the carrier. Initially, all parties walked the roofs of the buildings, explaining their positions and identifying supporting physical evidence. At the onset of this portion of the process, the public adjuster stated that the roofs had not sustained hail damage; therefore, there was no reason to address the hail damage portion of the claim. However, he remained adamant that the roof had sustained wind damage, which had caused several roof leaks. Because areas similar to that shown in **Figure 2** were claimed to be wind damage — and therefore paths of intrusion — it was proposed that the roof be cut open in these areas to determine if this was the case. While the public adjuster was adverse to this, the umpire decided it should be done. Several areas were cut open (chosen at random by the public adjuster), and all demonstrated adhesion between plies with no evidence of leaks.

Upon completion of the physical examination of the roofs, attempts were made to interview tenants to address discrepancies between the provided statements. Only one tenant was available who had been in the buildings prior to the storm. This tenant refused to speak with anyone, reportedly because she was upset that previous statements she had made were misrepresented. At that point, the proceedings moved to a conference room nearby where the matter was discussed, and references were reviewed. During this discussion, the umpire stated that he had been presented with no physical evidence that the building had sustained wind or hail damage. During this hearing, maintenance records were reviewed with the umpire that established the roofs had a significant number of leaks prior to the subject event — and that the property management company (both in writing and at the hearing) had misrepresented this information.

After the umpire reviewed the facts of the case (spending well over 100 hours), he decided that the roofing systems were damaged by the identified storm and that they therefore needed to be replaced by the carrier. He stated in writing that he was presented with no physical evidence of storm damage or storm-generated openings. However, because tenants had stated that the roof leaked more after the storm than it did prior (more than three year's difference in time), the systems must have been damaged by the storm.

Case Study #2 – Five Building Hotel Complex

This claim involved a relatively large hotel complex in Tucson, AZ. The property contained four two-story buildings with BUR systems covered with gravel ballasting. However, in some areas, the gravel was displaced/removed, and the roofing was covered with granulated cap sheets (of varying color) or an elastomeric coating. The roof over the office and banquet hall was covered with built-up roofing with an elastomeric coating (the cap sheet did not appear to originally contain roofing granules). Finally, there was a detached restaurant associated with the hotel with a steep pitched roof covered with metal tiles and a low pitch roof covered with built-up roofing with an elastomeric coating. **Figure 4** provides an overview of the complex taken from Google Maps.

When the matter was initially presented, a report had been issued by an out-of-state engineering firm with four authors — a certified environmental inspector, two professional engineers, and an engineer in training. This report contained the following opinions:

- "The granulated modified bitumen roof covering would require 1¼ inches or larger size hard density hailstones with a perpendicular impact velocity of 55 to 75 mph to produce impact energy large enough to puncture or tear the exposed surface of the membrane."

Figure 4
Image of roof from Nov. 20, 2009.

- According to the National Climatic Data Center (NCDC), the area had experienced hail up to 1 inch in diameter on Sept. 10, 2011, July 15, 2012, and Aug. 21, 2012. (Reported date of loss was July 7, 2011.)

- Any roof areas without ballast were damaged by hail.

- A section of the roof over the office area had been displaced due to wind forces.

The report did not contain any historical weather data or analysis other than mentioning the three dates where 1-inch hail was experienced in the city. There were no photographs of hail spatter indicating the size experienced, and none of the photographs of the roof demonstrated hail damage. Instead, photographs provided large overviews depicting severe deterioration and splitting of the membrane, and highlighted two large dents in a rooftop appurtenance. There was a photograph showing the roofing pulled up from a corner and folded on itself over the office area.

The insured in this matter was represented by a public adjuster. In support of allegations that the failing condition of the roof was a recent occurrence — and due to storm damage — the public adjuster also submitted a letter from an in-state architect dated Aug. 6, 2012. The letter discussed a building review performed for the owner 60 days prior, stating: "As part of our general review, we performed a visual inspection of the roofs. We found the roofs to be well maintained with no visible damage."

After review of these documents, the property was researched. Information provided through the county assessor revealed the buildings were originally constructed 44 years prior. Historical aerial images obtained from Google Earth showed the roofs in a deteriorated condition in 2009 — two and a half years prior to the reported date-of-loss. **Figure 4** provides a portion of this image. The date has been magnified in **Figure 4**. The darker areas of the roof are locations where the ballast material is displaced or removed, and the underlying roofing is exposed.

A site inspection revealed roofing systems that were severely aged and littered with patchwork, ranging from added layers of roofing to large sections covered with an elastomeric coating. There were also numerous soft spots and one area experiencing structural failure. **Figure 5** presents a photograph showing the cracked and peeling nature of the roofing.

Areas similar to that shown in **Figure 5** were observed throughout the roofing systems over the two-story buildings. No areas of impact damage were observed on any of the roofs. Spatter marks observed throughout the property were consistent with only minor hail, approximately 0.25 inches in diameter. Additionally, conversations with onsite maintenance personnel during the inspection revealed that the roof had been leaking for years. This was consistent with observations of the interior spaces.

Figure 5
Split/failing section of roofing.

Regardless of this information, the public adjuster continued to pursue the claim, and several documents were produced by the opposing engineer, providing personal and technical criticisms. In lieu of this, a second report was authored on April 14, 2014, addressing the technical criticisms, providing photographs from other investigations where large hail was experienced and caused damage, and providing extensive weather data.

The uplifted section of roofing in this matter was clearly from wind, and payment for repair was provided by the carrier. The public adjuster did not claim that any other portions of the property were damaged by wind.

The umpire selected for the appraisal process was a local attorney. A site inspection was conducted as part of the appraisal hearing; however, experts were not asked to attend. At the conclusion of the hearing, the umpire did not make a ruling, but wanted additional time to review all of the information. On May 12, 2014, the umpire submitted the following in a letter addressed to both appraisers:

> *We met at the property and looked at portions of the roof. We then conferred at my office and could not reach an agreement… I have reviewed again all of the reports including all the photographs. I have thought it out, and my conclusion is that based on the preponderance of the evidence there was no hail damage…*

Conclusions

In both cases discussed, the claims were filed well over a year after the reported event, the claims alleged water intrusion resulting from the storm, and the buildings had roofing systems that were poorly maintained, worn, had leaked for years, and were in need of replacement.

Case Study #1 was unique in that the claimed source of damage changed from hail to wind over a year and a half after the claim was filed — and only after the hail damage claim was investigated and shown to be without merit. In addition, all technical arguments and claims made regarding the presence of wind damage were offered by the insured's appraiser, not a qualified expert. Finally, the umpire did not appear to have taken the physical evidence and established scientific literature into account when making his determination.

In Case Study #2, damages were alleged that were unsupported by any of the physical evidence or established scientific literature. However, in this matter, the umpire placed credence on the importance of scientifically backed expert opinions and the available physical evidence.

While laws exist that govern the admissibility of expert witness opinions in litigation matters, they are not applicable in appraisal forums. Comparing the two, the appraisal process is much less formal, allowing technical opinions to be offered by persons not established as experts, and there is no formal discovery process, which inhibits the ability to disprove junk science or the lack of science altogether. Two matters were presented where technical opinions contradicted the facts of the case (including onsite testing) as well as established scientific principles and data. However, both cases had entirely different outcomes, likely due to the abilities of the umpires selected, including the way in which they approached expert testimony and dispute resolution.

References

1. Fennig D. 2013. 2010-2012 United States hail loss claims and questionable claims (public). Des Plaines IL: National Insurance Crime Bureau; [accessed March 21, 2014]. https://www.nicb.org/File%20Library/Public%20Affairs/2010-2012-US-Hail-Loss-Claims-and-QCs---Public.pdf
2. Giffin CW. 2009. Evaluating storm damage to flat-roof assemblies. Dallas TX: Roof Consultants Institute; [accessed June 17, 2013]. http://www.rci-online.org/interface/2009CTS-Proceedings-giffin-brown.pdf
3. Greenfeld SH. 1969. Hail resistance of roofing products. Washington D.C.: National Bureau of Standards.
4. Marshall TP. 2006. Hail damage to built-up roofing. Paper presented at: 22nd Conference of the American Meteorological Society, Hyannis MA, October 6, 2004.
5. Roofing Industry Committee on Weather Issues. 2007. Hurricane Katrina investigation report. Powder Springs GA: Roofing Industry Committee on Weather Issues, Inc.
6. Roofing Industry Committee on Weather Issues. 2012. Hailstorm investigation Dallas/Fort Worth TX. Place of publication: Roofing Industrey Committee on Weather Issues, Inc.; [accessed December 27, 2012]. http://www.ricowi.com/docs/reports/RICOWI_DFW_Hail_Report.pdf

Development of a Computer Model to Predict Curling of Poured Concrete Slabs on Grade

By George A. Merlo, P.E. (NAFE 142S) and Anthony C. Merlo, P.E. (NAFE 636S)

Abstract

This paper addresses the causative factors associated with curling of concrete slabs poured on grade. The study was initiated when the owner of a newly constructed warehouse brought legal action against the designer/contractor for excessive concrete slab curling. Subsequent to settling with the owner, the designer/contractor brought legal action against the subcontractors who prepared the subgrade and placed the concrete. A computer model was developed by the defendant's expert to evaluate the effect selected parameters have on curling of the concrete slab on grade. The parametric study was used to evaluate the most probable causes of the curling, which led to settlement of the case.

Keywords

Forensic engineering, construction defect, curling of concrete slab on grade, foundation modulus, concrete shrinkage

Introduction

This case involves curling of a 7-inch unreinforced concrete slab on grade (SOG) at a newly constructed warehouse facility. Subsequent to settling with the owner of the warehouse for excessive slab curling, the designer/contractor proceeded to bring legal action against the subcontractors who prepared the subgrade and constructed the concrete slab.

The concrete subcontractor entered into a contract with the designer/contractor to form, place, and finish 388,000 square feet of 7-inch unreinforced SOG, excluding weather protection, concrete material, and concrete pumping. The designer/contractor was responsible for the concrete design mix and selection of the slab thickness and joint spacing. The slab covered an area 970 feet by 400 feet and was poured in sections as noted in **Figure 1A, 1B** and **1C**.

After placing the concrete slab, it was saw cut into 15-foot by 13-foot sections, providing control joints. Subsequent to the slab installation, the ends of the slab began to curl, resulting in voids between the subgrade and underside of the slab. Numerous elevation measurements were conducted with differential curling — ranging from approximately .25 inch up to 1 inch (see **Figure 2A** and **2B**). These differentials were detrimental to the equipment operating in the warehouse.

Factors Affecting Slab Curling

All SOG concrete slabs curl due to the inherent nature of concrete shrinkage during the curing process. It is noted that *"Evaporation of moisture from the upper surface of slabs is what causes drying shrinkage. Curling is caused by the difference in drying shrinkage between the top and bottom of the slab* [1,2,3]."

The primary factor associated with slab curling is the shrinkage gradient that develops through the slab thickness during the curing process. Placement of concrete on a dry subgrade provides two surfaces for excess water to be reduced, thus providing a lesser shrinkage gradient. Placement of concrete on a moist subgrade will increase the tendency of the slab to curl because the top surface will shrink more than the bottom, resulting in a slab with a concave shape. A similar condition will occur if the slab is poured on a vapor barrier.

Factors affecting shrinkage[1,2,3] are the water/cement ratio (higher water content results in greater shrinkage), temperature of concrete at discharge point, high concrete slump (higher slump indicates higher water content), excessive haul time in transit mixer, too long of a waiting period at the job site, too many revolutions at mixing speed, use of cement having relatively high shrinkage characteristics, use of aggregates with potential of high shrinkage, and use of additives that produce high

George A. Merlo, P.E., and Anthony C. Merlo, P.E., 88 Inverness Circle East, Bldg. C102, Englewood, CO 80112; (303) 721-0100; george@merlo4n6.com

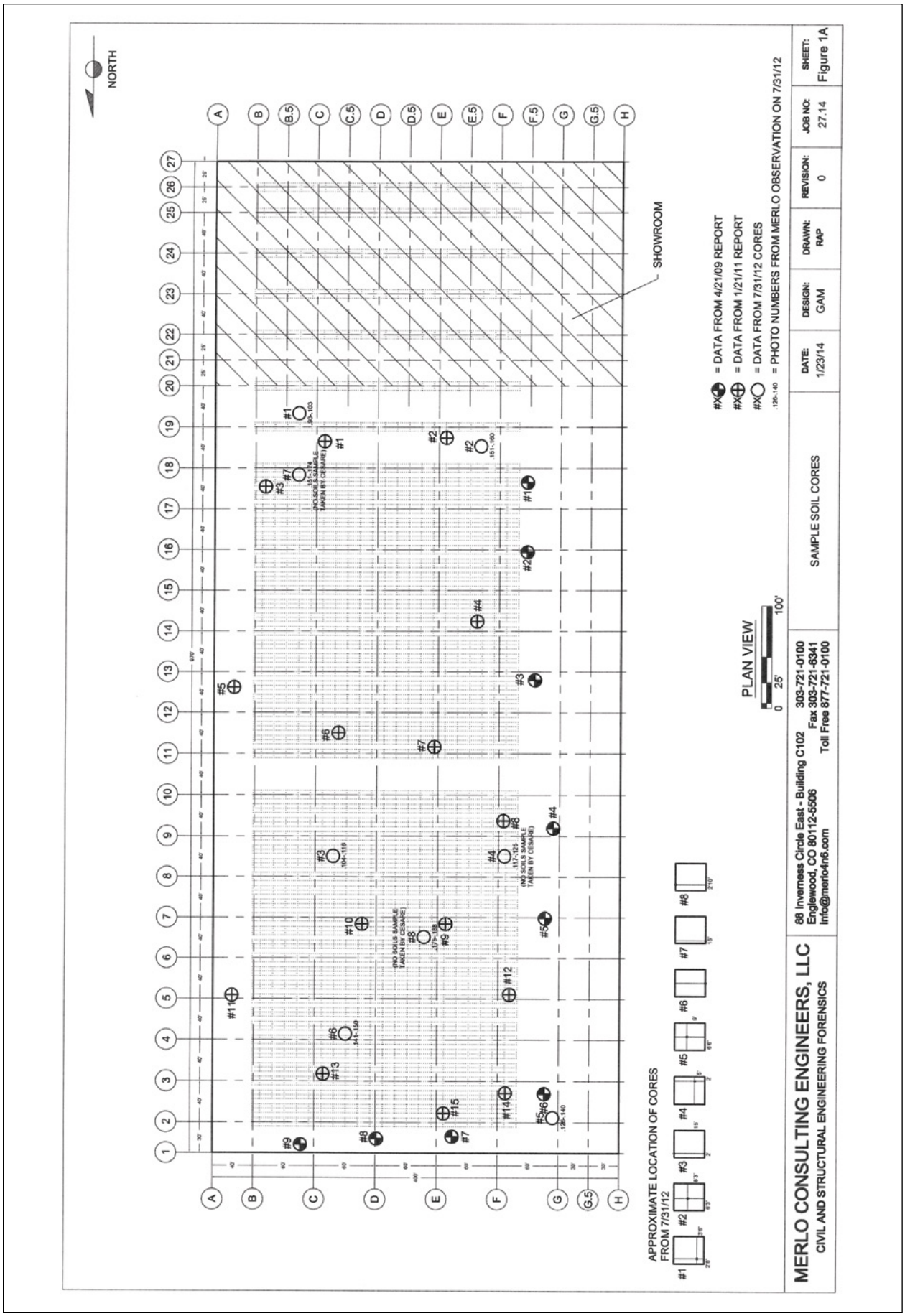

Figure 1A
Soil sample core locations.

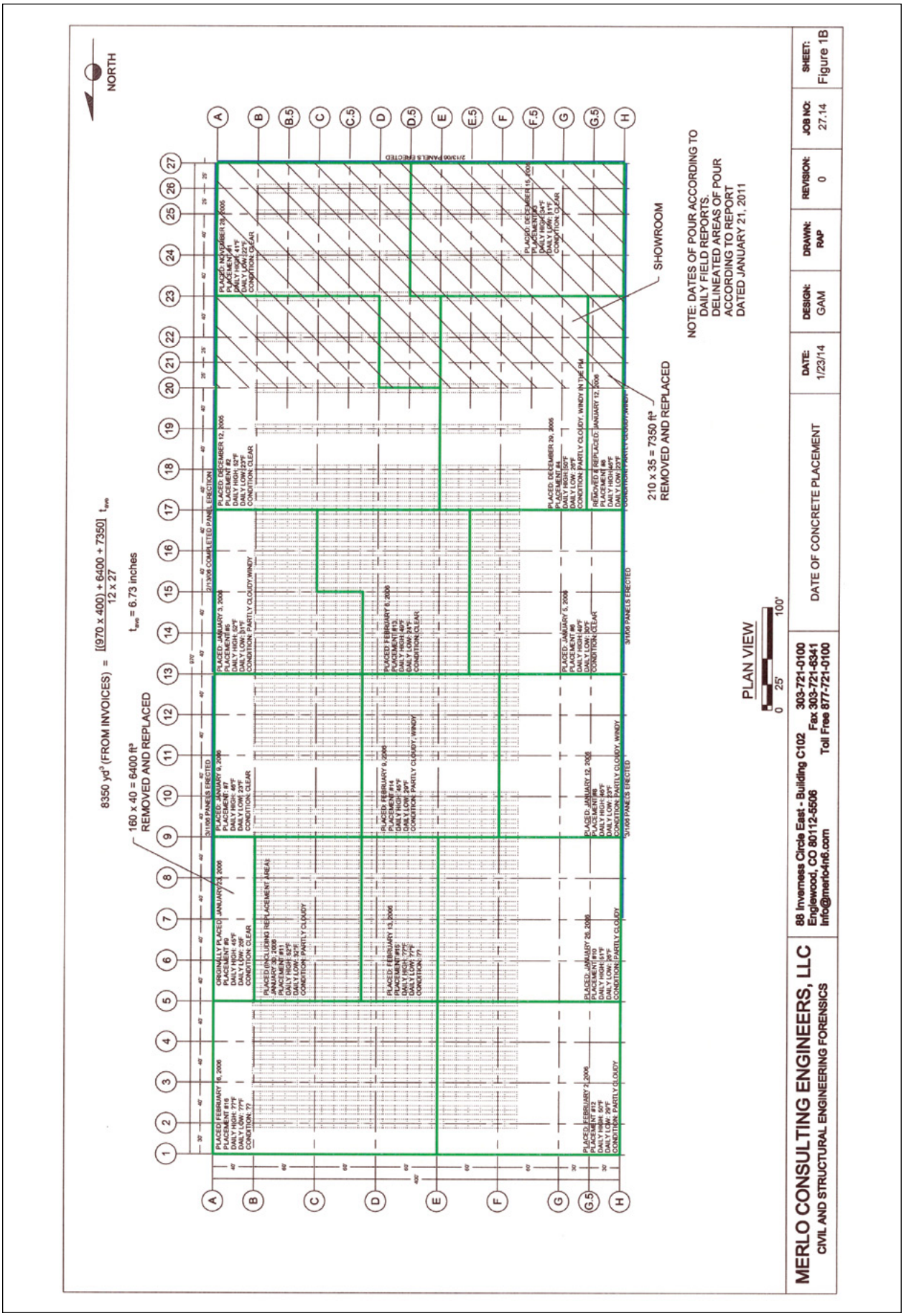

Figure 1B
Sequences of slab placement.

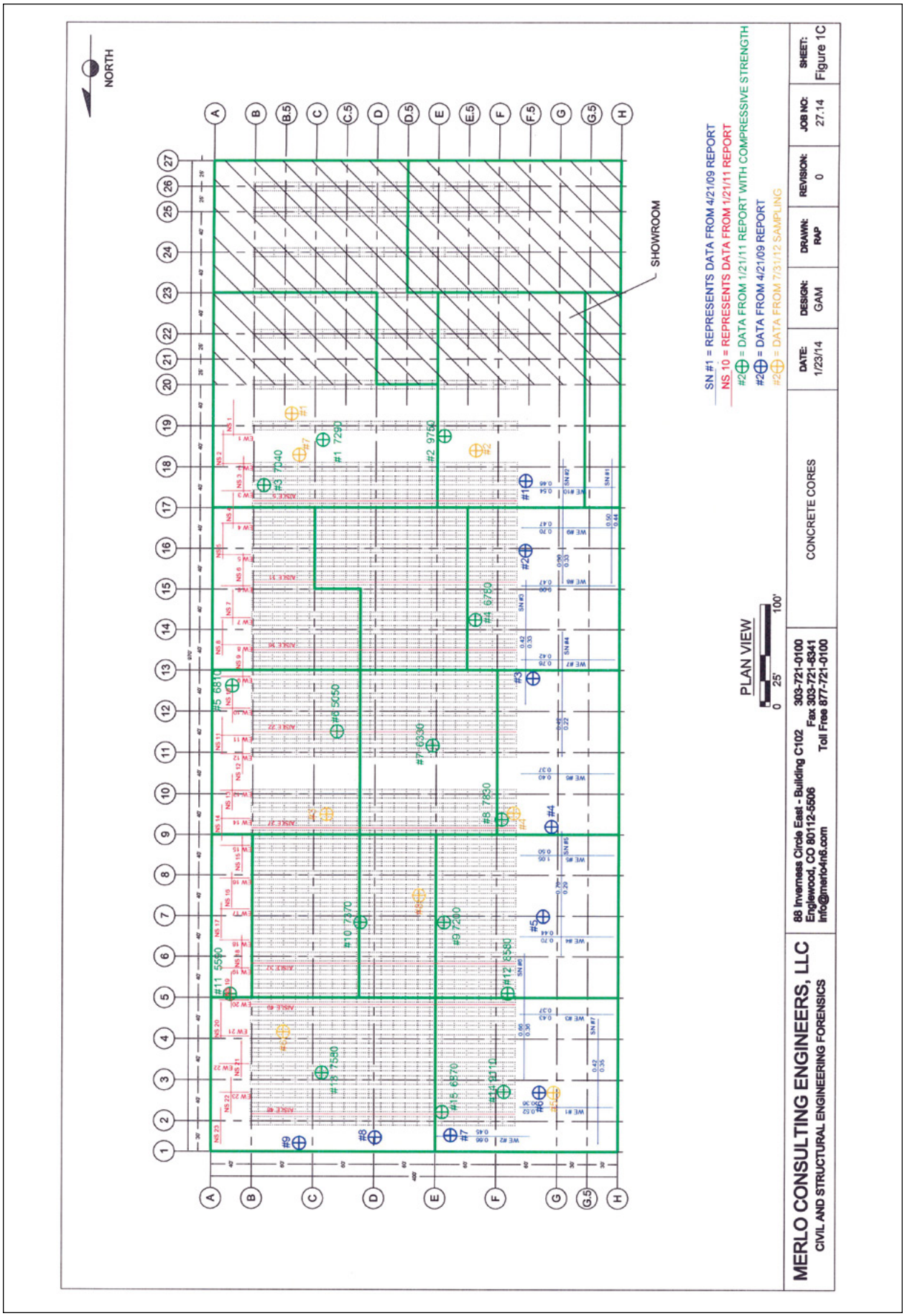

Figure 1C
Location of core samples.

Summary of Pour/Weather Data

Aisle Number	Location	Date Poured	Pour Area	Weather Data			Historical Data Period 7 Days after Pour					Elevation Differences		Estimated Concrete Shrinkage Gradient, in/in (subgrade 100pci)	
				High	Low	Condition	High	Low	High	Average	Gust	Max. Diff., inches	Average Diff., inches	Maximum	Average
5	B to E	12/12/05	#02	52 F	23 F	Clear	46 F	5 F	5 F	2 mph	11 mph	0.50	0.27	0.0007	0.00041
5	E to F.5	12/29/05	#04	50 F	26 F	Partly Cloudy, Windy in the pm	58 F	19 F	5 mph	2 mph	11 mph	0.30	0.27	0.00046	0.00041
11	A to C	1/3/06	#05	52 F	31 F	Partly Cloudy	63 F	21 F	16 mph	4 mph	27 mph	0.40	0.175	0.00058	0.00029
11	E5 to F.5	1/5/06	#06	49 F	30 F	Clear	49 F	20 F	23 mph	9 mph	37 mph	0.40	0.275	0.00058	0.00042
11	C to E.5	2/6/06	#13	49 F	24 F	Clear	60 F	22 F	25 mph	9 mph	36 mph	0.40	0.28	0.00058	0.00044
16	B to C.75	1/3/06	#05	52 F	31 F	Partly Cloudy,	63 F	21 F	16 mph	4 mph	27 mph	0.35	0.24	0.00052	0.00038
16	E.5 to F.5	1/5/06	#06	49 F	30 F	Clear	49 F	20 F	23 F	9 mph	37 mph	0.35	0.30	0.00052	0.00045
16	C.75 to E.5	2/6/06	#13	49 F	24 F	Clear	60 F	22 F	25 mph	9 mph	36 mph	0.35	0.25	0.00052	0.00039
22	B to C.75	1/9/06	#07	46 F	23 F	Clear	41 F	18 F	22 mph	10 mph	37 mph	0.40	0.36	0.00058	0.00053
22	F to F.5	1/12/06	#08	46 F	23 F	Partly Cloudy, Windy	39 F	27 F	11 mph	2 mph	18 mph	0.40	0.40	0.00058	0.00058
22	C.75 to F	2/9/06	#14	45 F	29 F	Partly Cloudy, Windy	58 F	21 F	8 mph	2 mph	14 mph	0.40	0.275	0.00058	0.00029
27	B to C.75	1/9/06	#07	46 F	23 F	Clear	41 F	18 F	22 mph	10 mph	37 mph	0.70	0.46	0.00094	0.00065
27	F to F.5	1/12/06	#08	46 F	23 F	Partly Cloudy, Windy	39 F	27 F	11 mph	2 mph	18 mph	0.40	0.40	0.00058	0.00058
27	C.75 to F	2/9/06	#14	45 F	29 F	Partly Cloudy, Windy	58 F	21 F	8 mph	2 mph	14 mph	0.50	0.37	0.0007	0.00054
37	E to F.5	1/26/06	#10	51 F	26 F	Partly Cloudy	53 F	24 F	19 mph	6 mph	41 mph	0.40	0.33	0.00058	0.00049
37	B to C.75	1/30/06	#11	52 F	32 F	Partly Cloudy	53 F	24 F	19 mph	6 mph	41 mph	0.70	0.36	0.00094	0.00053
37	C.75 to E	2/13/06	#15	?	?	?	?	?	?	?	?	0.40	0.24	0.00058	0.00038
40	E to F.5	2/2/06	#12	50 F	29 F	Partly Cloudy	58 F	15 F	7 mph	3 mph	16 mph	0.60	0.35	0.00083	0.00051
40	B to E	2/16/06	#16	?	?	?	?	?	?	?	?	0.30	0.25	0.00046	0.00039
48	E to F.5	2/2/06	#12	50 F	29 F	Partly Cloudy	58 F	15 F	7 mph	3 mph	16 mph	0.25	0.25	0.00039	0.00039
48	B to E	2/16/06	#16	?	?	?	?	?	?	?	?	0.60	0.34	0.00083	0.0005

Figure 2A
Weather conditions during slab placement.

Summary of Pour/Weather Data

Sample #	Location	Date Poured	Pour Area	Weather Data			Historical Data Period 7 Days after Pour					Elevation Difference		Estimated Concrete Shrinkage Gradient, in/in (subgrade 100pci)	
				High	Low	Condition	High	Low	High	Average	Gust	Maximum Difference,in.	Average Difference,in.	Maximum	Average
sn1	15 to 17 & G.5	1/5/06	#06	49 F	30 F	Clear	49 F	20 F	23 mph	9 mph	37 mph	0.50	0.44	0.00068	0.00061
sn1	17 to 17.5 & G.5	1/12/06	#08	46 F	23 F	Partly Cloudy Windy	39 F	27 F	11 mph	2 mph	18 mph	0.46	0.45	0.00064	0.00062
sn2	17 to 17.5 & G	12/29/05	#04	50 F	26F	Partly Cloudy Windy	58 F	19 F	5 mph	2 mph	11 mph	0.22	0.19	0.00032	0.00029
sn2	15 to 17 & G	1/5/06	#06	49 F	30 F	Clear	49 F	20 F	23 mph	9 mph	37 mph	0.36	0.33	0.00052	0.0005
sn3	13 to 15 & F.5	1/5/06	#06	49 F	30 F	Clear	49 F	20 F	23 mph	9 mph	37 mph	0.32	0.28	0.00046	0.00042
sn3	12 to 13 & F.5	1/12/06	#08	46 F	23 F	Partly Cloudy Windy	39 F	27 F	11 mph	2 mph	18 mph	0.42	0.33	0.00058	0.00048
sn4	13 to 14 & G	1/5/06	#06	49 F	30 F	Clear	49 F	20 F	23 mph	9 mph	37 mph				
sn4	11 to 13 & G	1/12/06	#08	46 F	23 F	Partly Cloudy Windy	39 F	27 F	11 mph	2 mph	18 mph	0.42	0.22	0.00058	0.00034
sn5	6 to 9 & G.5	1/26/06	#10	51 F	26 F	Partly Cloudy	53 F	24 F	19 mph	6 mph	41 mph	0.70	0.29	0.00092	0.00043
sn6	5 to 6 & F.5	1/26/06	#10	51 F	26 F	Partly Cloudy	53 F	24 F	19 mph	6 mph	41 mph				
sn6	3 to 5 & F.5	2/2/06	#12	50 F	29 F	Partly Cloudy	60 F	22 F	25 mph	9 mph	36 mph	0.66	0.36	0.00086	0.00052
sn7	1.5 to 4.5 & G.5	2/2/06	#12	50 F	29 F	Partly Cloudy	60 F	22 F	25 mph	9 mph	36 mph	0.42	0.35	0.00058	0.0005
we1	2/3 & F.5 to H	2/2/06	#12	50 F	29 F	Partly Cloudy	60 F	22 F	25 mph	9 mph	36 mph	0.52	0.36	0.0007	0.00052
we2	1/2 & E to F.5	2/2/06	#12	50 F	29 F	Partly Cloudy	60 F	22 F	25 mph	9 mph	36 mph	0.66	0.45	0.00086	0.00062
we3	4/5 & F.5 to H	2/2/06	#12	50 F	29 F	Partly Cloudy	60 F	22 F	25 mph	9 mph	36 mph	0.43	0.37	0.0006	0.00053
we4	6/7 & F.5 to H	1/26/06	#10	51 F	26 F	Partly Cloudy	53 F	24 F	19 mph	6 mph	41 mph	0.70	0.44	0.00092	0.00061
we5	8/9 & F.5 to H	1/26/06	#10	51 F	26 F	Partly Cloudy	53 F	24 F	19 mph	6 mph	41 mph	1.05	0.50	0.0013	0.00068
we6	11/12 & F.5 to H	1/12/06	#08	46 F	23 F	Partly Cloudy Windy	39 F	27 F	11 mph	2 mph	18 mph	0.40	0.37	0.00056	0.00053
we7	13/14 & F.5 to H	1/5/06	#06	49 F	30 F	Clear	49 F	20 F	23 mph	9 mph	37 mph	0.76	0.42	0.00097	0.00058
we8	15 & F.5 to H	1/5/06	#06	49 F	30 F	Clear	49 F	20 F	23 mph	9 mph	37 mph	0.90	0.47	0.0012	0.00065
we9	16/17 & F.5 to H	1/5/06	#06	49 F	30 F	Clear	49 F	20 F	23 mph	9 mph	37 mph	0.70	0.47	0.00092	0.00065
we10	17/18 & F.5 to G.5	12/29/05	#04	50 F	26F	Partly Cloudy Windy	58 F	19 F	5 mph	2 mph	11 mph	0.34	0.30	0.00048	0.00044
we10	17/18 & G.5 to H	1/12/06	#08	46 F	23 F	Partly Cloudy Windy	39 F	27 F	11 mph	2 mph	18 mph	0.54	0.46	0.00072	0.00064

Figure 2B
Weather conditions during slab placement.

shrinkage. None of these factors were under the control of the subcontractor responsible for forming, pouring, and finishing the slab. The designer/general contractor (plaintiff) was responsible for selecting the design mix, purchasing the concrete, and supervising the delivery and discharge of the concrete at the job site.

Counteracting the tendency for the edge of the slab to curl upward is the dead weight of the slab (slab thickness). Also affecting curling is the soil subgrade modulus *k* (coefficient of subgrade reaction), which can be defined as the ratio between the bearing pressure against the slab and deflection of the subgrade.

Typical units for *k* are pounds per cubic inch (pci) or psi per inch of deflection with values ranging on the order of 80 to 350 pci; the larger the *k* value, the stiffer the subgrade. Placement of a slab on a less-than-stiff subgrade will result in the curled slab "sinking" into the soil, reducing the net curling. On a stiffer subgrade, less area is required to support the dead weight of the slab, resulting in greater net curling.

Plaintiff Allegations

With the plaintiff being responsible for the factors adversely affecting concrete shrinkage, the allegations were directed at the subcontractors responsible for preparation of the subgrade and placing the concrete.

With respect to the concrete subcontractor, the allegation was directed at the slab thickness being less than specified. The allegation directed at the subcontractor responsible for the subgrade preparation and compaction was that the subgrade was prepared too stiff (450 pci vs. specified 150 pci). It should be noted that the project specifications did not require field testing of the subgrade, nor did they require measured finish slab elevations within 72 hours of completion of the pour.

Computer Model

In order to evaluate the effects slab thickness and subgrade modulus have on the net curling of the SOG, a computer model was developed using the commercially available finite element program STAAD.Pro (licensed by Bentley Architectural and Structural Software). This involved treating the SOG as a mat supported by springs representing the soil subgrade modulus. The springs were treated as compression springs — only with no resistance when subjected to uplift due to curling. The shrinkage gradient was represented by an equivalent temperature difference between the top and bottom of the slab.

In order to substantiate the validity of the model, it was first compared with the test results[4]. The test slab consisted of a 6-inch-thick concrete slab 24 feet by 13 feet with a modulus of elasticity of 3,000 ksi, subgrade modulus of 80 pci, and an equivalent shrinkage gradient of 30.5°F.

Results of the test indicated that the maximum curl at the edges was on the order of .10 inches above the original floor finish, with an unsupported length at the edge of 4 feet. Maximum deflection at the center of the slab was measured at -.02 inches. Results of the computer analysis indicated the maximum curl equaled .102 inches with an unsupported cantilever length of 4.25 feet and a maximum deflection in the middle of the slab equal to -.021 inches (see **Figure 3**). Therefore, it was concluded that the computer model was verified with the test results and could be used to analyze the SOG at the subject warehouse.

Effects of Slab Thickness and Soil Subgrade Modulus

The plaintiff alleged that the curling of the slab was the result of inadequate slab thickness and improper preparation of the subgrade. Specifications defined the slab thickness as being 7 inches founded on a subgrade modulus equal to 150 pci. The plaintiff concluded based on 31 core samples that the average slab thickness was 6.5 inches; this was less than the specified 7 inches (see **Figure 4**). Laboratory testing of the plaintiff's core samples resulted in a concrete modulus of elasticity equal to 5,000 ksi (see **Figure 5**), and the plaintiff's geotechnical expert concluded that the soil subgrade modulus equaled 450 pci.

A parametric analysis was conducted to evaluate the effects of varying the slab thickness and the soil subgrade modulus. With typical shrinkage strain for Portland cement of approximately .0004 to .0008 inches/inch, the finite element computer analysis was conducted to predict slab curling.

Using a shrinkage strain of .0006 inches/inch, and based on an evaluation of the elevation measurements (see **Figure 2A** and **2B**), the slab thickness and subgrade modulus were varied to evaluate the predicted curl. Results of the analysis, which are contained in **Figure 6A, 6B,** and **6C,** can be summarized as follows for a shrinkage strain of .0006 inches per inch (see **Figure 7**):

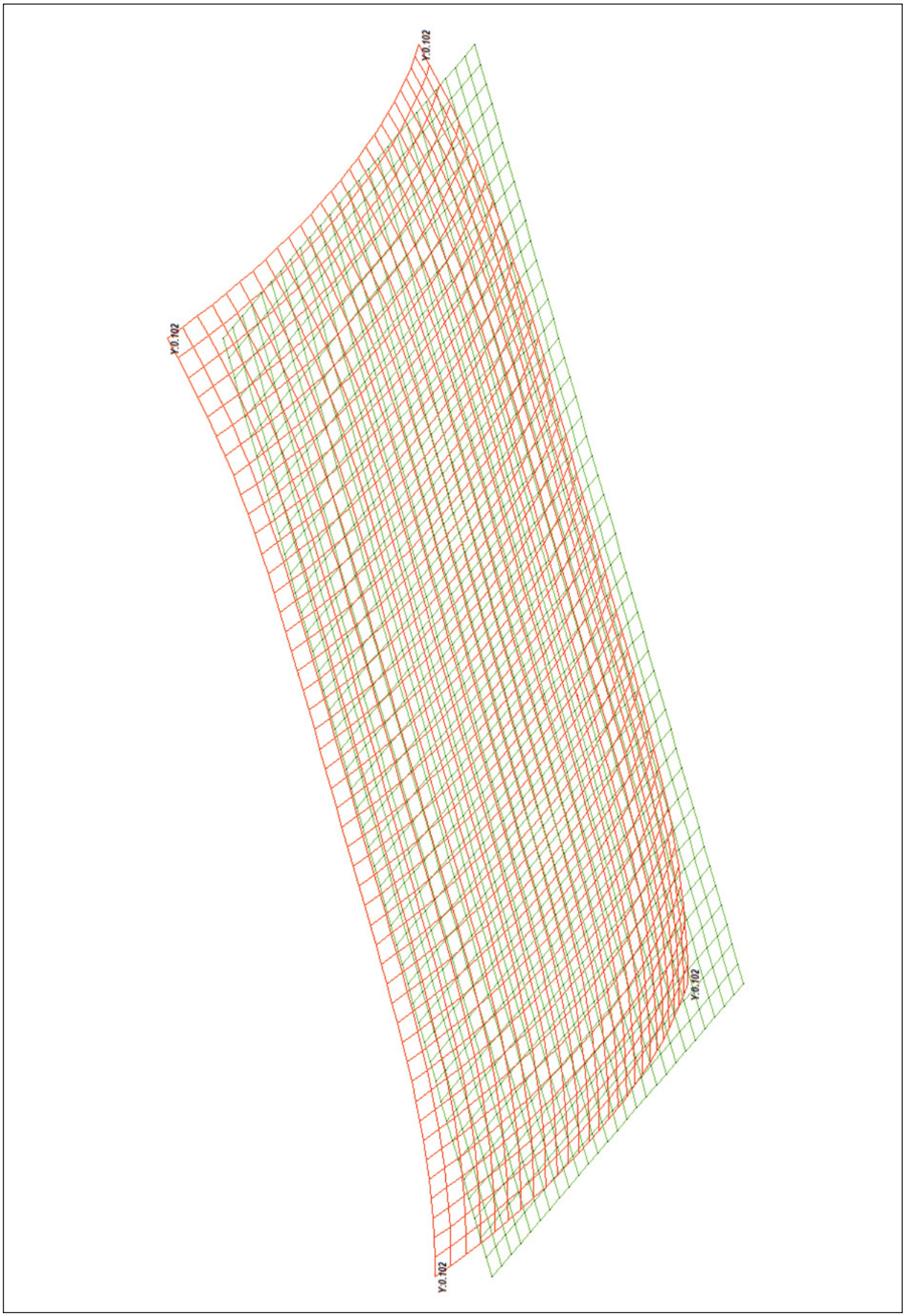

Figure 3
Computer model verification.

AVERAGE SLAB THICKNESS
MERLO CONSULTING ENGINEERS, LLC

File Name STAT1
File No.
Date August 1,2012

Jan. 21,2011 Data	1	5.125
Jan. 21,2011 Data	2	5.000
Jan. 21,2011 Data	3	5.875
Jan. 21,2011 Data	4	7.750
Jan. 21,2011 Data	5	8.500
Jan. 21,2011 Data	6	6.500
Jan. 21,2011 Data	7	7.000
Jan. 21,2011 Data	8	5.375
Jan. 21,2011 Data	9	7.000
Jan. 21,2011 Data	10	6.000
Jan. 21,2011 Data	11	6.500
Jan. 21,2011 Data	12	6.000
Jan. 21,2011 Data	13	6.000
Jan. 21,2011 Data	14	6.500
Jan. 21,2011 Data	15	6.750
April 21,2009 Data	1	7.000
April 21,2009 Data	2	7.000
April 21,2009 Data	3	7.000
April 21,2009 Data	4	7.000
April 21,2009 Data	5	5.000
April 21,2009 Data	7	6.500
April 21,2009 Data	8	6.000
April 21,2009 Data	9	6.500
July 31, 2012 Measurements	1	6.500
July 31, 2012 Measurements	2	7.000
July 31, 2012 Measurements	3	7.000
July 31, 2012 Measurements	4	6.375
July 31, 2012 Measurements	5	6.500
July 31, 2012 Measurements	6	6.625
July 31, 2012 Measurements	7	7.000
July 31, 2012 Measurements	8	6.625
	Average	**6.500**
	Standard Deviation	**0.75**

68% fall within 6.5+/- .75 inches

Figure 4
Measured slab thickness.

MERLO CONSULTING ENGINEERS LLC

File Name STAT

Title: Estimated Modulus of Elasticity

Date June 26,2012

Core Number	Compressive Strength,psi	Density,lbs/ft^3	Estimated Modulus Of Elasticity,psi
1	7290	150.7	5.21E+06
2	9750	148.6	5.90E+06
3	7040	148.4	5.01E+06
4	6780	146.2	4.80E+06
5	6810	146.2	4.81E+06
6	5050	147.9	4.22E+06
7	6330	147.4	4.70E+06
8	7830	146.7	5.19E+06
9	7200	148.4	5.06E+06
10	7370	149.0	5.15E+06
11	5590	148.5	4.46E+06
12	8580	150.9	5.67E+06
13	7580	147.5	5.15E+06
14	9110	150.5	5.82E+06
15	6870	146.1	4.83E+06
Average	**7279**	**148.2**	**5.07E+06**
Standard Deviation	**1224**	**1.60**	**5.E+05**

Figure 5
Core sample properties.

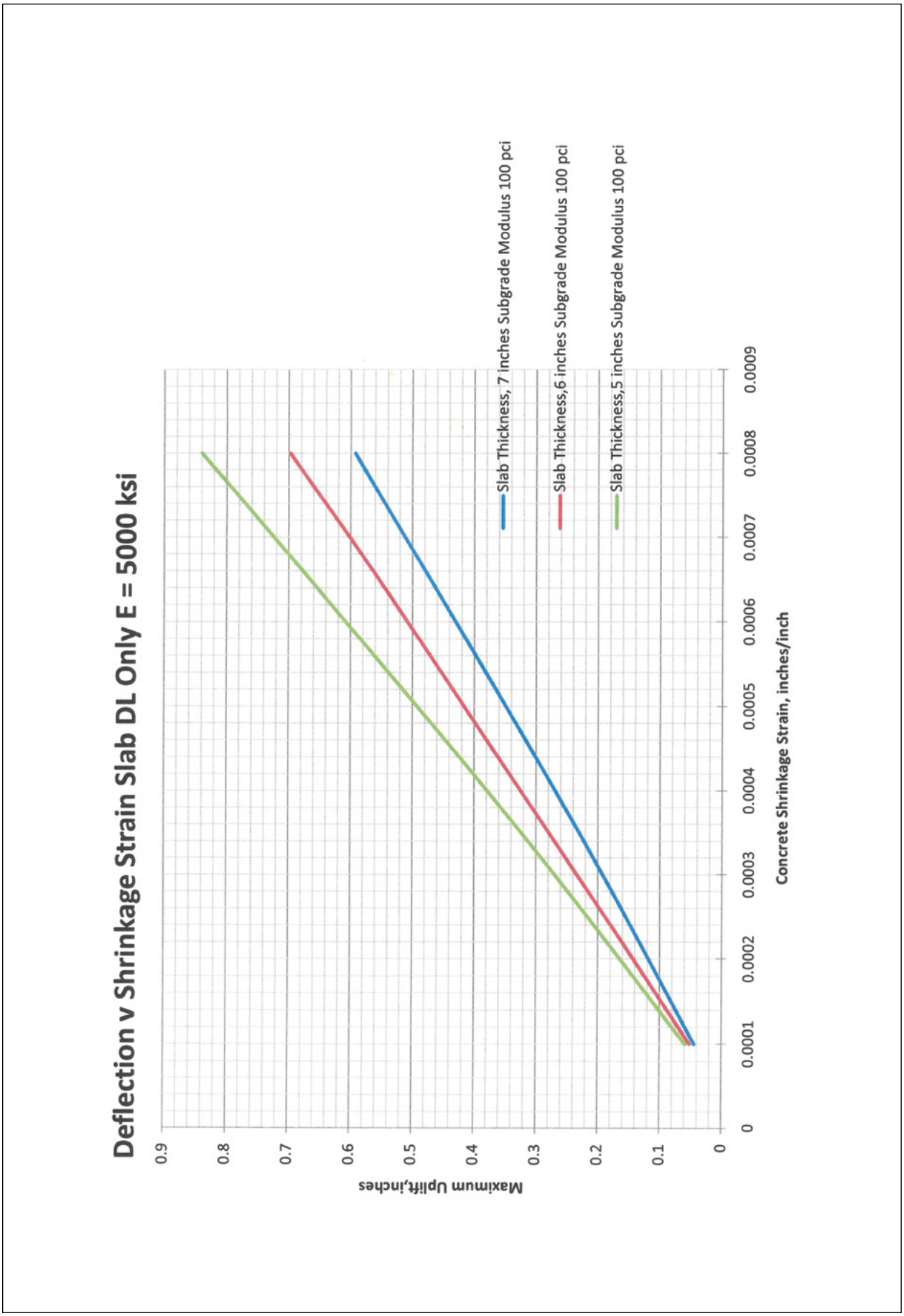

Figure 6A
Shrinkage strain vs. slab uplift for subgrade modulus 100 pci.

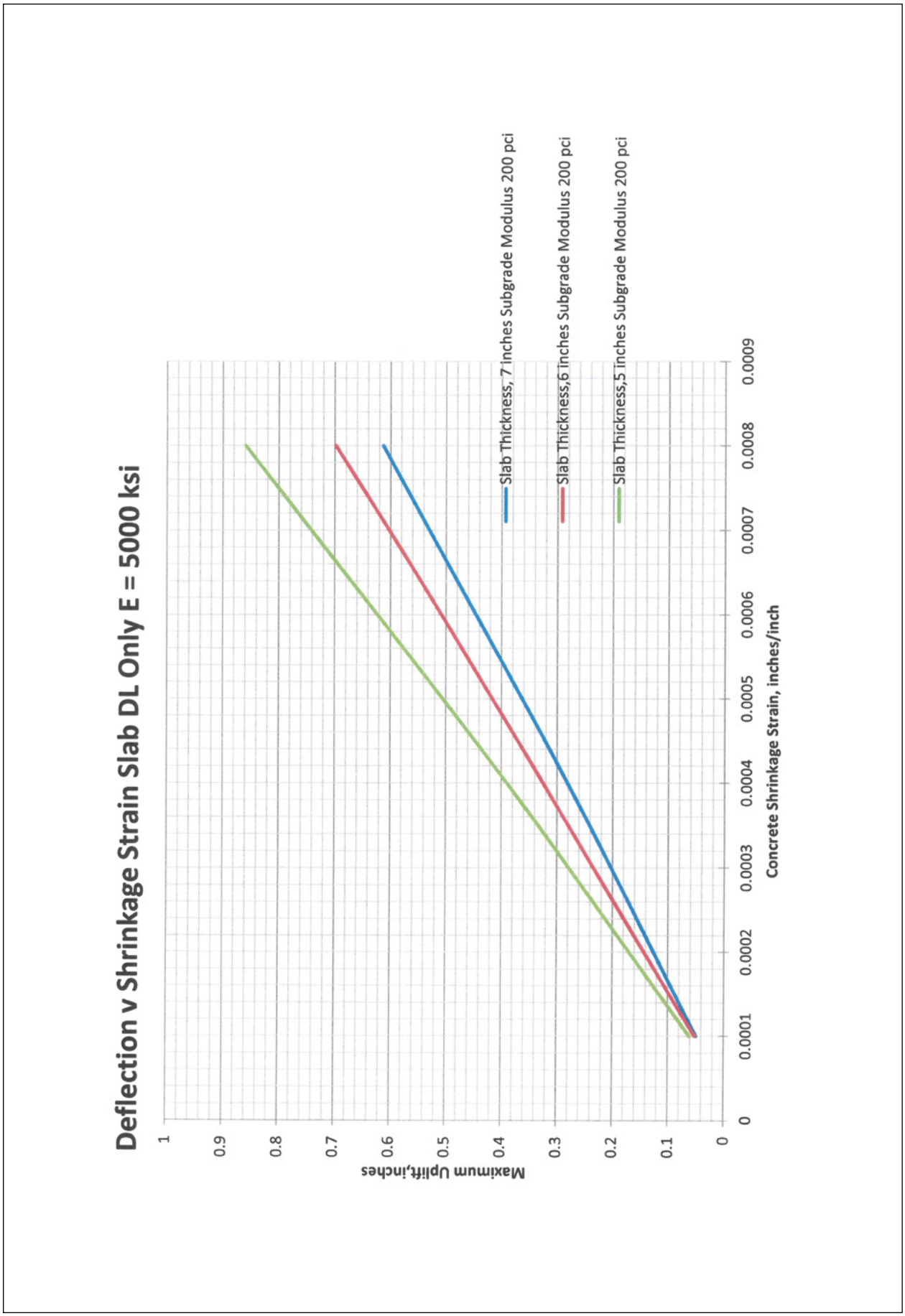

Figure 6B
Shrinkage strain vs. slab uplift for subgrade modulus 200 pci.

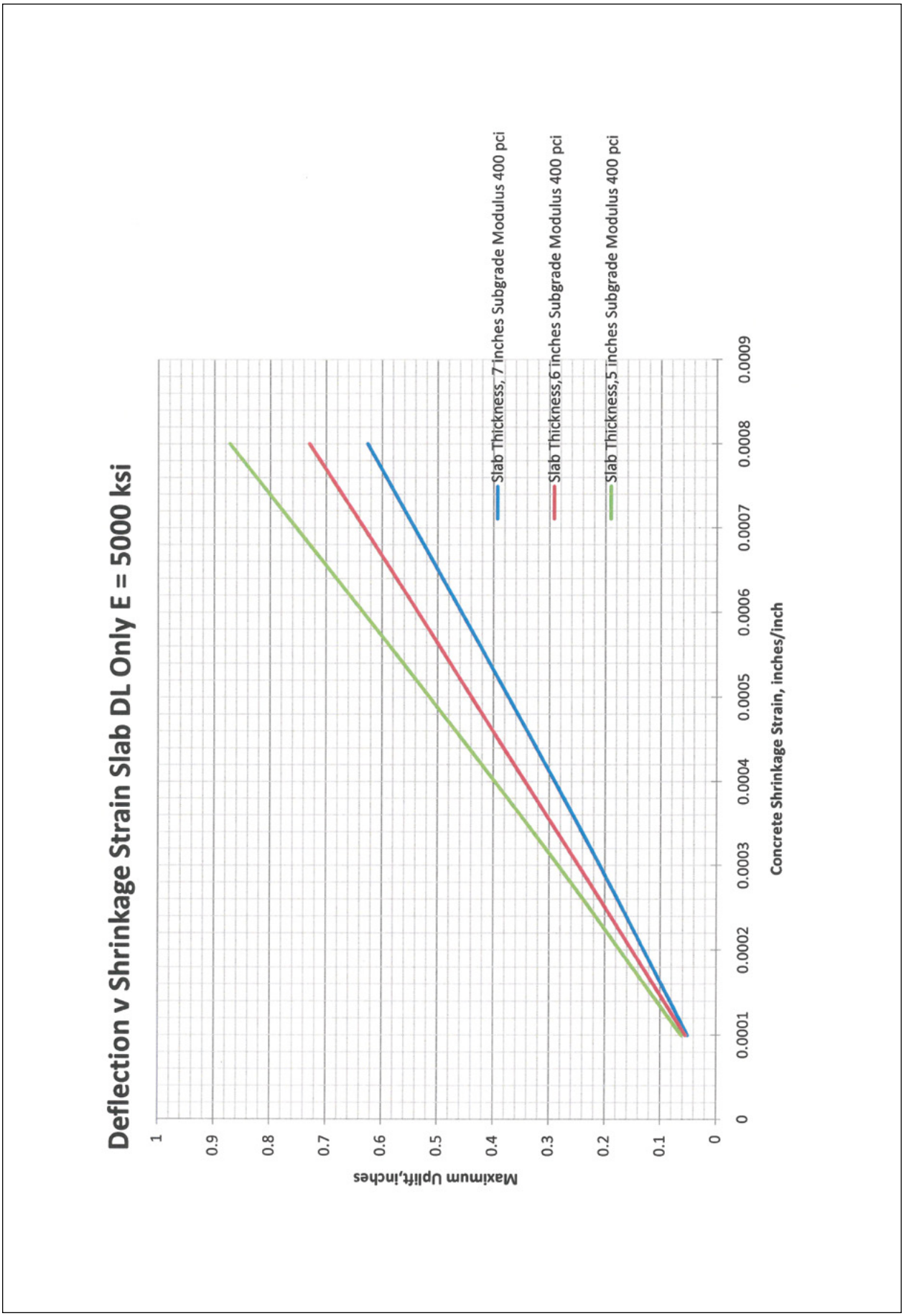

Figure 6C
Shrinkage strain vs. slab uplift for subgrade modulus 400 pci.

Subgrade Modulus, pci	Slab Thickness, inches	Maximum Curl, inches
100	7	.42
100	6	.51
100	5	.60
200	7	.44
200	6	.52
200	5	.62
400	7	.46
400	6	.54
400	5	.64

Figure 7
Shrinkage strain summarized.

As can be observed, the degree of curling is for all practical purposes independent of the subgrade modulus. However, the extent of the curling is to a minor degree dependent on the slab thickness. The plaintiff was asserting that the primary cause of the curling was attributable to the slab thickness measured as low as 5 inches in some locations (see **Figure 4**). The fallacy with this rationale is twofold.

First, the 5-inch cores do not represent the average thickness around the perimeter of the slab. It should be noted that the weight of the slab around the perimeter provides the dead weight, counteracting the effects of curl with lesser importance given to thicknesses toward the middle.

Secondly, no correlation exists between core thicknesses vs. slab curl based on the physical evidence. A comparison was made between core thicknesses and elevation differences. In several instances, areas with a 7-inch thickness exhibited greater than or equal curl as compared with areas of lesser thickness (see **Figure 1A, 1B,** and **1C**). For example, sample WE7 (with a 7-inch slab thickness) exhibited the same curl as sample WE4 with a thickness of 5 inches. The same can be stated with respect to aisle 27B to C.75 vs. aisle 27 C.75 to F.

It was the authors' opinion that the number of core samples taken were statistically inadequate to support the conclusion that slab thickness caused the curling. A review of the concrete delivery tickets indicated that a total of 8,350 cubic yards was delivered to the job site for the slab. It was calculated that the average thickness of the poured slab equaled 6.73 inches — approximately equal to the specified 7 inches.

With the slab thickness and subgrade modulus ruled out as causative factors, the cause of the slab curling remained unresolved. Clearly, the primary parameter affecting the degree of curling is the amount of shrinkage during the curing process. The subcontractor cured the concrete utilizing blankets furnished by the plaintiff. A comparison of the weather conditions vs. slab curl did not reveal any correlation (see **Figure 2A** and **2B**).

Only one factor remained as a possible consideration: the shrinkage characteristics of the mix itself. The designer/contractor should have conducted shrinkage tests of the design mix to ensure that the shrinkage was within allowable expectations. More important is the fact that the batch tickets contained evidence that calcium chloride was added to the approved mix at the request of the designer/contractor. With the slab being placed during periods of cold weather, calcium chloride was added to the mix to enhance curing and minimize freezing. The addition of the calcium chloride resulted in an increase in the heat of hydration and thus an increase in slab curling.

Conclusions

As a result of the authors' testing and analysis, the following opinions were presented:

1. Based on the range of parameters considered, neither slab thickness nor subgrade modulus were primary factors associated with the slab curling.

2. The primary cause of the curling can be attributed to one or both of the following: lack of proper evaluation of the design mix or the addition of calcium chloride to the design mix (both of which were under the control of the designer/contractor).

3. No allegations were made that the slab thickness and subgrade modulus adversely affected the structural integrity of the unreinforced slab. Repeated attempts requesting the design calculations (including the loads imparted by storage racks and warehouse equipment) proved unsuccessful.

References

1. Ytterberg R. Shrinkage and curling of slabs on grade part 1 – drying shrinkage. Farmington Hills MI: American Concrete Institute; April 1987.
2. Ytterberg R. Shrinkage and curling of slabs on grade part 2 – warping and curling. Farmington Hills MI: American Concrete Institute; April 1987.
3. Ytterberg R. Shrinkage and curling of slabs on grade part 3 – additional suggestions. Farmington Hills MI: American Concrete Institute; April 1987.
4. Leonards G, Harr M. Analysis of concrete slabs on ground. Soil Mechanics and Foundations Division Proceedings of the American Society of Civil Engineers. June 1959; Reston VA.

Forensic Engineering Analysis of Toilet Connector Failures in a Class-Action Lawsuit

By James William Jones, Ph.D., P.E. (NAFE 778F)

Abstract

A major manufacturer of water supply lines that connect flushable toilets to house water piping was the object of a class-action lawsuit. The author examined a large number of failed and exemplar connectors, complete fill lines, and similar injection-molded products as well as visited failure sites with the goal of ascertaining the root cause of the failures. Forensic work included strength tests and finite element analyses to determine the expected life of the nuts, including single overload failure strength and creep analysis to predict life. Tightening tests using random subjects were conducted. A statistical analysis of the failures was also performed. The products of competing manufacturers were evaluated for comparison of similar designs. After much investigation and analysis, it was concluded that the design of the connector was not defective and met relevant industry standards.

Keywords

Forensic, plastic connector, finite element, creep, class action, water leak, water damage

Introduction

The author was retained to investigate the cause of failure in acetal ballcock coupling nuts used to attach the water supply line to the tank of a standard home toilet tank. Failure of the supply line connector can result in considerable water damage to homes and offices. Several incidents cited in the lawsuit involved failure of the connector while the owner/occupant was away for several days. Damage caused by water leakage can run into the hundreds of thousands of dollars in extreme cases.

The ballcock coupling nut, hereinafter referred to as the "nut" for brevity, is a component of a supply line manufactured and sold in the United States. Work performed to prepare an expert report for this case included many different tests and analyses to determine the cause of failure and expected life of the nuts (if used properly). A list of tasks undertaken to resolve this matter is provided below. The action taken for each task is discussed in this paper.

To qualify for a class-action lawsuit, the class must consist of a group of individuals or business entities that have suffered a common injury or injuries. Class-action matters typically result from an action on the part of a business or a particular product defect/policy that applied to all class members in a typical manner. The plaintiff must show that there is an underlying root cause common to all of the failures. Thus, to defend a class-action, one legal strategy is to show that there is no common root cause of such failures. For example, if failures in Texas are caused by chemicals in the water that are only found in a particular location, then they may be excluded from the class. Alternatively, if it can be shown that failures are caused by damage resulting from abuse, then there is no demonstrable product defect. By showing that failures have multiple causes and are not related, the evidence would suggest no common root cause. Of course, any necessary warnings and instructions regarding installation and proper use/care must be considered and may influence the outcome of the cases. Further, the product design can be defended by showing that all relevant codes and standards are met, that the materials used are suitable for the application and of sufficient quality, and that the manufacturer of the parts meets or exceeds industry standards. Finally, the design can be compared to similar products and other competitive products in the marketplace and shown to be of equal or superior design and quality.

Scope of Work

The following tasks were performed in this matter.

- Inspection of sites where failures occurred.
- Examination and characterization of nuts from failure claims.
- Examination and characterization of nuts from different production sources of the manufacturer.

James William Jones, Ph.D., P.E., 5561 Ocean Terrace Drive, Huntington Beach, CA 92648; (714) 369-2703; bill@jwjce.com

- Examination and characterization of similar products and competitors.
- Sectioning of nuts from various sources to determine the details of thread geometry.
- Creating RTV silicone rubber molds of the internal features of the nuts and characterization of thread details. (RTV is the abbreviation for room temperate vulcanization, i.e., the rubber "cures" at room temperature. The two-part silicone rubber material can be easily cast into a void. It hardens quickly, has little shrinkage, and does not adhere to most surfaces.)
- Statistical analysis of failure data.
- Material characterization to determine strength and creep rate.
- Human factors testing to determine "hand tight" torque.
- Torque-to-failure tests for several different nut geometries.
- Torque vs. rotation angle tests.
- Finite element analyses to determine one-time overload failure.
- Finite element analyses, including creep and time-dependent effects to determine the expected life of nuts in service.

Failures Observed

Figure 1 shows several typical "failed" nuts that were provided to the author for evaluation. Failure typically occurs in the first thread of the injection-molded plastic coupling (nut).

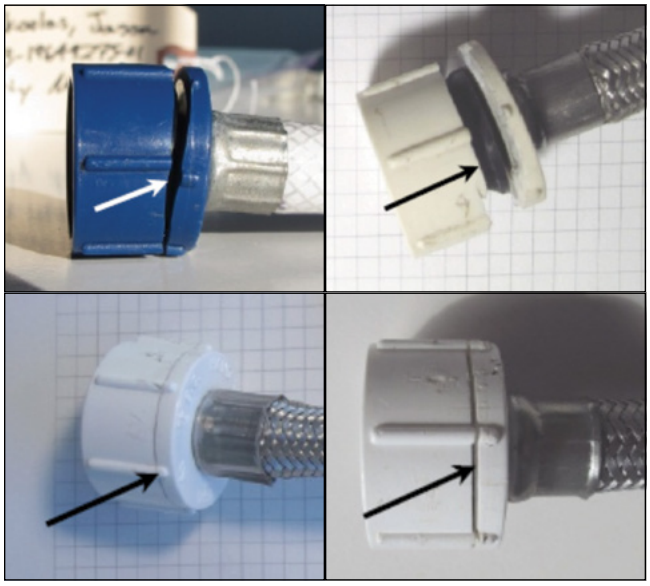

Figure 1
Failed coupling nuts.

Figure 2 is a photograph of a cross-sectioned nut showing the rubber cone washer and the end of the copper tube that form the water seal.

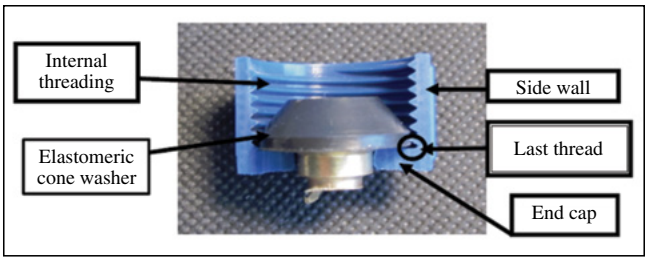

Figure 2
Cross-section of nut assembly.

Figure 3 is a photograph of a nut assembly that has been potted in a metallurgical laboratory, cut into halves, and polished. This nut fractured at the first thread.

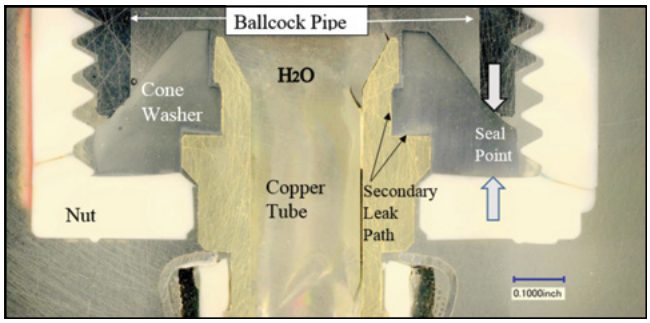

Figure 3
Cross-sectioned failed connector nut assembly.

How It Works

The connector nut is an injection-molded part that connects the supply line to the threaded ballcock pipe. The supply line terminates with a metal fitting that is swaged onto the supply line. The toilet nut has an internal thread to mate with the external ballcock pipe. A cone washer is stretched over the brass tube. This cone washer seals between the ballcock pipe and the nut by pinching the rubber cone washer.

If sufficient force is applied to this "seal point," then water will not leak through the connector. This force can easily be generated by hand tightening the nut. However, there is another possible leak path, as shown in **Figure 3** (denoted as a secondary leak path). If the cone washer inner diameter is not pressed against the brass fitting at the inside radius of the cone washer with sufficient force, water will leak through along this path. If water begins to leak at the inner radius of the cone washer, water can drip out through the annular space between the hole in the nut and the outside of the

brass fitting. Typical city water pressures range from a low of about 50 psi to over 100 psi. The cone washer is a rubber-like material (elastomer) with a Shore durometer hardness of approximately 70A. If water is leaking through the secondary leak path, then tightening the nut will not stop the leak.

Water-tight seals are typically provided in hydraulic equipment in two basic ways. The first is to apply sufficient force over a relatively small area such that the mating parts are tightly compressed together, removing all leakage paths. This is the mechanism employed at the ballcock. The second method is the "self-energizing" seal, such as an O-ring. This seal is affected by the pressure as it forces the sealing material against the sealing surface. The secondary leak path is sealed by the water pressure, forcing the rubber cone washer against the metal post. As previously mentioned, tightening the nut will not stop a leak along the secondary path.

What the Opposition Claimed

The counsel for the plaintiff claimed that the design of the nut was defective because the threads inside the nut formed a stress riser at the critical stress location, causing the nut to fracture when tightened. The sketch shown in **Figure 4** was produced by the plaintiff expert and was purported to accurately represent the nut design. Their expert cited plastic molding design guides that recommended against sharp corners and threads that end without tapering or rounding as design flaws.

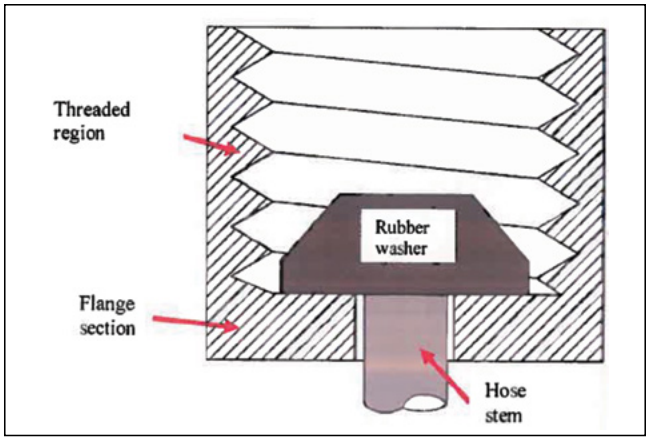

Figure 4
Schematic used by plaintiff to characterize nut.

The actual design, as shown in **Figure 5**, clearly incorporates local radii and a tapered or "feathered" thread termination. However, it is difficult to visualize internal threads even when a cross-section is used. A more visually effective technique was developed by using silicone RTV rubber to make a mold of the inside of the connector. As can be seen from **Figure 5**, the cast rubber replica provides a three-dimensional model of the thread profile. The RTV rubber castings provide a fast method of capturing and comparing thread profiles.

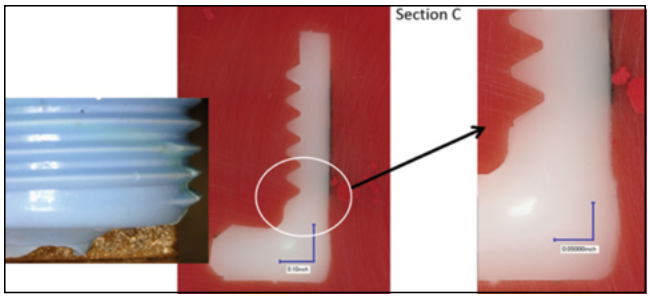

Figure 5
Cross-section of nut and RTV casting.

The plaintiff's accusation of "sharp corners" is clearly blunted by looking at the actual geometry. The next step in proving that there was not a design flaw is to show that the nut design (including the thread geometry) is capable of performing its intended service. The manufacturer testified that the design life of the connector is seven to 10 years (however, this information was not clearly conveyed to the customer). The nut is designed to seal with "hand tight only" torque. The "hand tight" instruction is imprinted on the nut during the injection molding process. The first question that comes to mind when attempting to analyze the loads on the nut is: "How tight is hand tight?"

Hand Tight Tests

A series of tests was conducted by an independent laboratory to attempt to ascertain the answer to this seemingly subjective question. The full extent and scope of the tests are too complex to describe in detail, and could probably serve as the basis of another paper. The tests used both registered plumbers and typical homeowners (picked at random) to tighten the nut. A complete bathroom environment was simulated, including toilet, lavatory, and walls that limited access similar to typical home bathroom installations. Thus, the test subjects functioned in approximately the same position as a typical toilet connector installer. Special torque measuring instrumentation was developed that was hidden in the toilet water reservoir. Tests were conducted using both the dominant and non-dominant hands. Subjects included both men and women. Test instructions were vetted such that the subjects were not aware of the purpose of the tests. Both "subject best estimate" of hand tight and "maximum possible" hand

tight torques were measured. The data were evaluated statistically, and mean and standard deviations values were calculated. These values were then used to determine a representative range of loading values in the finite element analyses.

Material Properties

Before finite element analysis can be performed, the properties of the material must be determined to a high degree of engineering accuracy. Because the failure of toilet nuts appears to be time dependent, it is necessary to not only know the short-term yield and ultimate strength of the material, but also the time-dependent (creep) properties. A series of creep tests was conducted by yet another laboratory. Tensile "dog bone" specimens were molded and tested in specially designed equipment to determine the creep strain as a function of load (and thus stress). Both notched and un-notched specimens were tested. Because the times to failure for actual nuts (even with high loading) is typically years, the tests were conducted in an elevated temperature environment to accelerate the creep strain. The data were used to determine an analytical creep/relaxation curve for the nut material that could be used in the FEA analyses. Additional tests were conducted using exemplar nuts to obtain one-time overload fractures. The details of these proprietary tests are too voluminous to include in this paper, but suffice it to say that the tests produced creep curves for the material and one-time overload fracture values that were considered sufficiently rigorous in procedure and accurate for use in the finite element analyses.

Finite Element Analyses

Knowing both the material properties of the acetal plastic and a defensible range of loading torques that covered the expected loading conditions, a series of finite element analyses was conducted to estimate the time to failure. Several different FEA analyses were conducted to determine the life of connectors subjected to various loads. The torque tests described earlier were used to determine the most likely "hand tight" loads. The torques found from the tests were converted to equivalent force on the connector bottom. The effect of water pressure was added to the torque loads to account for the additional end load caused by the supply line water pressure.

The finite element models shown in **Figure 6** were developed to calculate stress and strain distributions in the nut for various loading conditions. There were four different geometries sold by the manufacturer, and FEA models of each were developed and analyzed. The applied loads (torque values due to tightening the nut) for each were different due to the external geometries. Some of the connectors had "wings," (i.e., protruding grips that facilitated the user hand-tightening the nuts) while others had only small "bars" that gave the user less leverage for applying torque when tightening the nut. The thread geometries for each type were also different.

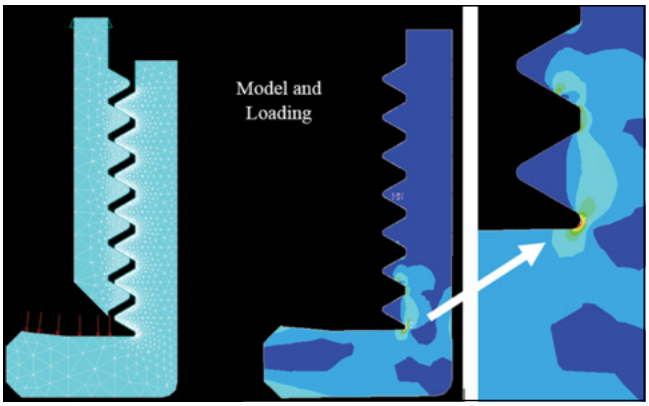

Figure 6
Finite element model of nut.

The first FEA analyses were conducted to determine if one-time overload failures, which were known from test results, could be calculated using the FEA analysis procedure. The one-time overload FEA models were run using an elastic-plastic material model (no creep because of the short time to failure). Test data from the tensile specimens indicated that the fracture strain for the tensile specimens was approximately 39%. The failure criteria for the FEA models were based on the assumption that fracture will begin when the peak strain (anywhere in the nut) reaches the fracture strain for the tensile specimen (i.e., 39%). The one-time overload analyses involved gradually increasing the applied load on the end cap until the nut failed. The analysis attempted to simulate the one-time overload tests.

The one-time overload FEA results correlated well with test data. The FEA-calculated peak strains occurred at the point of crack initiation. Because both the location of the failure as well as the load to cause failure were correctly predicted, this provided confidence that limiting total strain to 39% was a reasonable predictor of failure.

Having proven that the FEA was capable of predicting short-term failures of the nuts, the next step was to model the long-term behavior. Because most, if not

all, of the reported failures occurred when the homes were unattended (when presumably there was no external loading), it was concluded that the mode of failure was due to time-dependent material effects. Creep is known to occur in plastic parts that are subjected to relatively high stress levels. The creep data obtained from the tests described earlier were converted to creep strain rate material properties. It was assumed that the nuts remained at room temperature for the entire life of the component. This simplified the creep analysis because most analyses involve both stress level and temperature variations over time.

The analysis procedure used to model creep was to apply an end load on the nut that was equivalent to the sum of the torque load and internal pressure loadings. The load was held constant for the duration of the analysis. The creep analyses were run to simulate a total of 200,000 hours (approximately 23 years). The maximum strain in the nut was monitored. When the strain reached 39%, it was assumed that the nut would fail. **Figure 7** provides the results for these analyses. The different nut geometries are shown as Type 1 through 4. The plots show the last thread before the end cap. The first column provides the load applied and the resulting strain after 23 years at that load. For example, column 1, row 1 represents a load of 58.2 pounds, which is the equivalent end load for a hand-tightened nut plus water pressure. The 5.7% is the total strain at the worst-case location at the end of 23 years. The failure strain is 39.1%, as shown in the seventh row down. The second row is the load for hand tight plus one sigma standard deviation. This load results in a maximum strain of 7.2% at the end of 23 years. As can be seen from **Figure 7**, none of the connectors failed under the applied loads in the 23-year time frame. Type 2 exhibited the greatest accumulated strain. The last row shows runs made to determine the expected life of a nut loaded well beyond the expected worst-case loading. For a 200-pound end load, the Type 2 nut shows an accumulated strain of 32.9% at the end of 23 years.

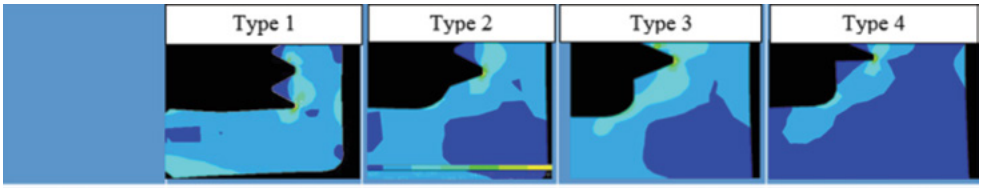

	Type 1	Type 2	Type 3	Type 4
Hand Tight	58.2 / 5.7%	58.2 / 6.3%	72.6 / 5.3%	72.6 / 5.3%
Hand Tight + σ	68.2 / 7.2%	68.2 / 7.8%	92.8 / 7.4%	92.8 / 7.5%
Hand Tight +2σ	78.3 / 8.7%	78.3 / 9.5%	117.3 / 10.3%	117.3 / 10.4%
Hand Tight -σ	48.2 / 4.4%	48.2 / 4.8%	54.7 / 3.6%	54.7 / 3.6%
Hand Tight - 2σ	38.1 / 3.2%	38.1 / 3.5%	34.5 / 1.9%	34.5 / 1.9%
Hand Tight + 1/4 Turn	106 / 13.2%	106 / 14.4%	118.9 / 10.5%	118.9 / 10.5%
Limiting Total Strain	39.1%	39.1%	39.1%	39.1%

End Load (pounds) Corresponding to Stated Loading Condition / Maximum Accumulated Strain Calculated at the End of 23 years (Above) – Maximum Accumulated Strain for a Limiting End Load of 200 pounds (Below) - for all Connector Geometries

200 Pound Load	30.4%	32.9%	21%	21.5%

Figure 7
Maximum strains for various loading conditions.

Thus, the FEA analyses indicate that the nuts should not fail over the seven- to 10-year expected life of the nuts. This begs the question: "Why did the nuts fail?"

First, it is instructive to determine the frequency of failure. No matter how rigorous quality assurance requirements are, there will always be some components that are outliers on the normal distribution curve. A statistical analysis was performed by a consultant retained by the defense. Her analysis, based upon the total number of connectors sold by the manufacturer, indicated that the probability of a reported claim for a seven-year-old connector is three to four connectors for every 100,000 sold. Because the expected life of the connector is seven to 10 years (per the manufacturer), the statistics consultant opined that this failure rate was among the lowest of any consumer product. Clearly, there will be some failures when so-called consumer products are sold in the volume (more than 40,000,000 over a nine-year period) involved in this case. Based on the statistical analysis, the failure rate is exceedingly small. Therefore, it is highly unlikely that a single "root cause" can be identified. A root cause would imply that a defect was present, either in the design or manufacture of a product, which was responsible for a rash of failures. Further, in a class-action matter, the plaintiff typically must show that a large number of people have been injured by the same defendant in the same way. Certainly, it is difficult to imagine that such a low failure rate could rise to the level of a systemic failure of a consumer product — and that the failure mode was the same in all cases.

Having shown that the rate of failure was exceedingly small, what could cause these "random" failures? The most likely cause is overtightening the nut. Despite the fact that the plastic nut has "hand tight only" embossed on it via the molding process, it is clear that most of the nuts were tightened using a tool. **Figure 8** is a photograph of a failed nut that has tool marks on the outside surface. Most of the nuts examined by this author had indications that a tool was used to tighten the plastic nut onto the ballcock threads. It is also possible to use channel lock pliers or similar tools to grip the nut while using a rag to protect the nut from being scratched or gouged.

Why overtighten the nut? One reason they may be overtightened is when an old connector develops a leak, or when it is removed and reinstalled. When compressed for years under high stresses, the rubber

Figure 8
Failed nut showing distress marks from tool used to tighten the nut.

washer takes a "set." Permanent deformation of the cone washer can be observed when the nut is removed. When this occurs, the cone washer should be replaced. The rubber has hardened. If the initial seal is disturbed, it will no longer conform exactly to the surfaces to be sealed (see **Figure 3** for the seal points). In addition, chemicals in the water can cause deterioration of the rubber, resulting in surface cracking. When the nut is removed and then reused, the sealing surfaces may no longer "match up," and leak paths are formed. When water pressure is applied to the line, these small leak paths allow water to drip out of the connector. Instead of replacing it, the homeowner (or plumber) may use a tool to tighten the nut until the leak stops. This "brute force" fix overstresses the nut and accelerates creep at the highly stressed areas of the nut, particularly at the threads. If the leak returns later, more tightening of the nut is done, and eventually the nut will fail.

It is also interesting to observe that some of the experts for the plaintiff apparently did not understand how the nut seals against leakage.

As shown in **Figure 3**, there are two distinctly different leak paths in the nut assembly. The first seal is affected at the end of the threaded ballcock pipe and the cone washer. This seal point is at the top of the rubber cone washer. The seal is caused by forcing the end of the ballcock thread against the washer by torquing the nut. This seal requires only a low torque that can be applied by hand. The second possible leak path is at the inside of the cone washer. This seal is affected by the force of the water pressure pushing the cone washer against the copper tube. Tightening the nut will not stop

a leak through this path. **Figure 9** shows a cone washer taken from a failed nut. Note the calcium deposits on the inside and bottom surface of the cone washer. This indicates that leakage had occurred for quite some time through this secondary leak path. The user apparently continued to tighten the nut, hoping to stop the leak and finally caused the nut to fail.

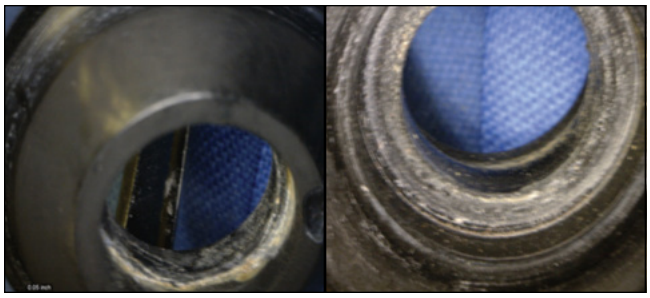

Figure 9
Inside and bottom of cone washer showing water deposits, indicating leakage.

Summary

This paper describes a number of tests and analyses that were performed in the course of defending against a plaintiff class-action suit. The injection-molded plastic connector nuts were failing in a time-dependent manner characterized by creep rupture of the plastic at or near the last thread. The plaintiff experts opined that the cause of the failures was a design defect resulting from a sharp thread configuration ending at or near the bottom of the connector. The potential liability to the manufacturer was in the hundreds of millions of dollars.

In order to investigate these claims, the experts retained by the defense attorneys performed a number of tests and analyses described herein. Material property testing was performed to determine the long-term creep properties of the plastic. Exemplar nuts were tested using an increased temperature environment to simulate longer term creep room temperature response. Test specimens were likewise tested to obtain the time-dependent creep properties of the material. The definition of "hand tight" was developed by another facility using more than 50 subjects selected at random. Some of the subjects were licensed plumbers; some were "typical" homeowners. These tests provided a range of torques and were sufficient in number to provide a statistically meaningful result, including mean, max, min, and standard deviation.

Having the material properties and a good approximation of the loading, detailed elastic-plastic-creep analyses were performed using two different commercially available finite element programs. The analyses confirmed the test data for short-term failure and provided an estimate of the expected life of the nuts. A statistical analysis of the failures was done that showed the failure rate is extremely low. It was shown that the nuts exceed the design life and that no defect in either the design or manufacturing was present. The matter was settled out of court.

Forensic Analysis of Wind Power Generator Tower Cracking

By James William Jones, Ph.D., P.E. (NAFE 778F)

Abstract

Generators that produce electricity for modern wind farms are mounted atop large steel towers. The hollow cylindrical towers, which are typically more than 250 feet in height, are fabricated from mild steel plates (approximately 1-inch-thick and 10 to 12 feet in diameter). Cracks in the steel plates measuring more than 4 feet long were observed in such a tower. The author was retained to determine the cause of the cracking and if that cause was a result of incorrect design (owner) or poor fabrication quality (contractor). Laboratory examination of the crack morphology and finite element analyses techniques were used to characterize the root cause of the failure. Cyclic loading on the tower was developed from wind rose data for the site. It was ultimately shown that the cause of the steel plate cracking was flow-induced vibrations resulting from von Karman street vortex shedding — not the fore-aft loads of the direct wind forces on the blades.

Keywords

Forensic, wind tower, flow-induced vibration, vortex shedding, crack initiation due to vibration

Background

A forensic analysis was performed to determine the cause of failure of a wind turbine tower at a wind farm in New Mexico in the spring of 2011. A review of documents revealed the following facts: During a routine inspection of the tower, a technician noticed a crack in the middle splice of the steel tower structure. At that location, a forged flange is welded to the rolled tower shell section. According to a report issued by a large, nationally recognized metallurgical laboratory, a crack initiated at the toe of the full penetration weld that joins the flange to the rolled shell section. The laboratory report provided a detailed description of the failed section and how the origin of the crack was determined.

The flange of the tower section is fabricated from ASTM A694 Grade F42 material. The tower shell is fabricated from ASTM A572 Grade 50 or ASTM A709 Grade 50F. The flange is welded to the shell at the neck by means of submerged arc welding using a complete joint penetration (CJP) weld preparation (groove). The welding was performed in accordance with American Welding Society (AWS) specifications. The welded materials are compatible, including the welding rod, and have been used for this application for many years. The welding was performed in accordance with shop weld procedures prepared by the fabricator and approved by the owner, using certified welders that were qualified in the process used. All welding was inspected before the towers were shipped. **Figure 1** shows a schematic drawing of the wind tower. The failure was observed between Section 2 and Section 3. No other weld failures were found in the tower.

Wind turbines are almost always located at sites that experience prevailing winds from one dominant direction. Locations for wind farms are selected very carefully. Typically, a wind and enviromental measuring station is placed at a candidate site and monitored for at least one year. The wind velocity and direction are measured and recorded. In order to be economically viable, the average wind velocity at the site must be more than approximately 18 to 20 mph for a large percentage of the time. Some basic definitions for wind speed (relative to turbines) include:

- *Start-up speed* — This is the speed at which the rotor and blade assembly begins to rotate.
- *Cut-in speed* — The minimum wind speed at which the wind turbine will generate usable power. This wind speed is typically between 7 and 10 mph for most turbines.
- *Rated speed* — The minimum wind speed at which the wind turbine will generate its

James William Jones, Ph.D., P.E., 5561 Ocean Terrace Drive, Huntington Beach, CA 92648; (714) 369-2703; bill@jwjce.com

designated rated power. For example, a "10 kilowatt" wind turbine may not generate 10 kilowatts until wind speeds reach 25 mph. Rated speed for most machines is in the range of 25 to 35 mph. At wind speeds between cut-in and rated, the power output from a wind turbine increases as the wind increases. The output of most machines levels off above the rated speed. Most manufacturers provide graphs called "power curves" that show how their wind turbine output varies with the wind speed.

- *Cut-out speed* — At very high wind speeds, typically between 45 and 80 mph, most wind turbines cease power generation and shut down. The wind speed at which shutdown occurs is called the cut-out speed or sometimes the furling speed. Having a cut-out speed is a safety feature that protects the wind turbine from damage.

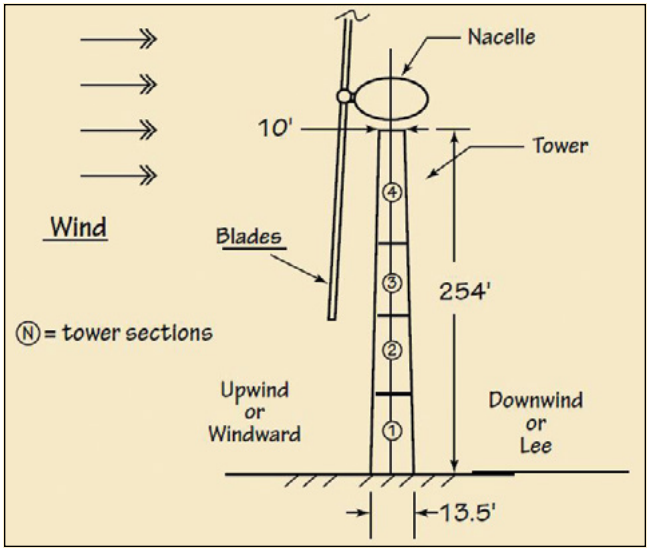

Figure 1
Wind tower schematic drawing.

The data obtained from the site measuring station is used to develop a "wind rose," which is shown in **Figure 2**. The wind rose graphically displays the overall wind flow hours and the direction of the wind. The prevailing wind direction can be clearly seen from **Figure 2** to be from the southwest. Since only the nacelle (on which the blades are mounted) is rotated such that the blades face the wind, the upwind/downwind directions for the tower change (depending upon wind direction). However, when the prevailing wind is predominately from the southwest (as in this case), the loading on the tower is dominated by a primary load path shown in **Figure 3**. The location of the crack in the tower is also shown in **Figure 3**. **Figure 4** shows the crack in the tower before the section was removed and taken to the laboratory. The presence of iron oxide stains indicates that the crack existed in the steel for a considerable length of time before it was discovered, which could suggest that maintenance at the site was inadequate. The crack extended a total of 2,110 mm (83 inches) around the circumference.

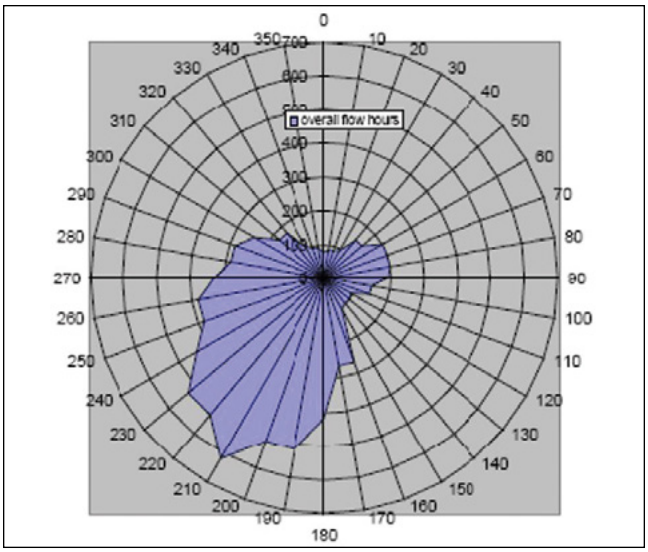

Figure 2
Wind rose for site of tower.

As can be seen in **Figure 2** and **Figure 3**, the primary loading on the tower is from the southwest toward

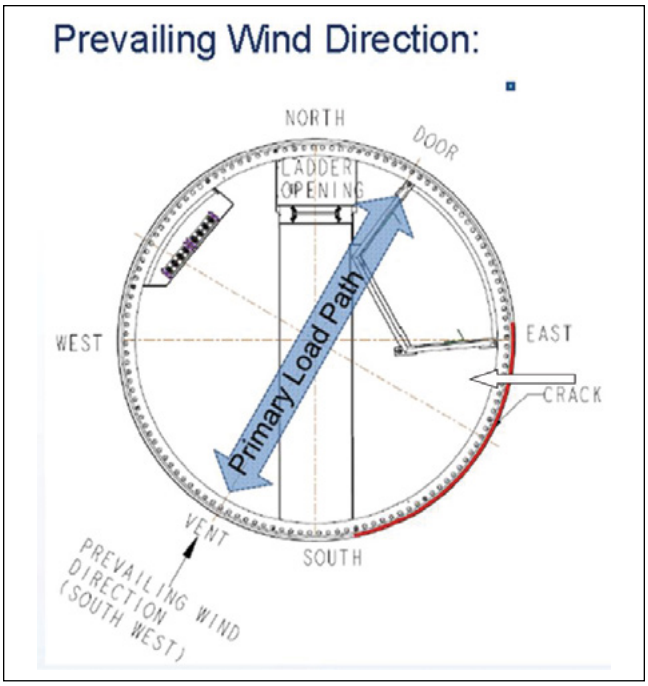

Figure 3
Location of crack with respect to wind direction.

the northeast. Further, the primary direction wind load will result in a tensile load on the southwest side of the tower and compression on the northeast side. The bending stress distribution is shown in **Figure 5**. The crack is located almost exactly at the neutral axis of bending, where the bending stresses are very low. Further, the wind history indicated that site was almost never becalmed. A more or less constant wind would not produce reversed cyclic loading because the upwind side will always be in tension, and the downwind side would almost always remain in compression. Even more confounding, the weight of the tower shell above the crack plus the weight of the nacelle and blades provide a downward force at the crack location. This loading results in compressive stresses on the tower shell at the location of the crack. Virtually all cracks that result from cyclic loading involve a stress cycle in which there is a tensile stress component. In other words, some part of the loading cycle must result in a net tensile stress at the origin of the crack face. Cracks in steel plates rarely, if ever, initiate in a location that is subjected only to cyclic compressive stresses.

Figure 4
Crack in tower.

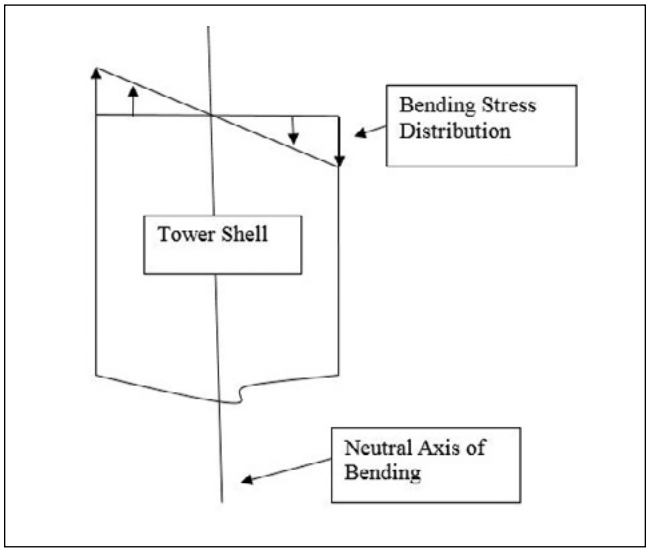

Figure 5
Bending stress distribution.

It would seem that the most logical point to initiate a crack would be the upwind side of the tower, which is subjected to the highest tensile stress. It would also seem logical to assume that the cyclic loading that initiated the crack was caused by the cyclic nature of wind velocity changes, including gusting. This type of loading would result in tensile stresses on the southwest side of the tower and almost no stresses at the actual crack initiation point (90 degrees away). Further, an examination of the tower indicated that there was no significant difference in the geometry at the crack initiation point than at any other point around the tower. The tower was axisymmetric, and no flaws were found at the crack initiation point. Thus, the question arose: Why did the tower crack at the lowest stressed area, and what was the mechanism that caused cyclic stresses of a magnitude to lead to cracking?

The most likely candidate for loading that could cause a crack to form at the observed location is vortex-induced vibration. In Chapter 2 of his seminal book on the subject, Blevins[1] provides an excellent discussion of the mechanism that causes vibration in cylindrical towers and stacks. For smooth cylinders, such as the wind generator tower, lift forces will be developed due to Bernoulli's principle* at the sides of the tower that result in lateral forces (forces perpendicular to the flow direction). The formation and subsequent shedding of vortices that disturb the flow around the cylinder (**Figure 6**) and alternate from side to side provide a harmonically varying (sine or cosine) load on the tower.

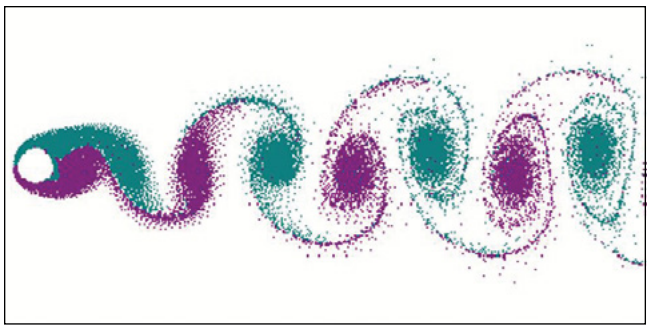

Figure 6
Von Karman street vortex shedding pattern.

* Bernoulli's principle, i.e., the Bernoulli equation that relates the effects of fluid velocity and pressure effects can be found in almost all books on fluid mechanics. A good introduction to the physics of Bernoulli's principle can be found on the NASA web site at https://www.grc.nasa.gov/www/k-12/airplane/bern.html.

The pattern formed by the vortices is known as a von Karman vortex street. When the frequency of vortex shedding frequency coincides with the first natural frequency of a long cantilevered cylinder, such as the wind tower, then the tower will begin to vibrate in a direction perpendicular to the oncoming wind direction. This is illustrated in **Figure 7**.

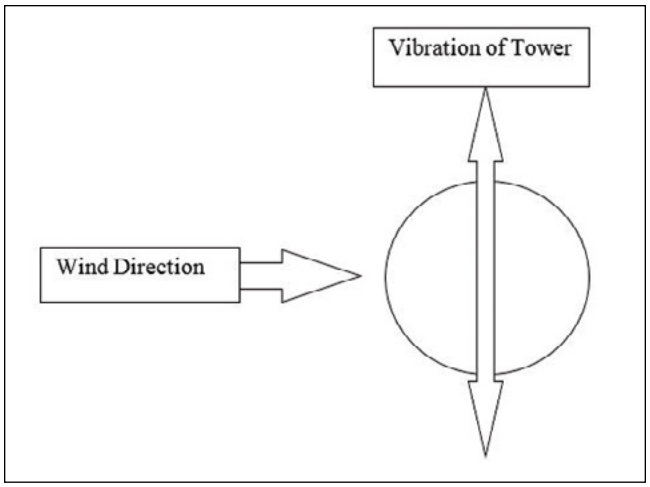

Figure 7
Schematic of wind and vibration directions for cylinder.

This phenomenon can be explained in greater detail as follows. The colors in **Figure 6** (dark and light areas) represent airflow around the cylinder. Vortex shedding is caused by a buildup of the boundary layer on each side of the cylinder, which as it happens, is always out of phase with the opposite side. As a boundary layer builds on the left side, for example, the velocity of the passing air is increased due to the Bernoulli effect — similar to the lift on an airplane wing. This produces a low-pressure zone on the left side of the tower, pulling the tower in that direction. However, the resulting boundary layer is unstable, and collapses into turbulent flow. This will greatly reduce the "lift" on the left side, since turbulent flow is not conducive to producing a net lift effect. This releases the "vortex" that is characteristic of the flow pattern shown in **Figure 6**. However, now the right-hand side of the tower begins to build up a boundary layer in a similar way to the left-hand side. The tower is now pulled to the right by the lower pressure acting on that side. This continues until the right side boundary layer collapses, and the left side begins to build up again. This alternating sequence of pressure patterns, which pulls the cylinder to one side and then the other, provides the sinusoidal driving force that, when occurring at the natural frequency of vibration of the cylinder, can result in large deflections of the tower. This harmonic driving force, while quite small compared to the force of the wind on the blades, causes lateral motion and therefore bending (like a fishing rod) from side to side. The motion is perpendicular to the direction of the wind.

Because the tower is being driven by harmonically varying loading at its natural frequency, the amplitude of the vibration will continue to increase until it is limited by inherent damping in the structure. The tower design is such that hysteresis damping (caused by flexing the steel cylinder and producing heat in the steel) is very low. It was determined that this damping was approximately one to two percent of critical damping. Thus, it is possible for the tower to experience deflection amplitudes of up to one diameter at the point of failure. The effect of the blades moving in air will also provide a form of Coulomb damping (damping that is the result of friction; in this case, motion of the tower and blades resisted by air). Thus, the calculation for maximum amplitude is not straightforward and was not attempted.

Calculation of Vortex Shedding Frequency

Having postulated an alternative loading mechanism for the subject tower failure, it is necessary to show that the tower natural frequency coincided with expectable vortex shedding frequencies. A detailed structural analysis had been performed for the tower by the design engineers and submitted to the local authorities as part of the permitting requirements. A detailed finite element dynamic analysis of the tower, including the nacelle and the blades, was performed. The author used these existing calculations, which showed that the first natural frequency of the tower was 0.341 Hz. The effect of gravity was not included in the design calculations for natural frequency; rather, the author derived an improved formula[2] for calculating the natural frequency of an inverted pendulum. This calculation was made as part of the structural design calculations and used to determine seismic loading on the tower. The mode shape is essentially a cantilever bending mode with the base of the tower fixed against rotation, and the top of the tower experiences the highest deflection.

The vortex shedding frequency can be calculated using the Strouhal number. The equation developed by Strouhal[3] for a smooth cylinder is:

$$f_S = (S)(U)/D \quad (1)$$

Where:

f_S = Vortex shedding frequency (Hz)

U = Free stream velocity approaching the cylinder (feet per second)

D = Cylinder diameter (feet)

Blevins (p 48) shows that for a wide range of Reynolds Numbers (encompassing this case), the value of the Strouhal number is approximately 0.2. Thus, from equation 1 above, the wind speed that will cause vortex shedding at the same frequency as the natural frequency of the tower (f_T) can be determined as follows.

$$f_S = (S)(U)/D = (.2)\ U/D = f_T = 0.341\ Hz \qquad (2)$$

Rearranging equation 2, find:

$$U = (.341)(D)/.2 = 1.705\ D \qquad (3)$$

The tower diameter varies from 4,120 mm (13.5 feet) at the bottom to 3,620 mm (11.87 feet) in the middle sections and tapers to 3,017 mm (9.89 feet) at the top. At each of these diameters, the free stream velocity (U) to cause vortex shedding (which has the same frequency as the tower natural frequency) can be calculated as follows:

Diameter (feet)	Free Stream Velocity (ft/sec)	MPH
13.5	23.00	16
11.87	20.23	14
9.89	16.86	12

Figure 8
Free stream velocity necessary to cause vortex shedding at the natural frequency of the tower.

Thus, (for example) if the free stream velocity (wind speed) is exactly 16 mph (**Figure 8**, for a diameter of 13.5 feet), the vortex shedding frequency will be exactly the same as the natural frequency of tower vibration, and the tower will resonate. Once the tower starts to vibrate back and forth (perpendicular to the wind direction), the amplitude of the motion will increase with each cycle until it reaches an equilibrium point where the energy dissipated by the tower motion equals the input energy from the vortex shedding. Of course, the theoretical calculations are never exact, and the wind doesn't blow at a constant speed. Thus, it is useful to investigate the effects of wind speed variation and how this affects the vortex shedding frequency predicted by the Strouhal number.

The available wind data from the site provided only average wind speed over rather long periods of time (reported as quarterly or monthly averages). In order to estimate the wind speeds and how they vary, a normal distribution or Gaussian curve was assumed. This assumption is justified by the fact that most naturally occurring phenomena exhibit a statistical distribution that can be reasonably represented by a Gaussian distribution. Based on this, it can be shown that the wind velocity will be within one sigma (standard deviation) from the mean (average in this case) value approximately 68% of the time. Thus, the wind velocity will tend to vary between plus or minus approximately 35% of the mean value about 68% of the time. Take, for example, a mean velocity of 20 feet per second. The actual wind velocity can be expected to be between a low of 13 feet per second and a high of 27 feet per second 68% of the time. Further, the wind velocity will be closer to the mean velocity more of the time than at the extremes of 13 and 27 feet per second.

As can be seen from **Figure 9**, the vortex shedding velocities for the various tower diameters fall within the measured wind velocities. Taking into account the Gaussian distribution (**Figure 10)**, which shows that the one-sigma variation of the wind speeds can vary significantly from the average, every diameter of the entire tower will have vortex shedding frequencies in the range of measured wind speeds. This velocity distribution, combined with measured wind velocities at the site, ensures that the tower could experience some flow-induced vibration over a significant portion of time during the course of every year.

However, there is yet another mechanism that will further increase the already high probability that the tower will resonate with the prevailing winds at the wind farm site. This is the effect of the cylinder *motion* on the frequency of vortex shedding. Blevins[1] states that:

"Transverse cylinder vibration (i.e., vibration perpendicular to the free stream), with frequency at or near the vortex shedding frequency, has a large effect on vortex shedding. The cylinder vibration can:

1. Increase the strength of the vortices.

2. Increase the spanwise correlation of the wake.

3. Cause the vortex shedding frequency of cylinder vibration. This effect is called lock-in or synchronization…"

Date	Wind Speed Average M/sec	Wind Speed Average Ft/sec.(MPH)
2009	7.38	24.0 (16.4)
Q2-2009	5.79	18.8 (12.8)
June 2009	5.79	18.8 (12.8)
Q3 2009	6.73	21.9 (14.9)
July 2009	6.43	20.9 (14.25)
August 2009	7.39	24.0 (16.4)
September 2990	6.36	20.7 (14.1)
October 2009	8.65	28.1 (19.2)
November 2009	7.28	23.7 (16.2)
Q4 2009	8.11	26.4 (18)
December 2009	8.38	27.2 (18.5)
Q1 2010	7.6	24.7 (16.8)
January 2010	6.92	22.5 (15.3)
February	6.91	22.5 (15.3)
March	8.92	29.0 (19.8)
April	10.39	33.8 (23)
Q2 2010	9.14	29.7 (20.3)
May 2010	9.59	31.2 (21.3)
June 2010	7.42	24.1 (16.4)
Data continues through 2011		
Grand Total (Undefined)	8.06	26.2 (17.9)

Figure 9
Measured average wind velocities at tower site.

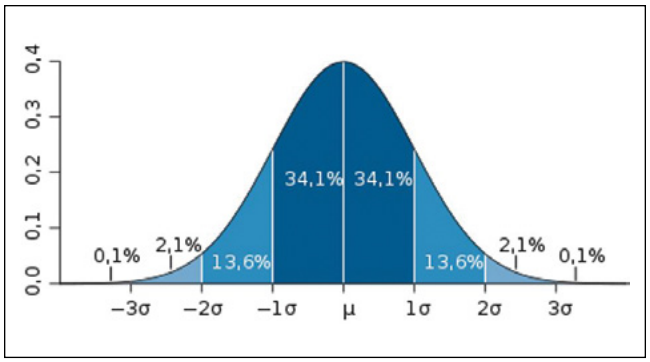

Figure 10
Gaussian distribution.

This so-called "lock-in" effect is explained by Blevins as the condition when the transverse vibration of the cylinder is at or near the shedding frequency; this organizes the wake. Thus, the vibration of the cylinder (tower), which will occur at its natural frequency, will cause a *shift* in the *stationary* vortex shedding frequency such that the frequencies are correlated. In other words, once the tower begins to vibrate at its natural frequency, the effect of the tower motion will cause the vortex shedding frequency to occur at that frequency. Thus, the two frequencies become correlated. Once the tower starts to vibrate at any particular wind velocity, the vibration will continue even if the free stream velocity changes over a wide range of velocities. Blevins' book provides experimental verification of this lock-in phenomenon on page 55. It can be seen from the Blevins reference that lock-in can occur for ratios of vibration frequency to stationary shedding frequency that range from 0.5 to 1.5. Considering that the assumed Gaussian distribution of recorded free-stream velocities extend over and have mean values near the confluence of the vortex shedding/natural frequency of the tower, this lock-in effect virtually guarantees that flow-induced vibration will occur for the towers at this site.

Discussion of Results

The assumption that the tower bends as a cantilever beam is admittedly an assumption, but the author has used this analogy successfully to accurately estimate the natural frequency of a tower of varying cross section. When the results are compared to a computer calculated natural frequency — taking into account the actual cross sections — the simplified analysis is quite accurate. This is probably due to the fact that the natural frequency is a function of the square root of the stiffness, which reduces the error appreciably even if the stiffness is inexact.

The effect of torsional loading was considered as a possible source of stress that could result in a crack. Torsional loading due to the asymmetric geometry of the blades was evaluated and found to be very small compared to the high torsional resistance of a cylinder approximately 12 feet in diameter and an inch thick. Further, the point of crack initiation is on the neutral axis of bending with respect to the wind direction. Since torsional stresses are evenly distributed completely around the circumference, there is absolutely no reason to suspect that the torsional stress contributed to the failure. If torsion was a factor, failure would have occurred near the top of the tower where the diameter is much smaller and the thickness is less, resulting in a smaller torsional moment of inertia.

It is noted that the magnitude of stresses that can be developed by vortex shedding is quite large, which may not be obvious initially. When the vortex shedding frequency is at or near the natural frequency of the tower, the tower will go into resonance. This is a similar phenomenon to the failure that occurred during the 1940 collapse of the Tacoma Narrows Bridge in Washington. However, it was experiencing a similar phenomenon called aerodynamic flutter rather than vortex shedding. Flutter is typically associated with aircraft wing stability and is caused by having a torsional wing stiffness that results in vibrations that interact with lift on the wing surface. As the wing (or bridge surface) rotates about a torsional axis, the lift varies from positive to negative. This provides the driving energy for the oscillation and the fact that the torsional frequency/wind velocity can become synchronized such that the fluid-structural interaction is at a natural frequency of the structure. The motion can become extreme — as was the case at Tacoma Narrows.

In the case of vortex shedding, it is not uncommon to get dynamic motions, side to side, equal to one or more diameters of the cylinder. While the aerodynamic forces on the tower are relatively small compared to the frontal wind forces acting on the blades, the fact that the shedding frequency is at or near the cantilever beam frequency of the tower can magnify the deflection, a result well-known in introductory vibration courses. The tower is, in effect, a single degree of freedom spring-mass oscillator driven by a sinusoidal driving force that has the same frequency as the spring-mass system. Thus, the peak excursions of the tower can be very large when excited at the natural frequency. Theoretically, the displacements can be "unbounded" for a simple spring-mass system driven at its natural frequency. However, there is always some damping in the system in real-world systems that limits the displacements. In welded towers such as this, damping is minimal, usually on the order of 2% of critical. Thus, it is possible to get large motion. In fact, the peak displacement can be approximated from the equation, $M = 1/(2\xi) = 1/(2x0.02) = 25$. (M = magnification factor, a multiple of the static deflection and ξ is the percentage of critical damping expressed as a fraction). Strain in the tower is related to deflection; therefore, bending stresses are developed when the tower sways from side-to-side. The author has personally witnessed this kind of vibration in several instances.

Conclusions

Based on the foregoing analysis, it was shown that the most likely cause of cracking of the steel plate shell comprising the wind generator support tower was flow-induced vibration due to vortex shedding at or near the natural frequency of the tower structure. The location of the crack, at an angle approximately 90 degrees away from the predominant wind direction, is explained by the direction of vibration due to the vortex shedding phenomena. Further, the side-to-side vibration of the tower can easily result in cyclic tensile/compressive stress cycles at the location of the crack. Cylindrical towers such as this are known to be susceptible to flow-induced vibration. Tall cracking towers at refineries and smokestacks are often fitted with "strakes" near the top of the cylindrical structures to prevent vortex shedding and side-to-side vibrations. Underwater cables and pipelines that are located in areas that have significant ocean currents also use this type of design to prevent unwanted vibration. Strakes are typically configured in the form of helical plates that wrap around the tower or stack (see **Figure 11**). A sub-sea riser fitted with strakes is shown in **Figure 12**, as well as smokestacks at an Alaska installation (**Figure 13**).

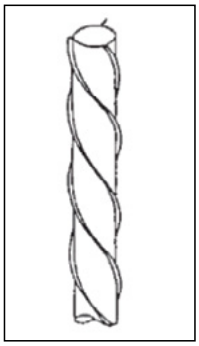

Figure 11
Helical strakes.

Figure 12
Strakes on subsea riser.

Figure 13
Strakes on stacks to prevent vibration.

References

1. Blevins R. Flow-induced vibration, 2nd edition. Malabar FL: Krieger Publishing Co.; 2001.

2. Jones J, Nickell R, Bulat W. The effects of gravity on structural vibration. Proceedings of the ASME Pressure Vessels and Piping Conference: 2013 July 14-18; Paris.

3. Strouhal V. Ueber eine besondere art der tonerregung (on an unusual sort of sound excitation), *Annalen der Physik und Chemie*, 3rd series, WILEY-VCH Verlag GmbH & Co. KGaA, Weinheim, 1878.

Forensic Investigation of Water Leakage Issues into Buildings, Recreating the Leaks Vs. Determining the Cause

By Kami Farahmandpour, P.E., FRCI, REWC, RRC, RWC, RBEC, CCS, CCCA (NAFE 854F)

Abstract

Forensic investigations of water leakage through building envelopes often involve complex investigation techniques and testing. In many cases, forensic investigators perform testing under controlled conditions to recreate the leaks and to determine whether design and/or construction defects resulted in leaks. However, construction-related litigation involves complex lines of contractual responsibility and multiple parties. As such, allocating responsibility to various parties requires an increased level of scrutiny. This paper provides an overview of typical construction defect cases and how the lines of contractual obligations can impact the scope of investigation by a forensic engineer. As a case history, a forensic engineering investigation of water leakage reported in a recently constructed building will be reviewed. The plaintiffs' experts performed testing to recreate the leaks, and adequately proved that the designs or construction methods of the exterior walls were defective. However, they were unable to prove causation attributed to one prime contractor who did not settle prior to trial. At trial, the defendant's expert demonstrated other potential paths of water leakage that were not attributed to the defendant, raising sufficient doubts about the liability of the sole defendant at trial.

Keywords

Building envelope, construction, project delivery, water intrusion, water leakage, water testing

Building Construction Litigation

Most construction professionals agree that the majority of building design and construction claims are related to water intrusion. In fact, one source suggests 70% of construction litigation is related to water intrusion[1].

Litigation related to building design and construction often involves several parties. The structure of each claim is dependent on the contractual relationships between such parties and the project delivery methods employed for the subject building. Understanding the contractual relationships between various parties is a key part of every construction litigation case.

Construction Project Delivery Methods

Building construction projects are typically delivered through a few project delivery methods, the most common of which include:

- Design-bid-build
- Design-negotiate-build
- Construction management
- Design-build
- Owner-build

The most traditional construction delivery method is design-bid-build. In this method, the project owner (owner) employs a design professional to design the building. The design of the building is conveyed through drawings and specifications that should detail every aspect of the construction and/or its performance requirements. The design documents are then sent to general contractors to provide bids for the work. The successful bidder is then contracted by the owner to construct the project as the general contractor. Design-bid-build consists of a simple contractual line of responsibility shown in **Figure 1.** The owner has a direct contractual relationship with the designer and a separate contractual relationship with the general contractor. The general contractor will often work with several subcontractors to construct various systems or supply materials. Having more than 30 subcontractors on one project is not uncommon for the construction of many buildings. In design-bid-build project delivery, no direct contractual relationship exists between the designer and the contractor, between the owner and subcontractors, or between the designer and subcontractors. The lack of direct contractual

Kami Farahmandpour, P.E., 1845 E. Rand Rd, Suite L-100, Arlington Heights, IL 60004; (847) 454-8814; kamif@btcpc.com

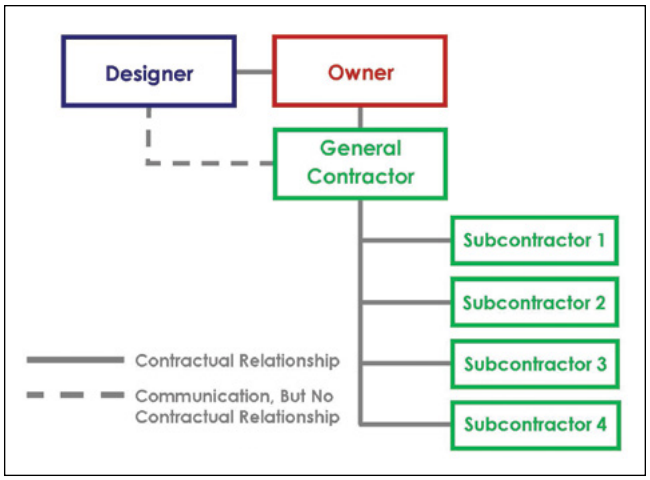

Figure 1
Design-bid-build project delivery.

relationships between these parties poses legal challenges in pursuing subcontractor and suppliers.

Design-negotiate-build project delivery is similar to design-bid-build. However, rather than bidding the construction of the project to several contractors, the owner negotiates with contractors to arrive at a mutually agreeable cost for the project. The contractual relationships between various parties are similar to design-bid-build.

When utilizing construction management project delivery, the owner retains a designer to design the project. The owner will also contract with a construction manager to assist in the construction of the project. Some construction managers also assist the owner in selecting the designer. Construction management project delivery can be further categorized into Construction Manager as Advisor (CMa) or Construction Manager as Constructor (CMc)[2]. CMc is also referred to as Construction Manager at Risk (CMr). When using CMa project delivery, the construction manager will not serve as a general contractor. Instead, the owner will contract directly with several contractors (typically referred to as prime contractors) to construct various portions of the project. This arrangement will result in the owner having a contractual relationship with multiple prime contractors. Although the construction manager will be responsible for overseeing and coordinating the work of these multiple prime contractors, it will have no direct contractual relationship with any of them. Instead, the construction manager will advise the owner on various aspects of the project and assist in managing the multiple prime contractors. When using CMc project delivery, the construction manager may serve as the general contractor. Discussing the differences between contractual responsibilities of these two categories of construction managers is beyond the scope of this paper. In either case, the construction manager's contractual obligations are usually to the owner. Typical contractual relationships between various parties for a construction management project delivery are shown in **Figure 2.**

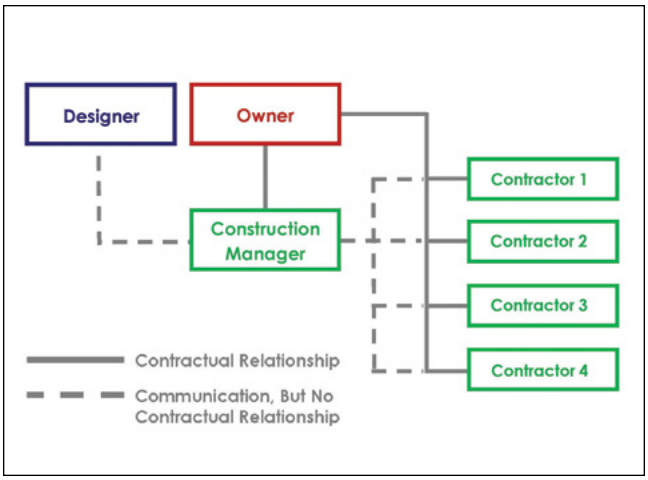

Figure 2
Construction manager project delivery.

In a project using design-build project delivery, the owner contracts with a single entity to perform the design and construction of the building. That entity is typically referred to as the designer-builder, who can then contract with various parties, such as architects, engineers, and contractors, to perform various tasks.

In many projects, a combination of these project delivery methods may be employed. For example, in the case of a residential developer, the owner (acting as the developer) will typically retain the designer and general contractor in a design-bid-build arrangement. However, in some cases, the developer may be the designer or the general contractor.

Challenges for Forensic Engineers Involved in Construction Litigation

Forensic engineers who specialize in the evaluation of moisture damage and water infiltration into buildings are often tasked with identifying the exact cause(s) of water infiltration or moisture (including condensation) in complex building envelope systems. This task is further complicated by the need to identify the responsible party (parties) and allocate responsibility.

When forensic engineers are retained by the plaintiff, their scope of investigation will likely be influenced by the contractual relationships between various parties and what the burden of proof will be. In a design-build project scenario, the plaintiff's forensic engineer may not need to allocate responsibility to the designer versus the contractor(s) because the plaintiff's contractual relationship was merely with a single entity with obligations to the plaintiff.

In building envelopes, most water leakage issues occur at interfaces between various systems. For example, water leakage can occur at the interface between the windows and the adjacent masonry walls. In such cases, allocation of responsibility will be complicated by the fact that several subcontractors may have played a role in constructing the interface. In addition, the design of the interface may have been faulty or omitted from the design documents. In the example of a window-masonry interface, the following parties may carry responsibility for the defects that led to water leakage:

1. The designer may have designed the interface improperly or specified incompatible materials at the interface.

2. The designer may have omitted the appropriate details at the interface, and one or more of the subcontractors may have constructed the interface incorrectly without seeking direction from the designer.

3. The window subcontractor may have installed the windows incorrectly.

4. The window supplier/manufacturer may have supplied defective windows.

5. The masonry subcontractor may have constructed the masonry through-wall flashings incorrectly around the windows.

6. The waterproofing subcontractor may have applied the weather-resistive barrier flashing around the windows incorrectly.

7. The sealant subcontractor may have improperly applied sealant at the interface between the masonry and the windows.

8. The general contractor or construction manager may have dictated incorrect sequence of work by the subcontractors.

9. The owner may have failed to maintain the building properly, or may have made modifications that may have adversely impacted the window-masonry interface.

In a construction defect case involving building envelope issues, it would not be uncommon to have more than 10 parties involved. This presents a challenge to the forensic engineer who may be tasked with quantifying the damages attributed to each party. While some forensic engineers render opinions regarding allocation of damages based on their judgement, there are more scientific methods for allocation of damages, including allocation by cost of repair for each component and allocation by percentage of damage caused by each source. A detailed discussion of these damage allocation methods and their potential shortcomings is beyond the scope of this paper.

Another challenge for forensic engineers is allocation of responsibility to design. In some cases, the designers may have delegated design responsibility for certain building systems to the contractor. For example, design of a curtain wall system is typically delegated to the curtain wall subcontractor because curtain wall systems are highly proprietary. However, the lines of responsibility for design of interfaces between various systems are more complicated.

All of the above challenges are exacerbated when considering that construction cases can involve hundreds of thousands of pages of background information. These documents are often provided to the forensic engineer in a disorganized manner. Sifting through the background information and finding relevant information is typically a significant challenge.

Typical Evaluation Methods Available to Forensic Engineers

Moisture issues through building envelopes can generally be divided into two categories: bulk water leakage and condensation issues. This paper focuses on bulk water leakage. Condensation within building envelope assemblies is a complex phenomenon that requires a separate discussion.

Evaluating bulk water leakage intrusion into buildings requires a thorough understanding of the building

envelope systems, the as-built condition of their interfaces, and how bulk water penetrates building envelopes. Several forces drive bulk water (or snow and ice) through openings in the building envelope. These include gravity, wind pressure, capillary action, kinetic energy, and surface tension. The author has evaluated building envelope water intrusion issues caused by all of the above factors. However, most building envelope water intrusion issues are driven by gravity or wind pressure.

One of the most widely recognized standards for investigation of exterior wall leaks in buildings is ASTM E2128, *Standard Guide for Evaluating Water Leakage of Building Walls*[3].That standard provides a good overview of the procedure a forensic investigator should follow to evaluate water leakage issues through building exterior walls. However, ASTM E2128 does not address building roofs or below-grade waterproofing.

The procedures prescribed in ASTM E2128 include background review, evaluation of the building's service history, a visual review, development of a hypothesis, confirmation of a hypothesis, and water leakage paths through testing and exploratory openings.

Background review is an important part of any forensic engineering investigation. In building construction, the as-built details often do not strictly follow the original design drawings and specifications. Many changes are made during the construction, and design intent and construction details sometimes change through multiple submittals that include shop drawings. As part of this review, a building envelope forensic engineer is often tasked with reviewing design drawings, specifications, contracts, shop drawings and submittals, test reports, reports produced by various parties during construction, meeting minutes, requests for information, change orders, payment applications, and many other forms of communication between multiple parties.

Once the relevant background information is reviewed and the service history has been established, a visual inspection of the building (or affected portions) is performed. Based on this information, the forensic engineer will develop certain hypotheses regarding potential water intrusion causes. Such hypotheses should then be verified (or ruled out) through water testing to recreate the leaks and to assess the path of water leakage through concealed components of the building exterior. In some cases, water testing may not be required. For example, where there is an obvious opening through the exterior wall at the location of a reported leak, it may be rationally concluded that the opening is one of the leak sources. However, the forensic engineer should also assess if there may be other water leakage sources.

Water testing will necessarily involve replicating the conditions that caused the water intrusion. Several water testing methods and standard procedures are available to building envelope forensic engineers. These include ASTM C1601[4], ASTM C1715[5], ASTM E1105[6], AAMA 501.2[7], and AAMA 511[8]. Discussions of these test procedures are beyond the scope of this paper. However, it is important to point out that the forensic engineer should understand the limitations of each test, and determine if the selected test procedure can sufficiently replicate the in-service conditions that caused the water intrusion.

It is also important to note that assessing the exact path of water leakage requires systematic and deliberate sequencing of testing. During such test sequences, various components of the building exterior should be isolated to evaluate their performance individually. Without such deliberate test sequencing and isolation, the leaks may merely be replicated, but their exact source or path cannot be determined.

Understanding What is Asked of the Forensic Engineer

The investigation methodology employed by each forensic engineer will greatly depend on what is asked of him/her. For example, a forensic engineer's assignment may be limited to determining if bulk water leakage occurs, or may be as detailed as determining the path of water leakage and attributing responsibility to various parties responsible for the design and construction of the building envelope.

In cases where the plaintiff files a claim against a developer who employed the designer and the general contractor, simply proving that water leakage occurs under in-service conditions may be sufficient for the purposes of convincing a jury or panel of arbitrators that the buyer (current building owner) did not get what it bargained for. However, in cases where allocation of responsibility is important, simply reproducing leaks under in-service conditions is not sufficient. In such cases, the forensic engineer will have the much more complicated task of proving that leaks occur

under service conditions and determining the path that the water travels to reach the building interior. This second component of the investigation is crucial for the purpose of allocating responsibility to various parties.

Case History

In a recent case, a residential condominium association filed a lawsuit against the developer of its building due to pervasive water leakage issues throughout the building. The leaks had manifested within several residential units within a relatively short time after completion of the building.

The subject building was a concrete frame high-rise structure with a combination of punched windows, strip windows, drainage masonry walls, and barrier metal panels forming the exterior of the building. The building exterior also included cantilevered balconies.

The building was developed by a development entity (the developer) who had constructed the building under construction management project delivery method. As such, the developer had retained a design firm to design the building, a construction manager to oversee the construction as an advisor, and several prime contractors who constructed various portions of the building.

In order to investigate the water leakage issues, the condominium association retained two forensic consulting firms who assigned multiple personnel to the project. The first consulting firm focused its efforts on investigating the windows, while the second reviewed the windows and exterior wall systems. The second consulting firm also acted as the plaintiff's expert during the subsequent litigation.

Through water tests, the condominium association's forensic consultants were able to replicate the water leakage through the exterior building components: Water leakage to the unit interiors was confirmed, proving that there were design and/or construction defects. The testing performed by the condominium association's consultants primarily consisted of ASTM E1105 and AAMA 501.2 tests. ASTM E1105 prescribes procedures for testing of installed windows and doors using a calibrated spray rack applying water on the exterior face of the assembly and a differential pressure exerted across the assembly to simulate wind pressure. AAMA 501.2 prescribes procedures for testing of inoperable windows and curtain walls using a hand-held calibrated spray nozzle with no applied differential pressure. In many cases, the ASTM E1105 testing (conducted by the condominium association's forensic consultants) was performed without employing any differential pressure across the tested system to replicate wind-driven rain events.

Although the tests replicated leaks, the path of the water leakage was not determined — with the exception of one test that conclusively demonstrated water leaks along the mullion joints of the strip windows.

Following the testing, the condominium association's consultants made exploratory openings to examine the as-built condition of the wall and window systems. Through those exploratory openings, several construction deficiencies were documented. These deficiencies were related to work performed by the window, metal panel, sealant, and masonry contractors. In addition, design deficiencies were also noted.

The condominium association's consultants attributed several of the noted deficiencies (observed through the exploratory openings) to the masonry prime contractor, including a lack of mechanical attachment along the top of through-wall flashings, inadequately constructed through-wall flashing end dams, lack of through-wall flashing end dams at some locations, failed sealant joints, lack of horizontal gaps for vertical expansion of brick, and missing through-wall flashing below window sills.

Based on their findings, the condominium association's forensic consultants developed repair schemes to address the leaks. These included a series of comprehensive repairs that addressed all of the deficiencies they had observed. In many cases, no water testing had been performed to verify that the components scheduled to be repaired were causing water leakage. Nonetheless, in an apparent attempt to ensure long-term performance of the building envelope, every potential source of water leakage was addressed.

Once the repairs were designed by the condominium association's forensic consultants, they were implemented by a qualified contractor. The costs for the design and implementation of the repairs were then attributed to the developer's prime contractors and the designer based on the cost of repair of each component. As the litigation process unfolded over several years, the condominium association was forced to pursue the

developer's prime contractors, and the designer was dismissed*. Subsequently, several of the defendant prime contractors settled with the condominium association shortly before trial†. Ultimately, the only remaining defendant was the masonry prime contractor.

The case against the masonry prime contractor proceeded to trial by a jury. During the trial, the condominium association's experts presented the results of their investigation. However, when challenged under cross-examination, they indicated that their water testing did not conclusively determine that the masonry deficiencies observed through their exploratory openings caused the water leakage issues. Using 3-dimensional modeling and computer-generated animations, the masonry prime contractor's expert demonstrated to the jury that other factors outside the masonry prime contractor's responsibilities were the likely cause of the water leakage issues. These factors included the windows (installed by another prime contractor), the design of the building envelope, and the sequencing of construction by the construction manager. An example of a 3-dimensional model used as a trial exhibit is shown in **Figure 3**. In addition, the masonry prime contractor's expert demonstrated that many of the repairs performed by the condominium association to address the water leaks may not have been necessarily related to the leaks.

Figure 3
3-dimensional model used to demonstrate where leaks could be due to a gap between the window frames and the window rough opening. That gap was left open by design.

* For several reasons, the developer of the building was not pursued, and under the state law, the condominium association was able to pursue its claims directly against the developer's prime contractors.

† In the author's experience, most construction claims are settled prior to trial. This is partially due to the complex nature of construction cases that cause uncertainty of outcome and the expenses related to such trials.

The jury found in favor of the masonry prime contractor, leaving the plaintiffs with no recovery from that contractor.

This case demonstrates that as the litigation process evolves, the burden of proof can change. Initially, the plaintiffs were pursuing the developer — a single entity who was responsible for the design and construction of the building. As such, their experts only needed to prove that the building did not perform acceptably without having to attribute causation to each prime contractor. The developer would then have the option of pursuing the designer and its prime contractors as third-party defendants, and allocating responsibility to each of those third-party defendants would be the developer's burden, not the plaintiffs'. However, as the case evolved over several years, the plaintiffs ended up pursuing the developer's prime contractors, making it the plaintiffs' burden to allocate responsibility among the prime contractors. To complicate matters further, since the building had been repaired, additional testing and investigation could not be performed to determine the responsible parties for the leaks.

In this case, it is not clear why the plaintiffs' experts did not determine the path of water leakage and properly formulate opinions regarding allocation of responsibility. However, evolving needs during a long construction litigation process spanning multiple years are common, and can certainly explain the process adopted by the plaintiffs' experts.

Uncertainty and confusion about burden of proof in building envelope water intrusion cases can occur due to many reasons, including:

1. In some cases, the client simply does not have the financial resources to authorize extensive testing and follow-up exploratory openings to determine the exact path of water leakage and allocation of responsibility through a thorough review of project documents.

2. In some cases, due to the long process of litigation, the initial objectives of the forensic engineer are defined properly. However, as the case evolves and burden of proof changes, the attorney or the forensic engineer fail to account for the changes in litigation strategies and the need to properly allocate responsibility to various parties.

3. In some cases, miscommunication between the forensic engineer and the attorney can lead to misunderstanding of the investigation objectives by the forensic engineer.

Conclusions

Prior to taking on an assignment, forensic engineers should thoroughly understand the client's objectives and what questions should be answered through their opinions. Based on this understanding, they should develop a scope of investigation that can yield useful and reliable results, which should then be used to formulate engineering opinions.

In building construction and water intrusion cases, a thorough understanding of each party's responsibility is often required. To determine each party's responsibility, the forensic engineer should perform a review of the project documents to understand the design, design changes during construction, and each party's role in changing and constructing the intended design. This will typically include a review of each party's contract and scope of work.

The initial document review should then be followed-up with an investigation of undisturbed conditions. This investigation will require the selection of an appropriate investigative testing protocol that can replicate the conditions that led to the water leakage, followed by exploratory openings to confirm the condition(s) that led to the water leakage and water leakage paths. Such investigative testing often involves methodical isolation of various building systems and their interfaces.

During the litigation process, the forensic engineer and client should routinely communicate and assess the need for further investigation as the case evolves.

References

1. Seward A. When it leaks it pours. Architect – The Journal of The American Institute of Architects. June 06, 2011 [accessed 2015 December 19] http://www.architectmagazine.com/technology/when-it-leaks-it-pours_o?o=1

2. The project resource manual: CSI manual of practice. 5th edition. Alexandria VA: The Construction Specifications Institute; 2005.

3. ASTM E2128-2012. Standard guide for evaluating water leakage of building walls. West Conshohocken PA; ASTM International.

4. ASTM C1601-2014. Standard test method for field determination of water penetration of masonry wall surfaces. West Conshohocken PA; ASTM International.

5. ASTM C1715-2015. Standard test method for evaluation of water leakage performance of masonry wall drainage systems. West Conshohocken PA; ASTM International.

6. ASTM E1105-2015. Standard test method for field determination of water penetration of installed exterior windows, skylights, doors, and curtain walls by uniform or cyclic static air pressure difference. West Conshohocken PA; ASTM International.

7. AAMA 501.2-2015. Quality assurance and diagnostic water leakage field check of installed storefronts, curtain walls, and sloped glazing systems. Schaumburg IL; American Architectural Manufacturers Association.

8. AAMA 511-2008. Voluntary guideline for forensic water penetration testing of fenestration products. Schaumburg IL; American Architectural Manufacturers Association.

Forensic Engineering Evaluation and Testing of Horizontal Intrusion Protection Equipment for Stand-Up Forklifts

By Ben T. Railsback, M.S., P.E. (NAFE 713S) and Richard M. Ziernicki, Ph.D., P.E. (NAFE 308F)

Abstract

In 2004, a report issued by the National Institute of Occupational Health and Safety (NIOSH) evaluated a fatal stand-up forklift accident where a warehouse forklift operator was crushed against a rack beam after it intruded into the operator's compartment. One of the recommendations of the report was that "Manufacturers of stand-up reach forklifts should include vertical framing or posts at the rear corners of their machines, from the operator's console to the overhead guard, to protect the operator from horizontal components entering the operator's station[1]." Other published studies have also recognized the risk associated with the hazard of a horizontal rack beam entering the operator's compartment of a stand-up forklift. It has been previously reported that there have been at least 250 incidences of horizontal intrusion as of June 2008[2]. The ANSI B56.1 "Safety Standard for Low Lift and High Lift Trucks" has recognized such guarding as permissible since 1993, and almost all stand-up forklift manufacturers have made such guarding standard equipment. The evaluation that is the subject of this paper is related to the fatal horizontal intrusion incident involving a stand-up lift truck (forklift) operated by a 44-year-old male.

Keywords

Stand-up, forklift, horizontal intrusion, under-ride

Introduction

This paper evaluates the performance of the forklift manufacturer's horizontal intrusion* protection system, or posts, through a series of four low-speed collisions with a rack system. The four tests were conducted at increasing kinetic energy levels to first evaluate whether the posts were compliant with ANSI B56.1 and at higher speeds/loading to assure that the operator of the forklift in the subject incident would have been protected by the posts.

The stand-up lift truck in the subject incident is a universal or fore/aft stance truck available with optional horizontal intrusion protection that consists of steel posts connecting the tractor portion of the truck to the overhead guard at the rear corners of the tractor. During this testing, the performance of the horizontal intrusion protection was evaluated based on deflection of the guarding system after a collision at low speed with a typical racking system consistent with the test methodology outlined in ASME/ITSDF/ANSI B56.1[3,4].

Testing shows that the optional steel posts are compliant with the ANSI B56.1 testing requirements and that the forklift operator would not have been crushed in the low-speed collision in the subject incident, had the forklift been equipped with these posts.

Reportedly, the forklift operator was using the stand-up lift truck in a "forks trailing" manner (in reverse) with the operator compartment leading while transporting a pallet of boxed books in the warehouse. The forklift operator was driving the forklift facing in the direction of travel with his left hand on the multi-function controller and his right hand on the steering tiller. As the stand-up forklift approached a rack, the forklift apparently experienced a brake code/braking error immediately before a horizontal rack beam intruded into the operator compartment above the tractor portion and below the overhead guard of the forklift. A police officer with the local sheriff's office described the incident/scene in a supplemental report. The officer stated the following:

* Horizontal intrusion incidents are also referred to as "underride" incidents.

Ben T. Railsback, M.S., P.E. 7185 South Tucson Way, Englewood, CO 80112-3987; (303) 925-1900; brailsback@knottlab.com

"The forklift was driven into an orange in color metal support beam used to hold pallets of books. The forklift was of a design that required the operator to stand upright during operation; no seat was affixed to the forklift. The height of the support beam allowed the forklift body to travel underneath, exposing the operator to the beam as it traveled in reverse. The victim's upper torso impacted the support beam, causing it to become bent."

The bottom of the rack beam pinned the operator to the top of the operator's console in the operator's compartment of the forklift. The operator sustained multiple injuries, including broken/fractured ribs, a transection of the aorta, lacerations to the lungs, laceration of the left hemi-diaphragm with herniation of the stomach and large bowel into the chest cavity, hepatic lacerations, splenic lacerations, transection of the duodenum, lacerations/contusion to the pancreas, and internal bleeding/hemorrhaging. The operator reportedly survived the initial collision, and expired some time after the impact while pinned between the forklift and rack beam.

In conducting this investigation, the following were reviewed: documents related to the incident, the manufacturer's literature (including the parts manual, maintenance manuals, and optional equipment brochure), and the ASME/ITSDF B56.1 standard. This information was referenced in evaluating the incident and developing a testing protocol to analyze the effectiveness of the manufacturer's horizontal intrusion protection relative to the incident. The complete listing of the reviewed documents is provided in **Appendix A**.

An exemplar forklift with the optional horizontal intrusion protection equipment and additional posts were obtained. In addition, vertical uprights, rack beams, and wire decking were obtained.

The authors reviewed the provided documents, analyzed the incident, performed research relative to lift trucks, analyzed engineering standards and literature related to lift trucks and safety, and evaluated the design of the lift truck based on known mechanical engineering and safety engineering principles. As a result of the investigation and testing, this paper addresses the following areas:

- Findings from a review of the incident
- Test protocol developed to evaluate the performance of the manufacturer's horizontal intrusion protection equipment
- Testing results
- Findings and discussion of testing
- Summary of conclusions

Findings from a Review of the Incident

STAND-UP FORKLIFT: The forklift operator was using a narrow aisle, end-controlled forklift with a universal or fore/aft stance. The truck is equipped with a deep or double-reach pantograph (scissor) mechanism that can extend a pallet into a racking system either one or two slots deep. Nominal capacity of the forklift is 3,000 pounds; the manufacturer's truck identification plate indicates that the truck can lift 3,000 pounds to a height of 246 inches (20.5 feet), and its capacity is reduced to 2,800 at a height of 252 inches (21 feet). The forklift has a triple-stage telescoping mast. The top speed of the forklift is 7.5 mph, but this can be electronically limited to a lower speed. The serial number indicates that the forklift was manufactured in 2007. A photograph of the forklift is shown in **Figure 1**.

Figure 1
Stand-up narrow aisle forklift.

The stand-up truck is operated from a "universal" or fore/aft stance. The operator typically faces either directly toward (fore) or directly away from the forks (aft). When the operator faces away from the forks, the operator's left hand is on the multifunction control or joystick, and the right hand is on the steering knob or tiller. In the aft stance, the right foot is the closest to the deadman brake on the floor of the operator compartment. In the fore stance, the feet and hands switch positions. The left hand operates the steering tiller, the right hand operates the multifunction control, and the left foot operates the deadman brake. The incident scene photographs indicate that the forklift operator was using the forklift in the aft stance, facing away from the forks at the time of the incident and in the direction of travel.

The operator's compartment of the forklift, which is located near the right rear corner of the truck, is entered through an opening at the rear of the truck. However, it is protected at the left, front, and right with a steel wall that varies in height from 47 to 50 inches above the ground. Above the steel wall, the operator's compartment is open and unguarded, except at the front of the tractor portion where the mast extends vertically. There is an overhead guard extending from the mast above the operator's compartment intended to protect the operator from falling objects.

RACKING: The racking in the warehouse was labeled with the manufacturer's brand labeling. The vertical upright columns are roll-formed steel with slots for rack beam connections. The rack beams are 5-inch structural steel. The first rack beam was installed with the top of the rack beam at a height of approximately 60 inches above the floor. The manufacturer's brochures indicate that the 108-inch structural beams have a capacity of 8,830 pounds per pair. A photograph of the general configuration of the racking system is shown in **Figure 2**. The racking in **Figure 2** has been modified to lower the first beam in the first section of the racking to a height below 60 inches. The majority of the racking has a first beam height of 60 inches.

The horizontal beam that the forklift operator and the forklift collided with deformed approximately 2½ inches at a location about 80 inches from the left side of the beam and 28 inches from the right end of the beam. The rear beam, wire decking, and beam braces do not appear to have deformed in the collision. The vertical uprights did not deform or appear to sustain damage from the collision either. The forklift operator's body, the forklift, and the rack beam appear to have absorbed all of the kinetic energy associated with the truck and load at the time of the collision.

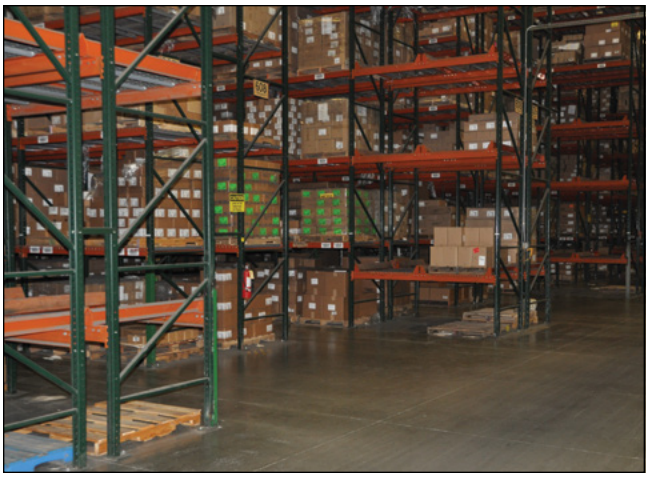

Figure 2
Warehouse rack (modified after the incident).

ENGINEERING STANDARDS: The American National Standards Institute (ANSI) published a standard in 1993 developed under the American Society of Mechanical Engineers (ASME) titled "Safety Standard for Low Lift and High Lift Trucks." In this 1993 revision of the standard, a new section was added, permitting the use of "guards or other means" to limit intrusions (into the operator's area) of horizontal members (e.g., rack beams) oriented generally transverse to the direction of travel. The standard also developed requirements for the performance and testing of the protection. The standard requires a collision between the forklift and a rigid barrier with a 3-inch vertical dimension performed at a speed of 1 mph with a truck carrying a full rated load. The performance of the horizontal intrusion protection is considered acceptable if there is no separation of parts or permanent deflection in excess of 4 inches in the horizontal plane.

Test Protocol Developed to Evaluate the Performance of the Horizontal Intrusion Protection Equipment

The authors developed a testing protocol to determine whether the optional manufacturer's horizontal intrusion protection meets the ANSI B56.1 standard requirements and whether the guarding would have prevented or mitigated the fatal crushing injuries sustained by the operator. The test consisted of four collisions between a section of typical warehouse racking and an exemplar stand-up forklift equipped with the optional

horizontal intrusion protection posts. The tests were conducted at increasing kinetic energy levels with impact speeds of approximately 1.4, 2.4, 2.8, and 3.4 mph. The acceleration distance required for speeds above 3.4 mph limited the top speed utilized in testing. Each test used a new post and new rack beam. Deflection in the post and racking were measured after each test. The forklift, racking, and testing are described below.

FORKLIFT: The forklift utilized for the testing was a narrow aisle, end-controlled, deep or double-reach forklift, with the same model number as the forklift involved in the incident. The serial number of the forklift indicated that the truck was manufactured in 2002 (approximately five years before the subject truck). The truck has a load capacity of 3,000 pounds at a 24-inch load center, and could lift to a height of 240 inches (20 feet). The truck in the incident had a lift height of 246 inches with a 3,000-pound load. **Figure 3** and **4** are photographs of the exemplar truck† (on the left) and the subject truck on the right.

The exemplar truck was equipped with the manufacturer's optional horizontal intrusion protection when it was purchased, and additional replacement posts were purchased through a forklift parts retailer. The retailer represented that the replacement posts were purchased from the forklift manufacturer and then repackaged as originating at the retailer‡. The chemistry and mechanical properties of a post from the retailer and a post from the manufacturer were tested. The chemistry and mechanical properties of the two samples were consistent, and, when combined with representations from the retailer, indicated that both sets of posts originated at the forklift manufacturer§.

Prior to the testing, maximum acceleration of the forklift as a result of maximum throttle input was measured using a SENSR GP1-programmable accelerometer. Maximum forklift acceleration was recorded to be approximately 0.06 g. Forklift acceleration appeared to remain relatively constant until top speed was achieved.

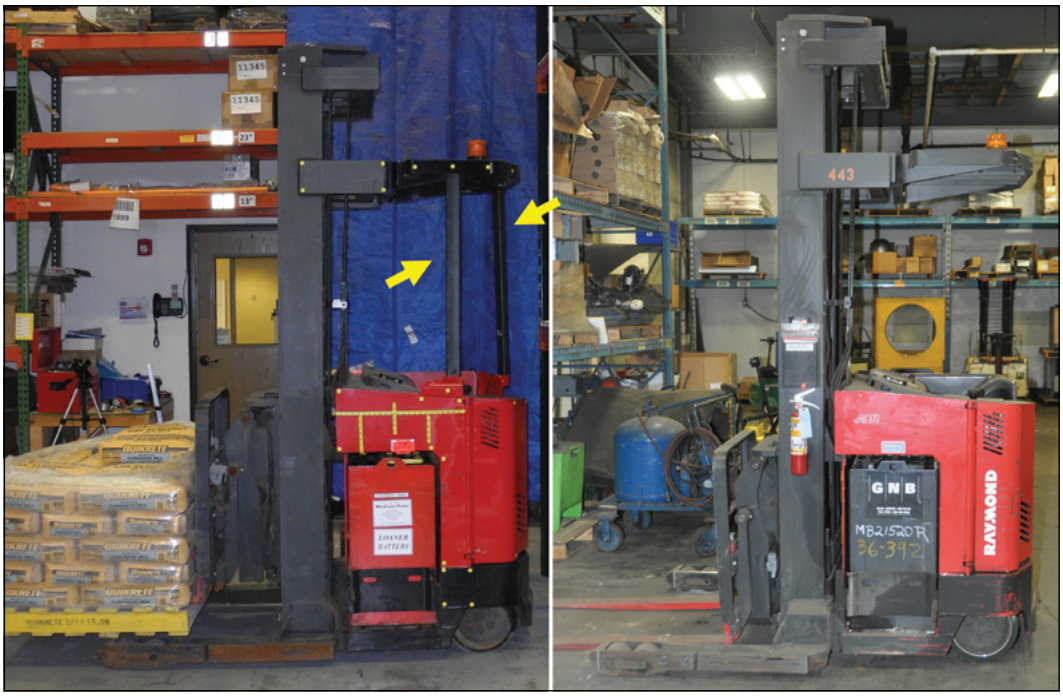

Figure 3
Exemplar truck with horizontal intrusion post protection (left) and subject truck without posts (right).

† The lift truck has been marked with round, yellow stickers and marking tape as a part of the testing.
‡ Despite ordering replacement posts based on the specific serial number associated with the forklift, the manufacturer supplied the retailer with posts longer than the posts on the truck. Because of the excess length, the authors cut the supplied posts to match the length of the post on the forklift, and a new mounting hole(s) was drilled. After the modification, the replacement posts matched the geometry of the original post. Additional posts were supplied that were obtained from the manufacturer's dealership using the serial number of the forklift. The posts supplied by the manufacturer's dealership were the same length as the posts supplied by the retailer.
§ Mechanical and Chemistry Testing Report prepared by Colorado Metallurgical Services, June 25, 2014.

Before the test, the multifunction controller of the forklift was removed from the operator compartment and extended outside of the operator compartment with an additional cable. The deadman brake pedal was disabled with weight to allow motion of the forklift without an operator present.

RACK: Vertical uprights, rack beams, and wire deck panels were used to conduct the collision testing. The vertical uprights were roll formed, slotted uprights (42 inches in depth and 12 feet in height). The uprights have a capacity of 22,100 pounds at a 48-inch lateral spacing. The rack beams were roll formed step beams (108.37 inches long and 4.65 inches tall). The beams have a manufacturer's rated capacity of 6,320 pounds per pair, with a factor of safety of 1.67 based on minimum yield strength of the steel. The decking was galvanized wire that was 42 inches deep and 52 inches wide with a capacity of 2,500 pounds.

The uprights were installed in a concrete floor using ½-inch x 5-inch wedge anchors. Two anchors were used per post leg (eight anchors total), utilizing all of the available mounting holes. Two rack beams and decking were installed at a height of 60 inches. A second pair of beams was installed at a height of 120 inches.

TESTING: During the first test, there was no load on the rack frame. In the second, third, and fourth tests, a nylon ratcheting strap was placed at each end of the rack and anchored to the floor using wedge anchors and angle iron brackets. The tension in each strap was approximately 1,000 lbf, simulating a 4,000-pound load on the rack system. Further, two sit-down forklifts were placed behind the rack system with masts raised and load carriages placed against the top of the rear of the rack system to increase the rigidity of the rack structure. **Figure 4** is a photograph of the forklift and rack configuration during the first test, and **Figure 5** shows the rack configuration for the subsequent tests. The simulated load and forklift placed behind the rack increased the rigidity or stiffness of the rack section.

Figure 4
Stand-up forklift and rack configuration during first test.

Figure 5
Rack configuration during second, third, and fourth test: Nylon ratcheting straps at each end of rack frame and sit-down forklifts. (Note that the 2x4 wood pieces in the foreground provide no structural support and are not part of the test equipment.)

Testing Results

The four tests of the manufacturer's posts were conducted at increasing speed and kinetic energy levels. The truck was accelerated for distances of 1, 3, 6, and 7 feet, respectively, to achieve the increase in speed prior to the collision. The tests are labeled sequentially 1-4 for the increasing distances. Tests labeled with an "L" denote a post supplied by the manufacturer through the retail parts distributor. The final test labeled "RL" denotes a post supplied by the manufacturer's dealer. **Table 1** summarizes the maximum impact speeds, peak kinetic energy levels, and peak accelerations (decelerations during the collision) achieved during testing. Impact speeds were obtained through numerical integration of the accelerometer data, and kinetic energy was calculated based on that impact speed and a mass of 11,178 pounds (truck

weight of 8,178 pounds and load of 3,000 pounds). Kinetic energy levels are reported for comparison of the testing to other incidents, since the load on the forks during testing represents 25% of the overall mass involved in the test collisions, and other incidents may or may not include a load on the forks. Peak accelerations are reported based on both raw accelerometer data and on a peak acceleration based on a 20-point moving average of the data for noise reduction (representing an average acceleration over a 200 millisecond time span). The peak acceleration reported is related to the maximum collision force and the acceleration (deceleration) that the operator will be subjected to. However, the noise in the accelerometer data (apparent in the oscillation between positive and negative acceleration values) shows that vibration and/or noise is overstating the peak acceleration values. Therefore, the authors concluded that further noise reduction was necessary to report meaningful peak accelerations. The accelerometer acquires data at a rate of 100 samples per second (100 Hz). A 20 point moving average reports the average acceleration over the last 20 points of data (200 milliseconds), removing most of the noise associated with vibration in the accelerometer in the system. Acceleration, velocity, and distance traveled by the forklift during the tests are presented in **Appendix B**.

The four tests produced increasing deflection in the rack beam and rack system but little or no deflection in the horizontal intrusion post. Post deflections are shown in **Table 2**. Post deflection or deformation was measured while the post was still installed on the forklift, and then again after removal from the forklift. Values of maximum deflection differ between the two methods because the first method reflects slight shifting of the post during the test relative to the weldment mounts, while the latter method documents only deformation in the post. **Figure 6** is a photograph of the posts after testing with little visible deflection.

Test	d (ft)	V (mph)	KE (ft *lbf)	Peak Acc. (g)	Peak Acc. 20 pt. (g)
1L	1	1.37	701	.87	.34
2L	3	2.42	2187	1.5	.52
3L	6	2.80	2927	1.2	.73
4RL	7	3.40	4316	1.37	.74

Table 1
Impact speeds, kinetic energy and accelerations. “L” denotes a post supplied by the manufacturer through the retail parts distributor. “RL” denotes a post supplied by a manufacturer’s dealer.

	Maximum Deformation On Truck (in.)	Height at Max. (in.)	Maximum Deformation of Post (in.)	Distance From Top of Post (in.)
1L	0.028	39	0	20
2L	0.052	29	0.063	20
3L	0.229	27	0.188	20
4RL	0.112	32	0.125	20

Table 2
Post deformation.

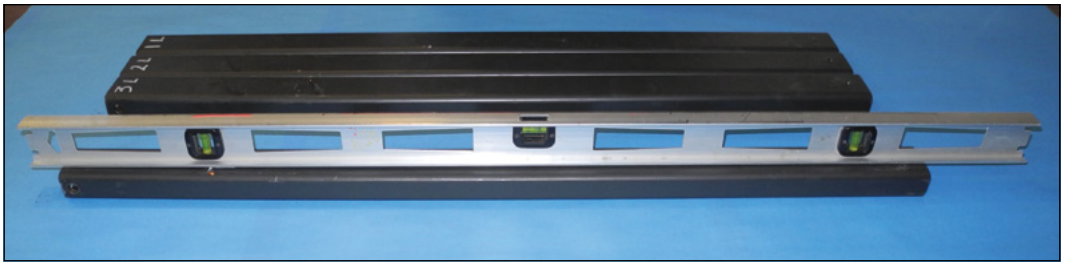

Figure 6
Posts after collision testing – little visible deflection.

Rack beam deformation is shown in **Table 3**. The deformation distance reported is the maximum deformation of the rack beam relative to the two ends of the beam. The test attempted to replicate the distance from the vertical upright during the subject incident of 28 inches; however, the forklift was driven into the rack, and the impact location varied slightly. The distance from the vertical upright is reported in **Table 3**. Static deformation of the rack system was also documented by the total distance that the forklift traveled after contact with the rack beam and consists of both rack beam deflection and the deformation of the rack system. While the forklift remained in close proximity to the area of contact in the first, second, and third test, it rebounded several inches in the fourth test. Therefore, forklift travel measured at rest after contact under-reports total rack deformation in the fourth test. In the first test, the vertical uprights deformed significantly while the rack beam did not. In the second and third tests (with the added reinforcement), the deformation occurred primarily in the rack beams, while the vertical uprights remained undeformed. In the fourth and final test, the rack beams and vertical uprights both deformed. **Figure 7** displays the deformed end of the rack beams after testing.

	Maximum Deformation of Rack Beam (in.)	Distance from Left End (in.)	Forklift Travel After Contact (in.)
1L	0.56	29	5.3
2L	6.13	25	6.6
3L	6.0	22.5	6.5
4RL	9.5	15	9.25

Table 3
Rack beam deformation and forklift travel after contact.

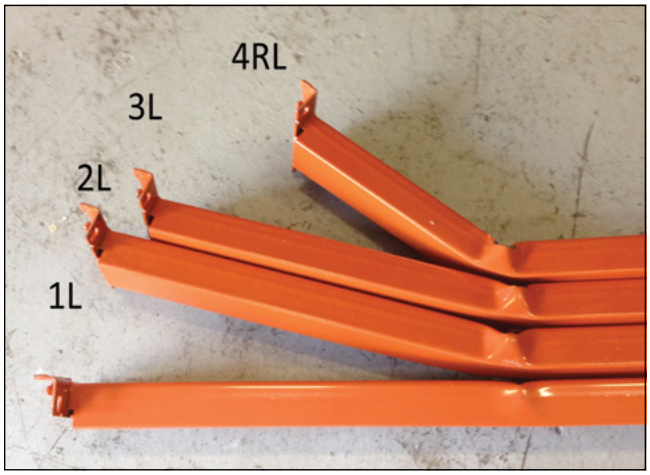

Figure 7
Deformed rack beams after testing.

Findings and Discussion of Testing

COMPLIANCE OF HORIZONTAL INTRUSION PROTECTION WITH ANSI B56.1: The primary requirements of the ANSI B56.1 test are an impact transverse to the direction of travel, an impact speed of 1 mph, and a rigid barrier simulating a rack beam with a 3-inch vertical dimension. Each test described in this paper exceeds the speed requirements of ANSI B56.1. The rigidity of the barrier requirement within the ANSI standard is not well defined; however, the racking used in the testing is prevalent throughout warehouses and distribution centers. The 4.65-inch vertical dimension of the rack beams exceed the height requirement in the B56.1 standard, which results in a higher moment of inertia in resistance to loading and bending. The first and fourth test dissipated energy in the rack beam and vertical uprights, while the vertical uprights remained undamaged in the second and third tests. The performance requirements of ANSI B56.1 specify no separation of parts or permanent deflection in excess of 100 mm (3.9 inches) in the horizontal plane. The manufacturer's horizontal intrusion posts and forklift tested met this requirement after four successive tests of increasing impact speed and energy levels. Based on the testing performed as a part of this research, the horizontal intrusion protection system of posts offered by the manufacturer met or exceeded the test requirements of B56.1.

The majority of the stand-up forklifts currently available on the market have some form of horizontal intrusion protection. The subject manufacturer's counter-balance stand-up trucks and sit/stand model of a reach truck also incorporate some horizontal intrusion protection. Given that the majority of forklift manufacturers have adopted standard horizontal intrusion protection, the benefits or utility of the protection clearly outweigh any trade-offs associated with the horizontal intrusion protection. Therefore, it is the authors' recommendation that the permissive language within the ANSI B56.1 standard should be modified to "require horizontal intrusion protection."**

The authors also recommend that the performance requirements of the ANSI B56.1 standard be strengthened in regard to horizontal intrusion protection. The

** It is the authors' further recommendation that the horizontal intrusion protection should not require modification of the end user's facility to make the horizontal intrusion protection effective. Vertical posts connecting the tractor to the overhead guard and extended backrests have proven effective in testing without significant modification.

maximum speed of stand-up forklifts is significantly higher than the performance requirement within the standard. The section within the standard regarding horizontal intrusion protection is also more than 20 years old. Manufacturers, including the subject manufacturer, have had more than sufficient time to develop robust horizontal intrusion protection equipment that can meet more stringent requirements than the current standard has.

ANALYSIS OF THE TESTING IN REGARD TO THE SUBJECT INCIDENT: While the subject incident apparently occurred as a result of a braking (plugging)†† failure with the forklift, other horizontal intrusion incidents also appear to have occurred through operator error or foreseeable misuse of the forklift. Regardless of the cause of the horizontal intrusion incident, the need for effective, standard operator protection is clear. The amount of deflection of the protective structure is the primary method of assessing the effectiveness of the horizontal intrusion protection because it determines how much intrusion will occur into the operator compartment. The subject incident produced a maximum deflection of 2½ inches of deformation in the rack beam that the operator and forklift collided with. The other components within the rack system appear undamaged, indicating that all of the kinetic energy of the forklift was absorbed, crushing the operator and damaging the rack beam. The testing performed in this research all produced more deformation (either in the vertical uprights or the rack beams) than the subject incident did. While the test performed at 1 mph produced less deformation in the beam than the subject incident, the vertical uprights were deformed at both ends of the rack. Further, the collision at approximately 2 mph produced 2.5 times as much deformation in the beam. While considering the difference between the testing and the incident (a rigid vertical beam colliding with the rack compared to the operator involved in the incident), the testing in this research shows that the subject incident occurred at a speed on the order of 1 mph, given the greater deflection in the 1 and 2 mph tests.

The authors consulted with another retained expert who analyzed the collision force and speed using a finite element analysis (FEA) of the rack system. The FEA indicated that the collision occurred at a speed between 1.9 mph and 3.0 mph. The FEA utilized assumptions that would produce maximum speeds rather than minimum speeds to consider the upper boundaries of the impact forces and speed. The FEA model was limited to the rack beams and end connections, and did not reproduce the whole system. Considering the FEA and the testing using similar (but not identical) rack components, the authors concluded (using this alternate analysis) that the collision occurred at a speed on the order of 2 mph. Both the testing and FEA analysis show that the collision took place at a low speed/energy level in comparison to a lift truck moving at full speed with a maximum capacity load.

Of foremost importance, the testing performed as a part of this research further shows that the manufacturer's horizontal intrusion protection was effective at a speed of 3.4 mph with a full load. The protection would therefore be effective at higher speeds as well. Since the subject forklift involved in the incident was reportedly operating with a load of approximately 972 pounds, the load used in this testing exceeded the load in the incident. Further, the incident occurred at a speed lower than the maximum test speeds — and at a significantly lower amount of kinetic energy. Even at a higher load, higher impact speed, and higher kinetic energy, the rack beam was held outside of the operator compartment by the post guarding system. Since the rack beam did not significantly intrude in the operator compartment, the volume or space required by the operator was not compromised. **Figures 8** and **9** show that the operator compartment space was maintained during the fourth test at 3.4 mph. Therefore, it is clear that the manufacturer's horizontal intrusion protection system would have prevented the crushing injuries sustained by the operator.

†† Plugging is the process of reversing the directional control (joystick) and using the electric motors to decelerate the forklift.

Figure 8
Operator able to stand inside compartment after fourth test.

Figure 9
Deformed rack beams outside of operator compartment after the fourth 3.4-mph test.

Conclusions

This study evaluated the effectiveness of a horizontal intrusion protection system. The system was found to be effective at preventing intrusion into the operator compartment on a fully loaded forklift at a speed of 3.4 mph — well in excess of the requirements of the ANSI B56.1 standard. The minimal deflection that occurred in the system at a collision speed of 3.4 mph shows that the system would be effective at higher speeds as well. The optional equipment provided by the manufacturer meets and exceeds the B56.1 standard, and provides protection in the event of a horizontal intrusion incident.

The subject incident occurred on a narrow aisle stand-up forklift at a speed on the order of 2 mph with a less-than-maximum load at less than the maximum speed of the forklift. While the optional horizontal intrusion protection offered by the manufacturer for the forklift would not have prevented the subject collision, it would have prevented the operator from being crushed between the rack beam and the forklift.

Appendix A

- Forklift arrival inspection checklist
- Autopsy report
- Sheriff's office news release
- Patient care report
- Sheriff's investigation report
- OSHA investigation
- News article
- Obituary
- Forklift photo index
- Forklift schematics
- Forklift incident news articles
- Incident site photographs

Appendix B

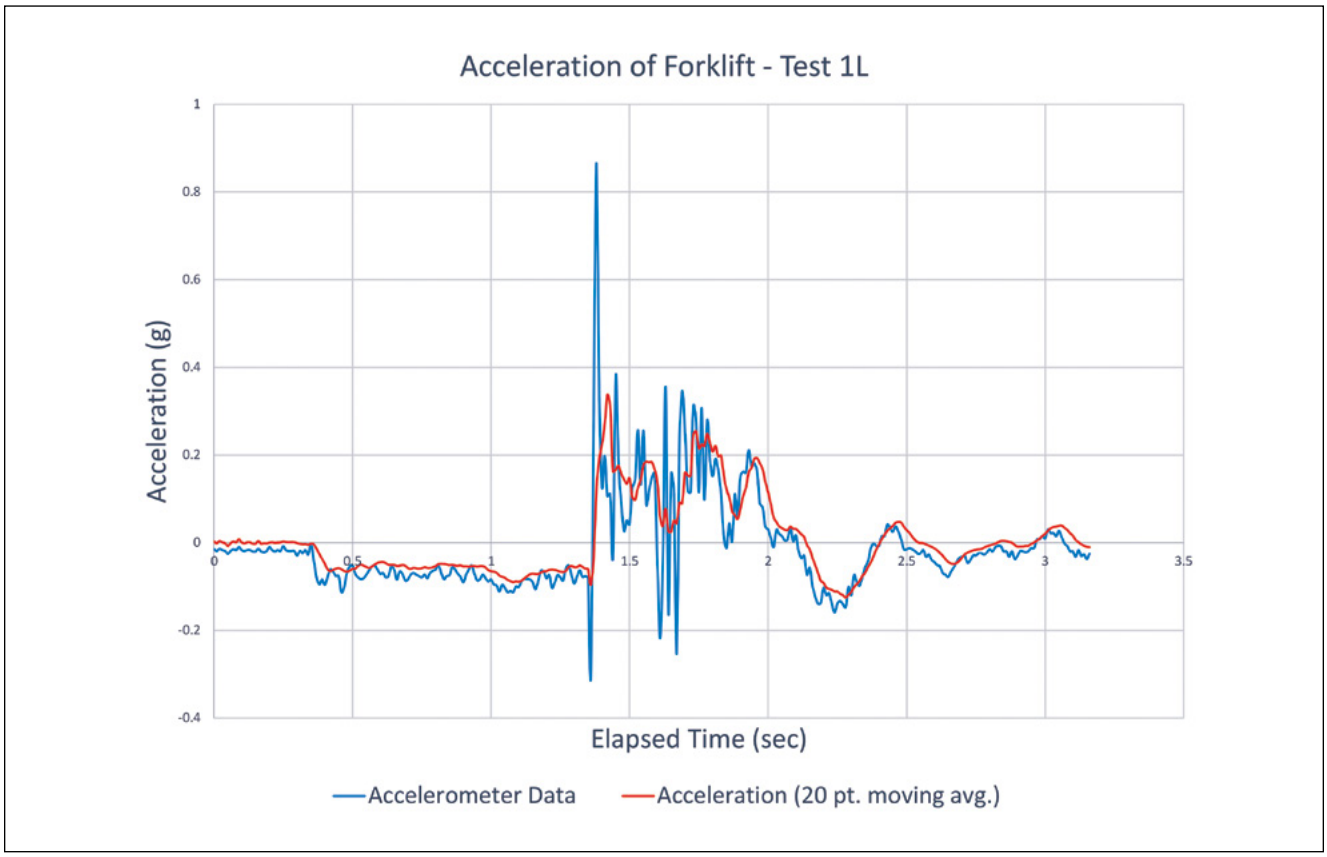

Appendix B-1

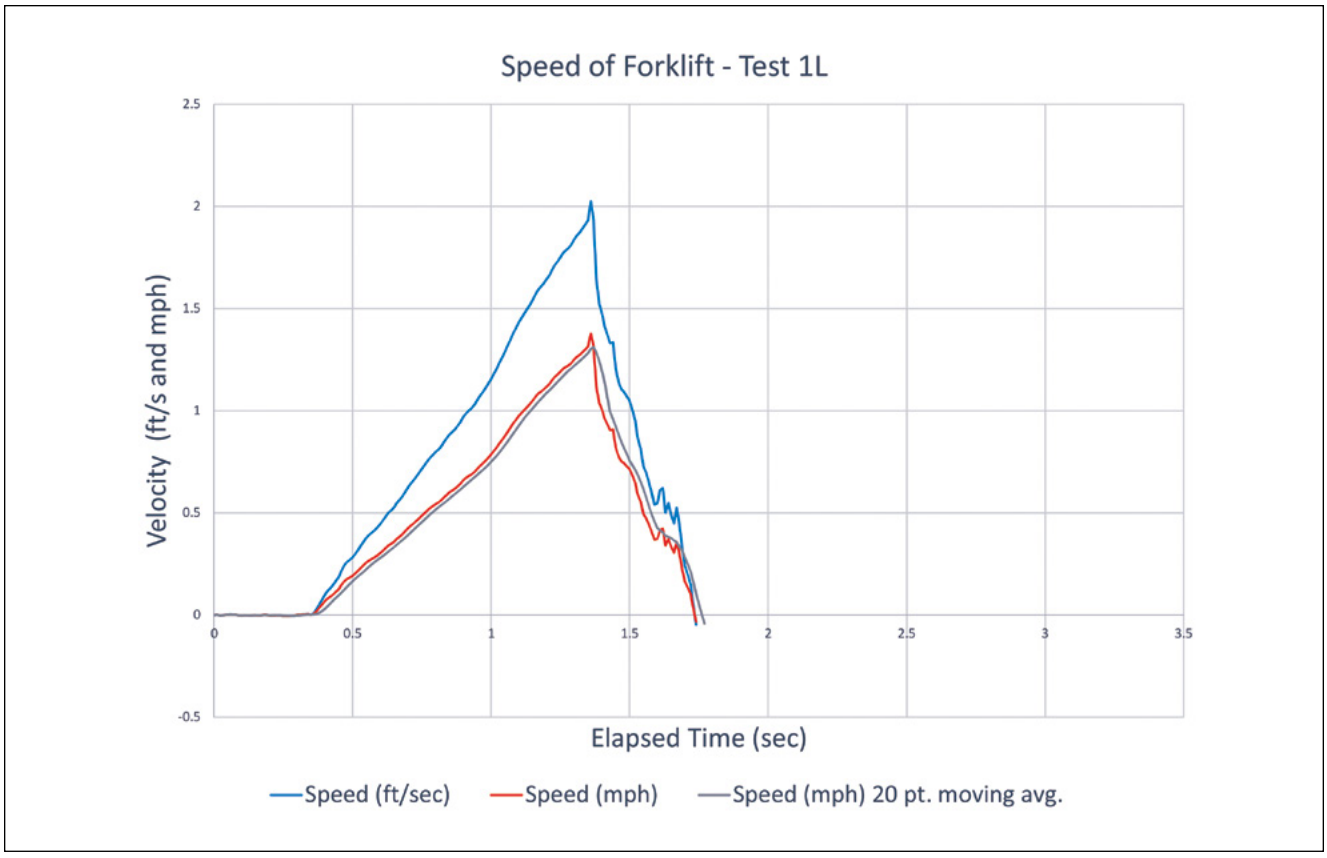

Appendix B-2

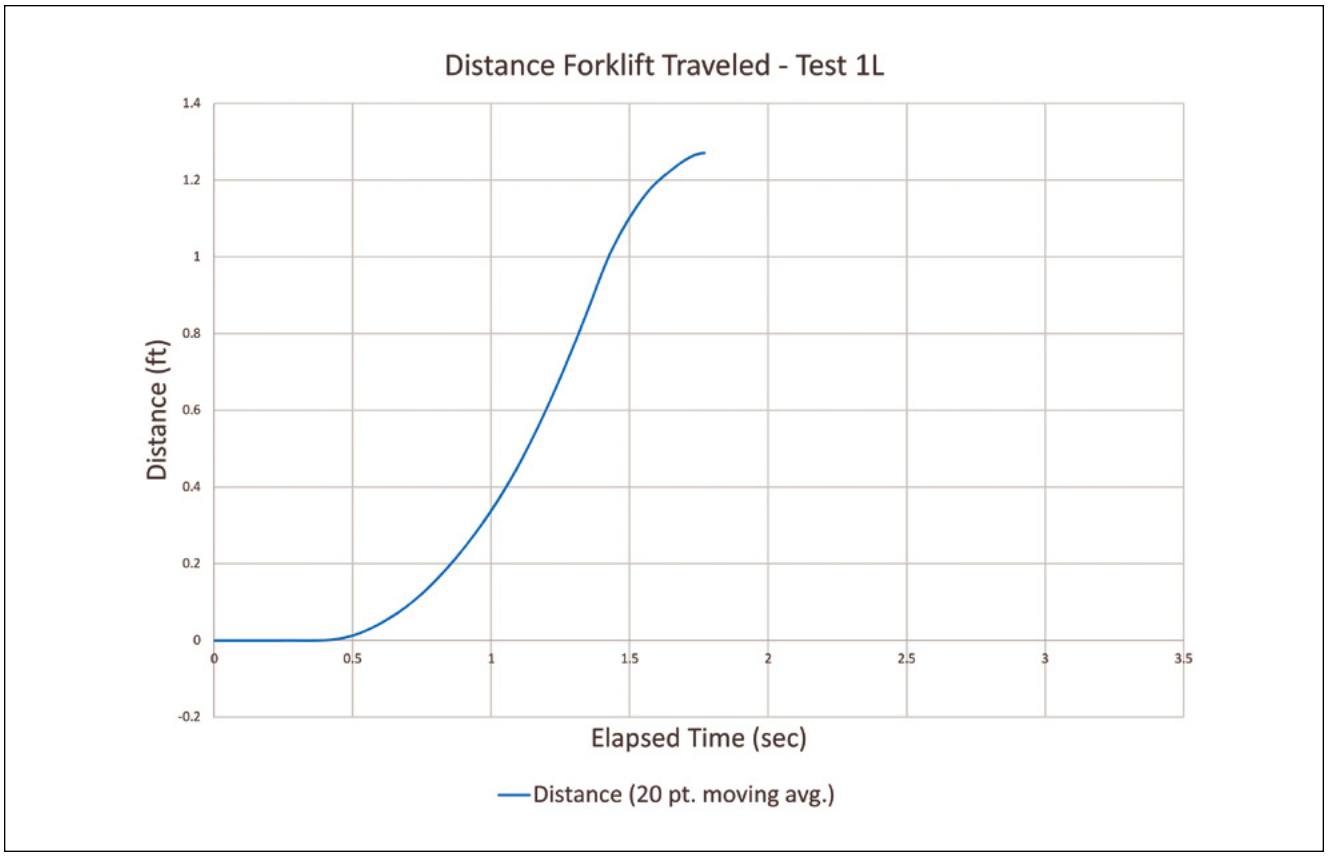

Appendix B-3

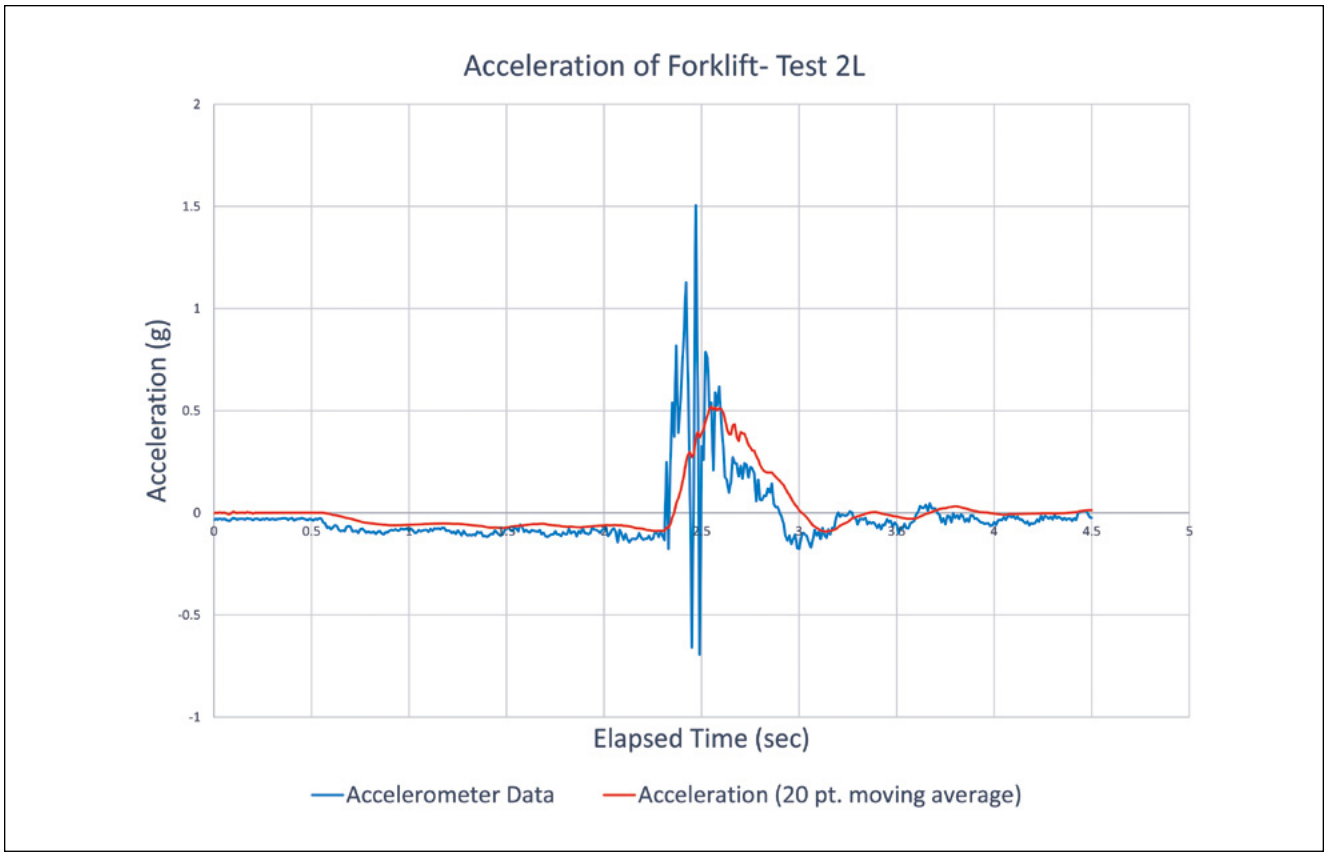

Appendix B-4

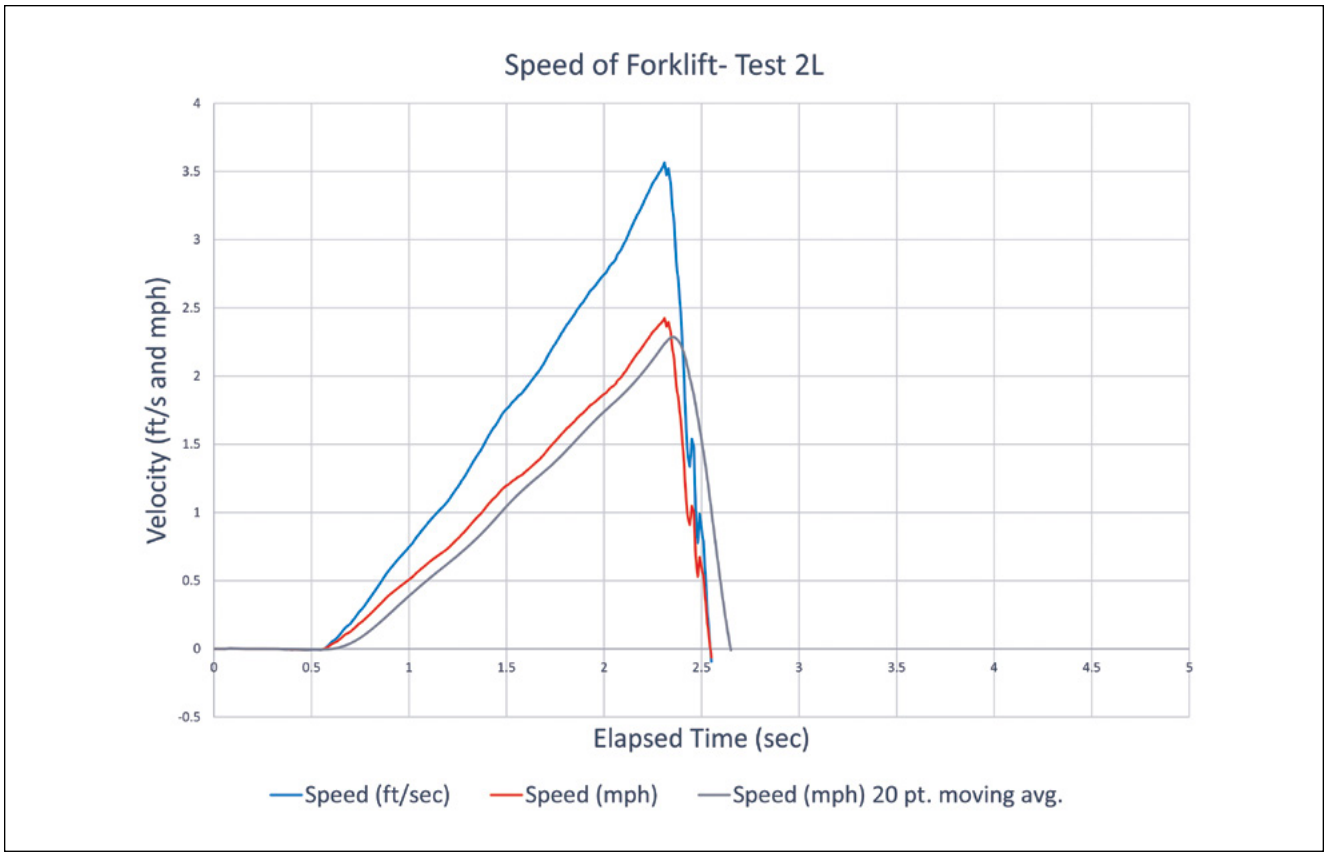

Appendix B-5

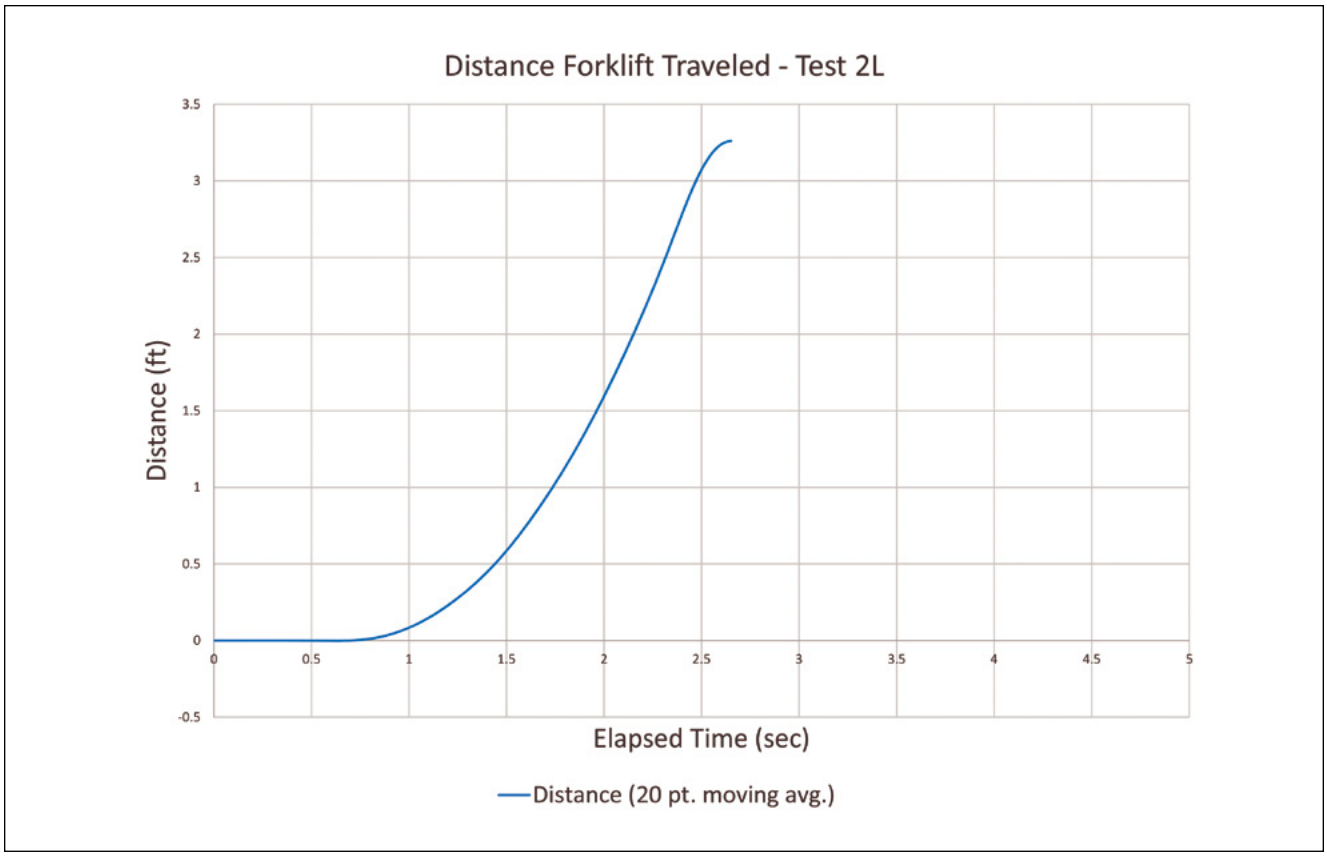

Appendix B-6

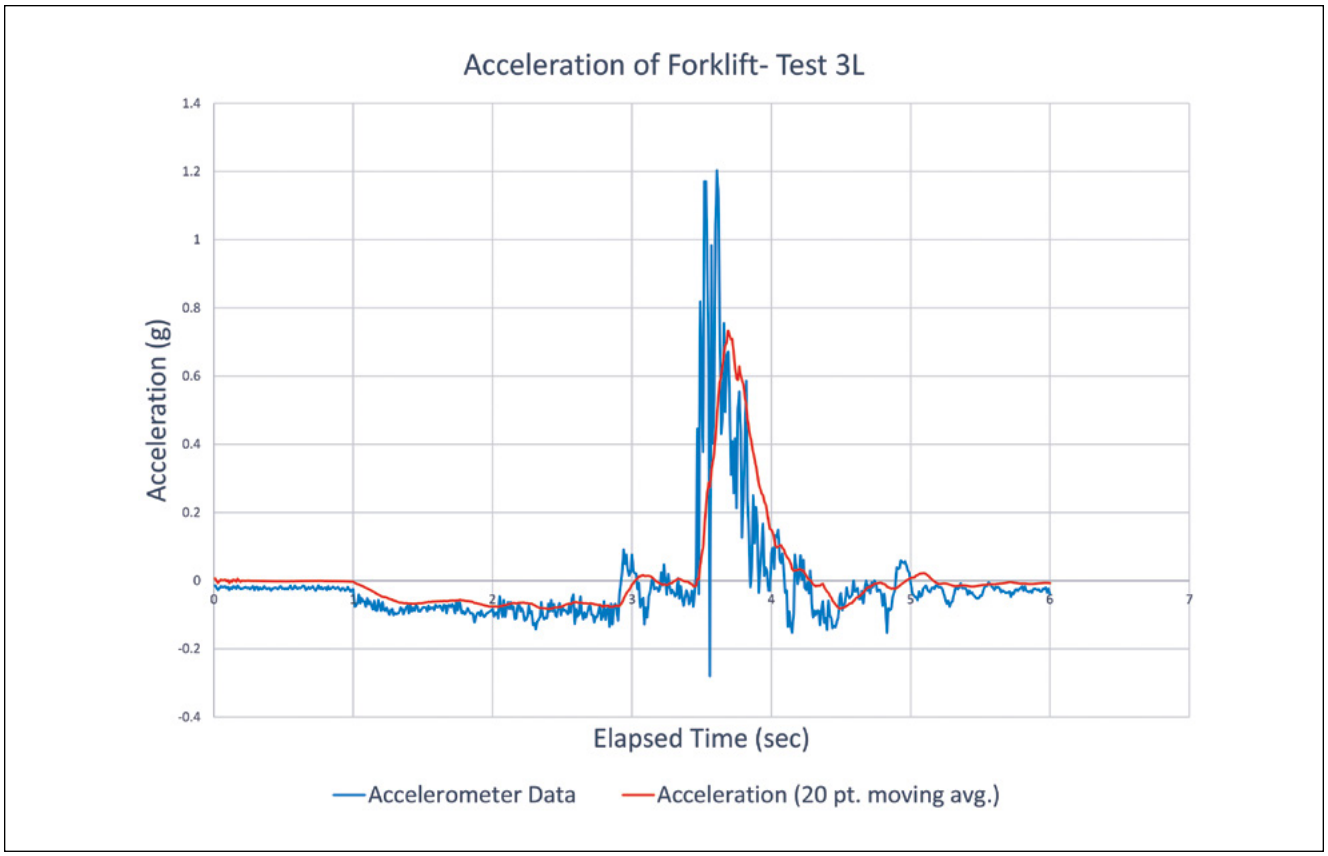

Appendix B-7

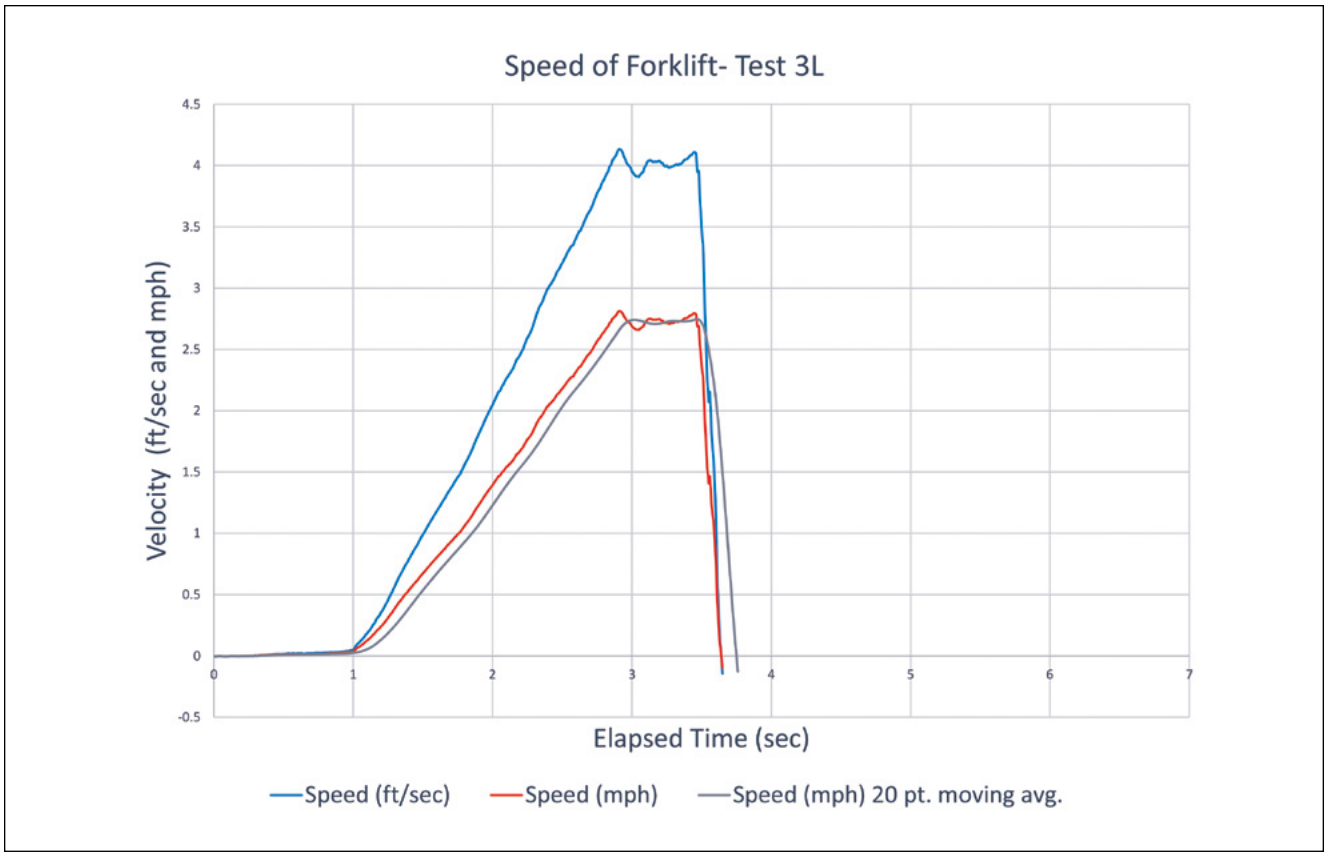

Appendix B-8

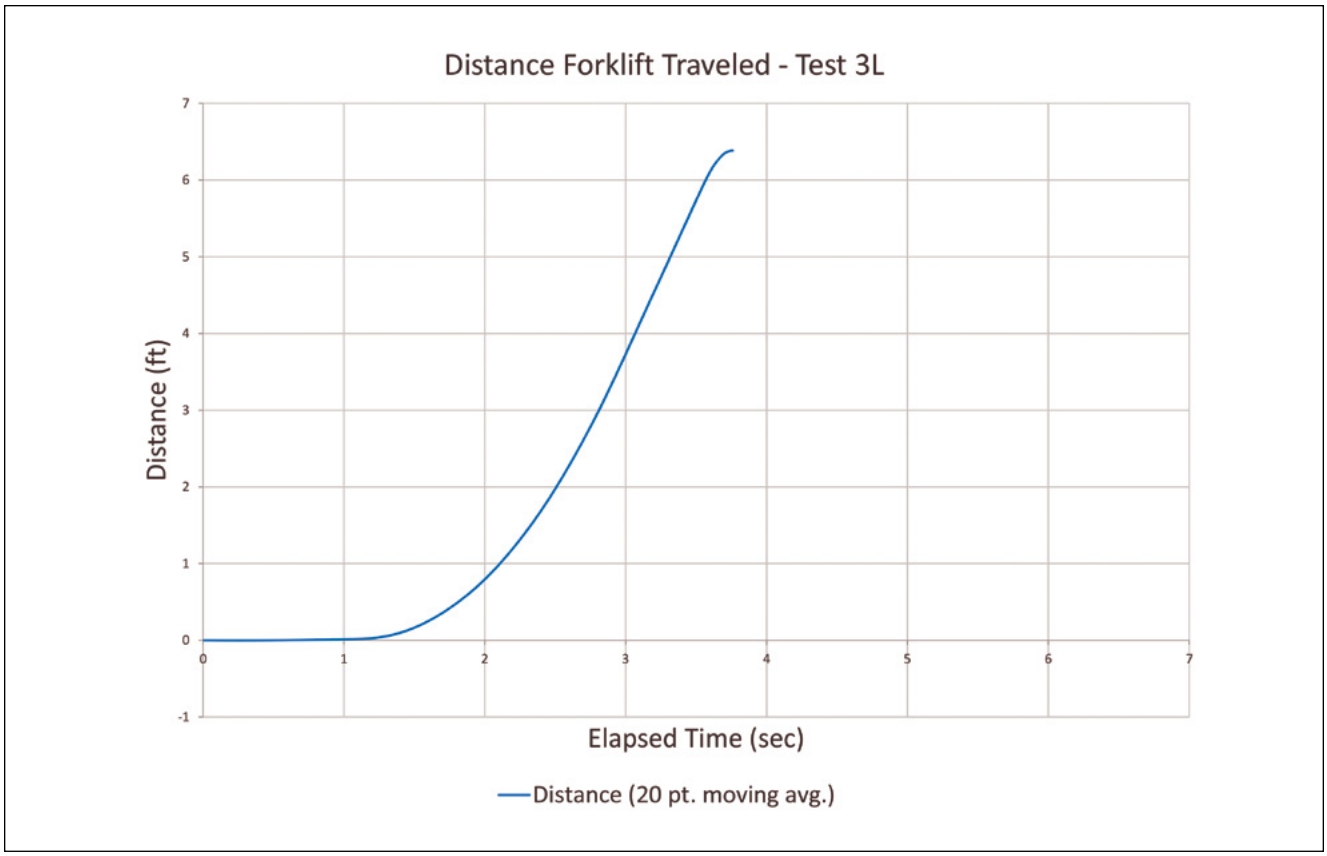

Appendix B-9

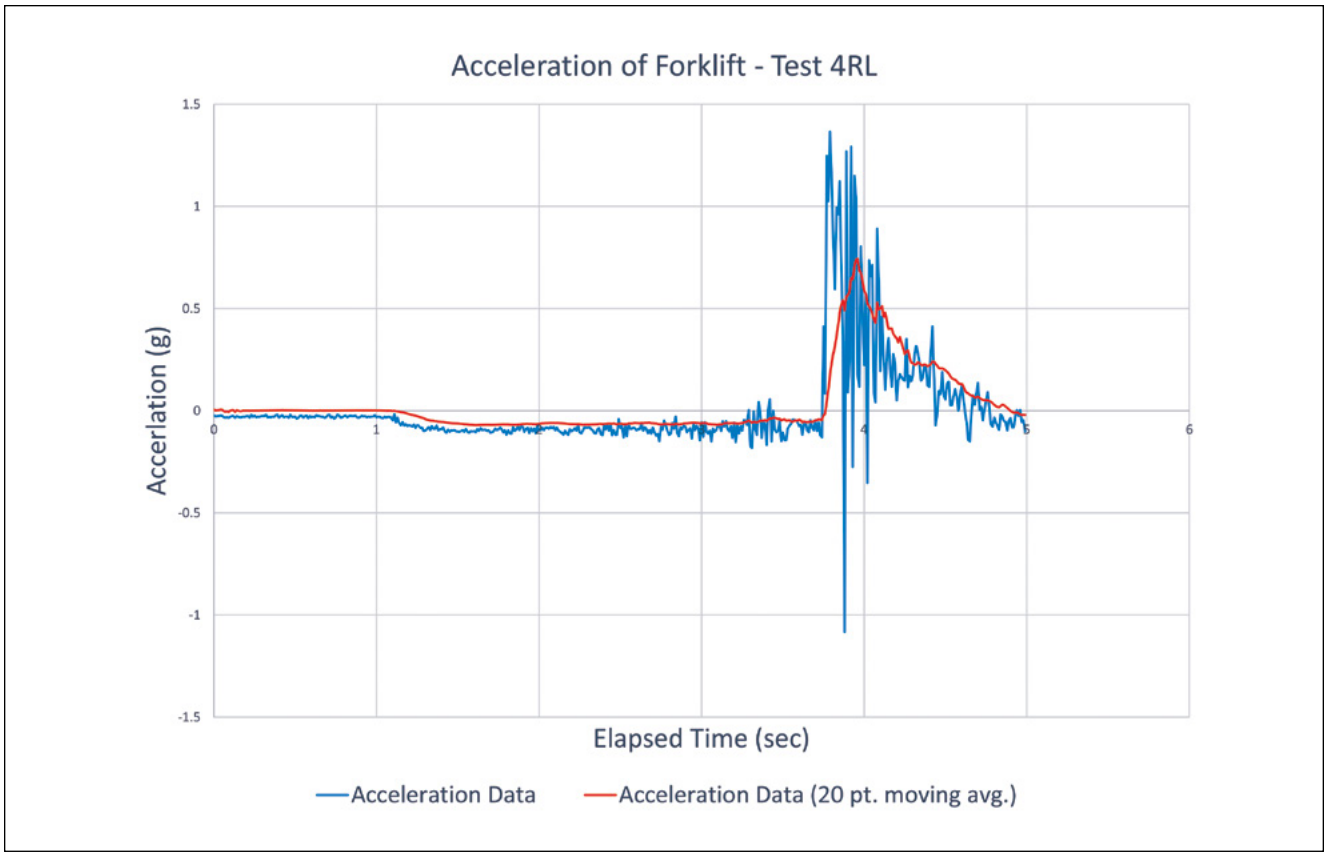

Appendix B-10

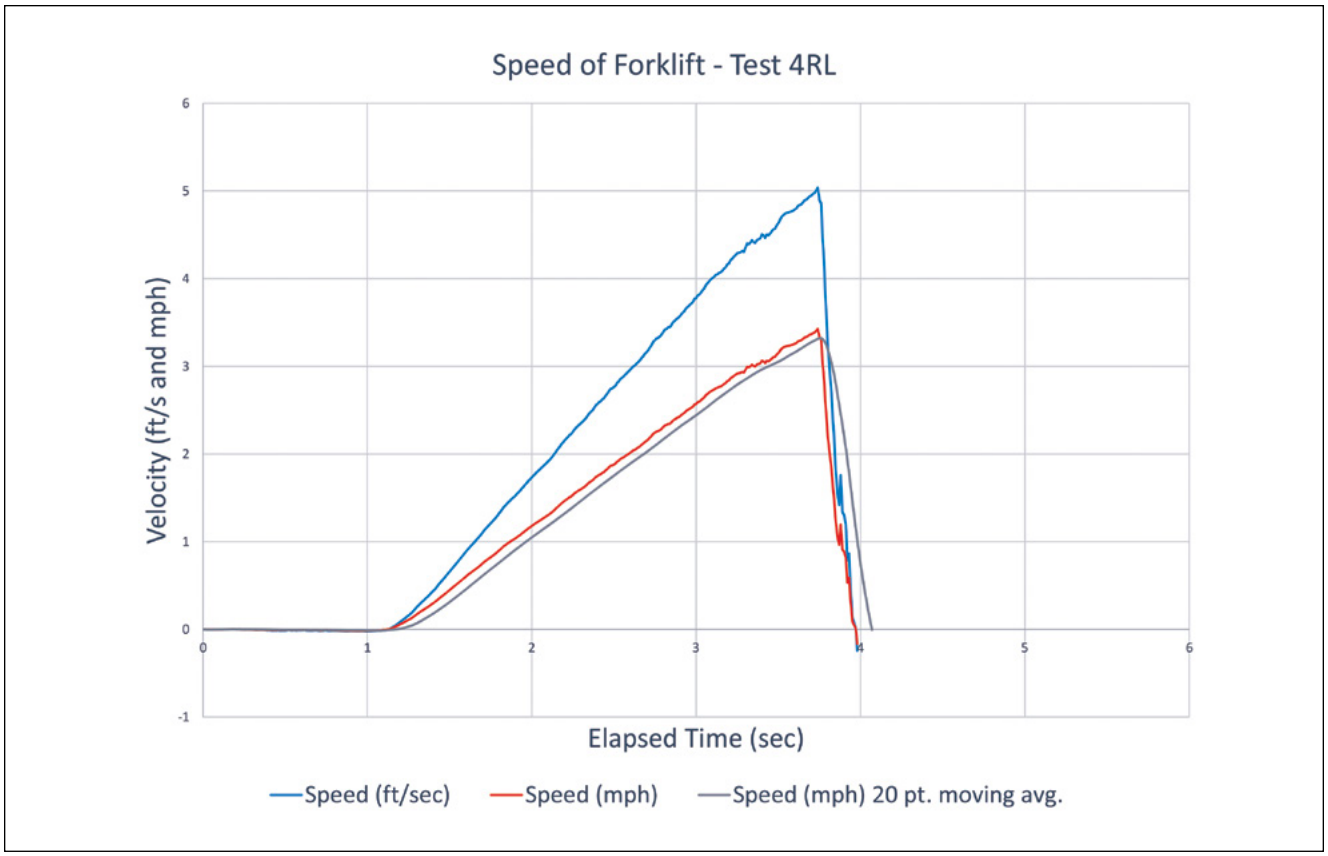

Appendix B-11

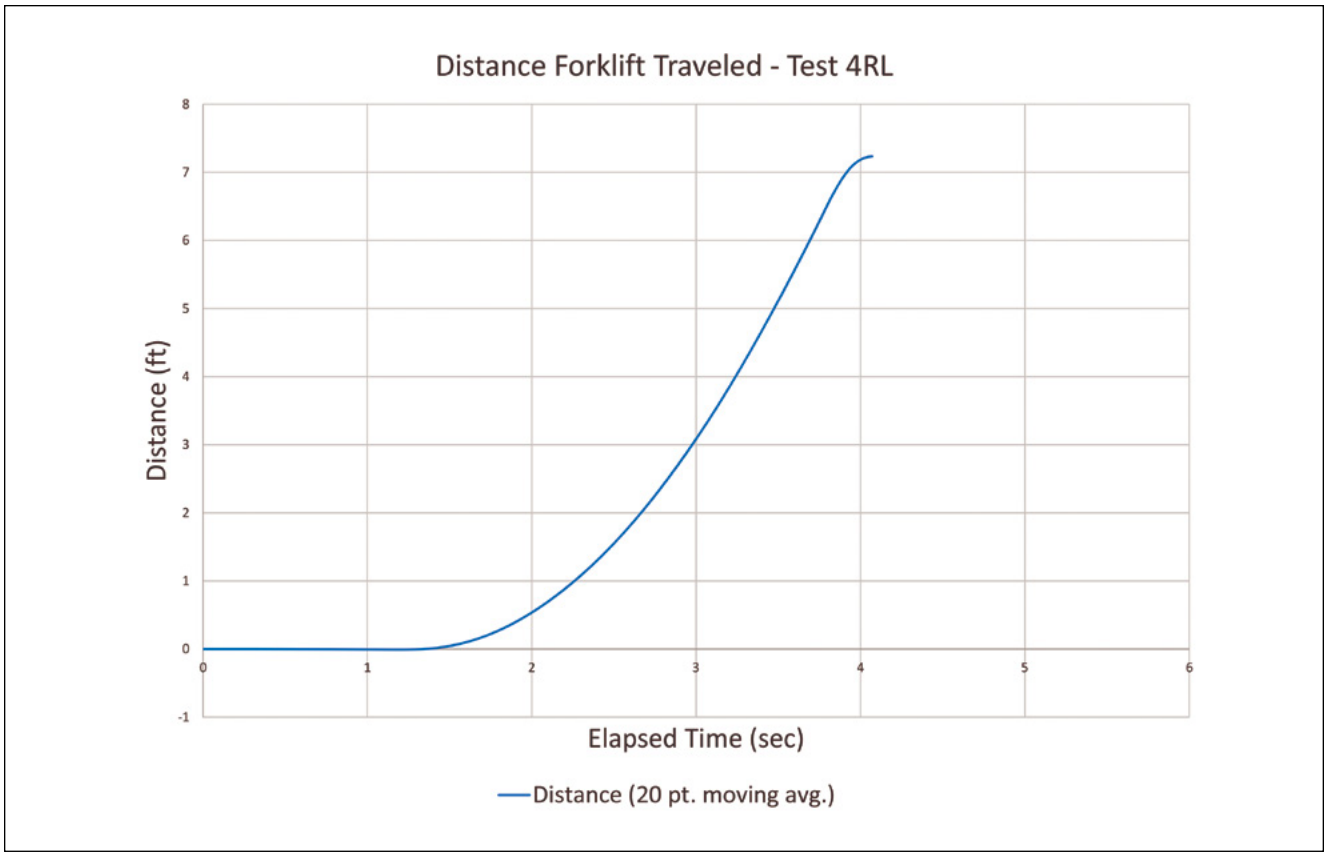

Appendix B-12

References

1. Warehouse forklift operator crushed against rack beam, case report 03IA057. Atlanta GA: National Institute for Occupational Safety and Health (NIOSH); August 24, 2004. http://www.cdc.gov/niosh/face/stateface/ia/03ia057.html.

2. Ziernicki R, Railsback B. Forensic engineering assessment of safety for stand-up forklifts. Journal of the National Academy of Forensic Engineers. 2008; 25(1):73-88.

3. ANSI/ASME B56.1-1993. Safety standard for low lift and high lift trucks. New York NY; American Society of Mechanical Engineers.

4. ANSI/ ITSDF B56.1-2012. Safety standard for low lift and high lift trucks. Washington DC; Industrial Truck Standards Development Foundation.

Forensic Engineering Applications of the G-DaTAΔV™ System of Equations to Real-World Collisions

By Jerry S. Ogden, Ph.D., P.E. (NAFE 561F)

Abstract

Analysis of vehicle deformation from impacts largely relies upon A and B stiffness coefficients for vehicle structures in order to approximate the velocity change and accelerations produced by an impact. While frontal impact stiffness factors for passenger vehicles, light trucks, vans, and sport utility vehicles are relatively prevalent for modern vehicles, stiffness factors for rear and side structures, as well as heavy vehicles, buses, recreational vehicles, trailers, motorcycles, and even objects, are essentially non-existent.

*This paper presents the application of the Generalized Deformation and Total Velocity Change Analysis to real-world collision events (**G-DaTAΔV™ System of Equations**) as developed by this author. The focus of this paper addresses the relative precision and accuracy of the G-DaTAΔV™ System of Equations for determining the total velocity change for oblique and/or offset vehicle-to-vehicle collisions involving light trucks and sport utility vehicles, which are largely under-represented with modern vehicle A and B stiffness values for side and rear surfaces. The previous paper presented by this author to the Academy addressed the relative accuracy and precision of the G-DaTAΔV™ System of Equations as they relate to a first validation using the RICSAC-staged collision database[1]. As a secondary and more comprehensive validation process, the G-DaTAΔV™ System of Equations will be applied to real-world collision data obtained through the National Automotive Sampling System (NASS), which provides the National Highway Traffic Safety Administration (NHTSA) with a comprehensive compilation of real-world collision events representing a broad-based collection of collision configurations from across the country. This data represents a reusable source of information that was collected using standardized field techniques implemented by NASS-trained field technicians. Through using a "core set of crash data components," NASS has demonstrated its utility and applicability to a vast array of statistical and analytical studies regarding traffic safety and vehicle collision dynamics[2].*

Keywords

Forensic engineering, force deflection, damage analysis, missing vehicle stiffness, total velocity change, crush energy, G-DaTAΔV™ System of Equations

Background

The G-DaTAΔV™ System of Equations, as presented in this Journal previously[1], provides the following significant advancements and/or enhancements to modern vehicle deformation-based analysis methodologies:

- Eliminates the dependence upon multiple structural stiffness coefficients for permanent vehicle structural deformation analysis, regardless of the impacted surface and vehicle type involved.
- Account for oblique and off-set collisions that result in principal direction of force that do not pass through the mass centers of vehicles and produce rotation.
- Account for inter-vehicular friction due to the colliding surfaces of vehicles sliding during the approach velocity change of an impact.
- Account for external tire-ground forces during the approach velocity change of an impact.
- Define the total velocity change resulting from any collision event, which considers the velocity

Jerry S. Ogden, Ph.D., P.E., P.O. Box 621519, Littleton, Colorado 80162-1519; (303) 795-1515; jogden@OEC4N6.com

change resulting from linear and rotational momentum (conservative forces) as well as the contributions due to inter-vehicular friction and tire/ground forces (non-conservative forces).

The G-DaTAΔV™ System of Equations showed excellent correlation to the RICSAC test data with an $R^2 = 0.989$ for piecewise damage profile analysis and an $R^2 = 0.991$ for the weighted average damage profile analysis. The $\chi^2 = 1.06$ for the piecewise and $\chi^2 = 1.08$ for the weighted average damage profile analysis methodologies ($\alpha = 0.99$, $n = 23$), which indicates the difference between the total velocity changes for the RICSAC tests and calculated values using either G-DaTAΔV™ System of Equations methodological approach, is not statistically significant when applied to the RICSAC-staged collision testing[1].

G-DaTAΔV™ Analysis Procedure

As mentioned, the application of the G-DaTAΔV™ System of Equations was outlined previously by this author[1]. In order to maintain uniformity between studies, the equation numbers from reference 1 will be used in this paper for the equations of the G-DaTAΔV™ System of Equations. Analysis using this approach starts with the documentation of vehicle deformation profiles for each vehicle into the form demonstrated in **Figure 1**.

After tabulating the deformation profiles for the numerical analysis, the following general analytical steps provide the *total velocity change* for two colliding vehicles:

1) Obtain vehicle weights, dimensions and determine inertial properties (Equation 10 from reference 1)

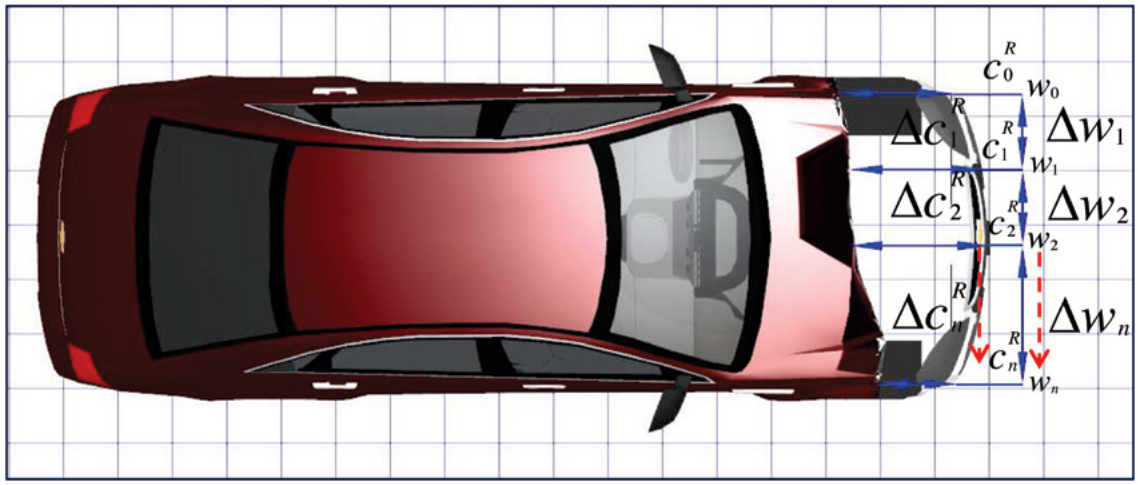

Description of point measured	Distance from Left Front (0)	Distance to undamaged profile
Left front corner	w0: +0 cm (0 inches)	c0: +81 cm (32 inches)
Left front frame rail	w1: +46 cm (18 inches)	c1: +81 cm (32 inches)
Center bumper reinforcement bar	w2: +92 cm (36 inches)	c2: +71 cm (28 inches)
C3…C(n-1)	w3…w(n-1)	c3…c(n-1)
Right front corner	w(n): +183 cm (72 inches)	c(n): +51 cm (20 inches)

So that, $$\Delta c_1^R = \frac{c_0^R + c_1^R}{2} = \frac{(81cm + 81cm)}{2} = 81cm \text{ (32 inches)}$$

$$\Delta c_2^R = \frac{c_1^R + c_2^R}{2} = \frac{(81cm + 71cm)}{2} = 76cm \text{ (30 inches), and so forth.}$$

And, $$\Delta w_1 = w_1 - 0_0 = (46cm - 0cm) = 46cm \text{ (18 inches)}$$

$$\Delta w_2 = w_2 - w_1 = (92cm - 46cm) = 46cm \text{ (18 inches), and so forth.}$$

Figure 1
Measured damage dimensions.

$$I_{zz} = \frac{m_{curb}}{K_G} \cdot \left(L^2 + b^2\right) \cdot \left(K_M \cdot \left(\frac{m_{loaded} - m_{curb}}{m_{loaded}} \right) \right) \quad 1$$

Where, I_{zz} = yaw moment of inertia (about *z-axis*)
m_{curb} = curb mass of vehicle (unloaded)
m_{loaded} = loaded mass of vehicle (curb plus occupants and cargo)
L = total length of vehicle
b = maximum width of vehicle
K_G = geometric empirically determined constant (see **Figure 2**)
K_M = geometric empirically determined constant (see **Figure 2**)

Vehicle type	K_G	K_M	R^2
All combined	13.1	0.696	0.85
Passenger car	13.8	0.769	0.86
Light truck	13.4	0.750	0.92
SUV	12.2	0.656	0.76
Light van	12.3	0.642	0.90

Figure 2
Yaw moment of inertia empirical constants[3].

2) Determine the PDOF acting upon each vehicle, which will be directly opposite in direction when the vehicles are placed together at maximum engagement; **Figure 3** as adapted from **Figure 5** from reference 1.

3) Obtain vehicle A/B stiffness values for the selected vehicle in determining the generalized force acting equal and opposite between the colliding vehicles (Equation 11 from reference 1) based upon the following hierarchy:

$$F^{Gen} = \sum_{j=0}^{n} \left(A_i + B_i \cdot \Delta c_j^R \right) \cdot \frac{\Delta w_j}{\cos(\Pi_i^{PDOF})} \quad 2$$

Where, A_i and B_i = unique structural stiffness values for the impacted surface of the selected vehicle of known A/B values.
Δc_j^R = the residual deformation, or "crush," of the j[th] deformation measured on the selected vehicle perpendicular to the damaged surface from its undamaged dimensions.
Δw_j = width of the j[th] deformation, measured parallel to the damaged surface of the selected vehicle.
Π_i^{PDOF} = angle of the PDOF acting upon the selected vehicle.

a) If both colliding vehicles have frontal stiffness values available, choose the A/B stiffness value for the vehicle with the greatest extent of measured damage (damage width and depth profile).
b) Frontal A/B stiffness for vehicle with frontal impact damage for oblique side, broadside, and rear-end impact configurations.
c) A/B stiffness by vehicle struck surface (front, rear, or side) if only one vehicle has an impact surface that is supported by test data regardless of impact configuration.
d) If neither vehicle impact surface is supported, use a range of A/B stiffness factors for similar vehicles to establish a higher and lower bounding for the analysis.

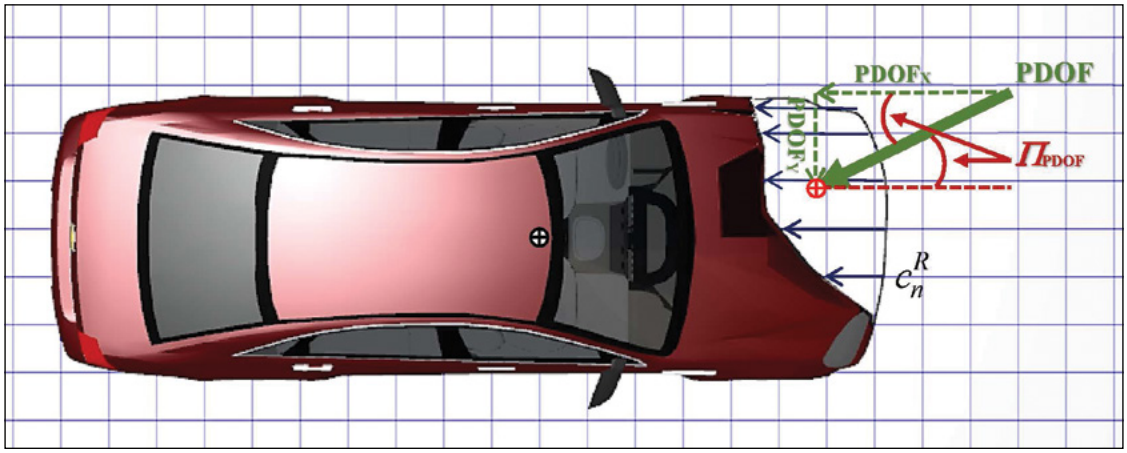

Figure 3
Oblique impact PDOF acting at damage centroid.

4) Determine the work due to the non-conservative inter-vehicular friction forces (Equations 17 and 18 from reference 1).

$$E_1^{friction} = m_1 \cdot g \cdot \mu_k \cdot \left(\frac{m_2}{m_1 + m_2}\right) \cdot \Delta w_{scrape} \quad 3$$

$$E_2^{friction} = m_2 \cdot g \cdot \mu_k \cdot \left(\frac{m_1}{m_1 + m_2}\right) \cdot \Delta w_{scrape} \quad 4$$

Where, m_1 and m_2 = masses of colliding vehicles 1 and 2, respectively (mass units)
μ_k = inter-vehicular friction due to surface scraping
Δw_{scrape} = difference in deformation contact widths (scrape distance)

5) Determine the weighted average deformation depth for the vehicle that is <u>not supported</u> by A/B stiffness data or where A/B stiffness data was not used (Equation 27 from reference 1).

$$\overline{C}^{unknown} = \frac{\sum_{j=1}^{n} \Delta w_j \cdot \Delta c_j}{\sum_{j=1}^{n} \Delta w_j} \quad 5$$

Δw_j and Δc_j from **Figure 1**

6) Determine the *generalized work* to produce compression of the vehicle structures in the form of permanent deformation (Equations 19 and 26 from reference 1).

7) Determine the time period to reach maximum impulse, which is <u>not</u> the total time of the impact to reach maximum velocity change, but the time in which the peak force is applied during the impact (Equation 24 from reference 1).

$$\Delta t^{Gen} = \sqrt{\left(\frac{2 \cdot m_1 \cdot \gamma_1 \cdot m_2 \gamma_2}{(m_1 \cdot \gamma_1 + m_2 \cdot \gamma_2)}\right) \cdot \frac{\left(E_1^{Gen} + E_2^{Gen}\right)}{\left(F^{Gen}\right)^2}} \quad 8$$

Where,

$$\gamma_1 = \left(\frac{I1_{zz}}{I1_{zz} + m_1 \cdot h_1^2}\right) \quad \text{and,} \quad \gamma_2 = \left(\frac{I2_{zz}}{I2_{zz} + m_2 \cdot h_2^2}\right)$$

And, h_1 and h_2 moment arms of PDOF from mass centers of vehicles 1 and 2, respectively.

8) Determine the roadway friction (μ) and equivalent braking efficiency (n) for the vehicle whose tires act against the direction of impact force application (struck vehicle).

9) Determine an appropriate coefficient of restitution for the impact. The following are general rules for determining appropriate coefficients of restitution:
   a) Minor impacts with minor damage will have higher restitution values[4,5].
   b) Even with extensive permanent damage profiles, ranging restitution between 0 and 0.1 may provide a greater confidence interval in the analysis results[1,11].
   c) When the impact involves an axle and/or wheel of a struck vehicle in an oblique side or broadside impact, restitution will range from 0.2 to 0.4 to account for the hardened zone of the axle and/or the "bounce" effect of impacting an inflated tire[1].

10) Determine the *total velocity change* for the vehicles produced by the impact event (Equations 22 and 23 of reference 1).

$$E_1^{Gen} = E_1^{Oblique} + E_1^{friction} = \sum_{j=0}^{n} \left(A_1 \cdot \Delta c1_j^R + \frac{B_1 \cdot \left(\Delta c1_j^R\right)^2}{2} + \frac{A_1^2}{2 \cdot B_1} \right) \cdot \Delta w1_j \cdot \left(1 + \tan^2\left(\Pi_{PDOF1}\right)\right) + m_1 \cdot g \cdot \mu_k \cdot \left(\frac{m_2}{m_1 + m_2}\right) \cdot w_1 \quad 6$$

$$\left(E_{work}^{Gen}\right)^{unknown} = \left(F^{Gen}\right)^{known} \cdot \left(\overline{C}^{unknown}\right) \cdot \left(1 + \tan^2(\Pi^{unknown})\right) \quad 7$$

$$\Delta V_1^{Gen} = (1+e)\sqrt{\frac{2\cdot m_2\cdot\gamma_2\cdot\left(E_1^{Gen}+E_2^{Gen}\right)}{m_1\cdot\gamma_1\cdot(m_1\cdot\gamma_1+m_2\cdot\gamma_2)}}+\frac{m_2\cdot(g\cdot\mu\cdot n)\cdot\Delta t}{m_1} \quad 9$$

$$\Delta V_2^{Gen} = (1+e)\sqrt{\frac{2\cdot m_1\cdot\gamma_1\cdot\left(E_1^{Gen}+E_2^{Gen}\right)}{m_2\cdot\gamma_2\cdot(m_1\cdot\gamma_1+m_2\cdot\gamma_2)}}-(g\cdot\mu\cdot n)\cdot\Delta t \quad 10$$

Outside of accurate deformation profile measurements, Step 3 is perhaps the most crucial in the application of the G-DaTAΔV™ System of Equations. The determination of the *generalized force* of the impact is completed for only one vehicle, not for both, since by Newton's third law the *generalized force* acting upon both vehicles is equal in magnitude but opposite in direction of application. If reliable stiffness data is available for both colliding vehicles and for the appropriate colliding surfaces (front, rear, or side), then the determination of the *total velocity change* for each vehicle can be calculated by applying the G-DaTAΔV™ System of Equations twice and comparing results as a useful crosscheck or for providing a reasonable confidence interval for the analysis[1].

The equations presented in this section comprise the G-DaTAΔV™ System of Equations as they relate to the determination of the *total velocity change* of a vehicle-to-vehicle or vehicle-to-object collision event.

Application of G-DaTAΔV™ to NASS Real-World Collisions

Twenty-five collisions were selected from the NASS Crashworthiness Data System (CDS) Case Viewer from the 2004 to 2013 approved data set, which met the following specific criteria for consideration:

- Two-vehicle collisions involving at least one light truck/van or one SUV category vehicle, with a preference to collisions involving only these category vehicles.
- At least one vehicle must have a complete Event Data Recorder (EDR) imaged report using the Bosch Crash Data Retrieval Tool (Bosch CDR Tool) without evidence of significant data clipping or incomplete data records due to power interruptions or system failures, with preference upon collisions involving both vehicles having a CDR report.
- Both colliding vehicles have complete measured damage profiles consistent with photographs documenting the post-collision condition of each vehicle.
- One vehicle must have Neptune Engineering NEI[6] database reported A and B structural stiffness coefficient values specific to the vehicle and impacted surface or applicable for sister model year runs or corporate manufacturer clones.

The NASS database provides the year, make, and model of each colliding vehicle and the standard curb weight from various sources, some of which are non-standard sources, as well as the occupant and cargo load at the time of impact (when known). However, the vehicles are not weighed by the field investigators, and the mass center or weight distribution is not determined for any vehicles. Therefore, in order to replicate real-world analysis procedures, which would likely be followed for individual collision reconstructions, the standard curb weights and distributions were determined using an industry resource[7] and while adding occupant and cargo loads. Additionally, the NASS database does not provide a measured drag factor for the individual roadway surfaces of the reported collisions. Accordingly, a uniform approximation of a dry roadway drag factor of m = 0.80 was used as the baseline roadway friction for each analysis. The structural stiffness data for one of the colliding vehicles was obtained through the NEI database. The following additional variables necessary for the G-DaTAΔV™ System of Equations analysis were available from the NASS database for each collision as follows:

- Vehicle collision deformation width and depth profiles (measured in SI units).
- Diagrams at impact, post-collision trajectories and tire marks, and vehicle final rest locations.
- Contact with wheel/tire hard zones for restitution considerations provided through vehicle photographic evidence, evidence (when appropriate).
- EDR output images using the Bosch CDR Tool for at least one of the vehicles, having both longitudinal and lateral total velocity change recordings.

The vehicles were positioned together at maximum engagement with the PDOF passing through the damage centroids as discussed in reference 1 and shown in **Figure 3**. The PDOF acting upon each vehicle was determined from the total velocity change vectors determined from the velocity recordings image from the vehicle EDRs. The moments of inertia for the vehicles were determined using Equation 10. Since all dimensions in the NASS-reported collisions were reported in SI units, the moment arm for the offset and oblique impacts were measured using the Faro Reality CAD program to within 0.1m[8]. Damage width and depth dimensions were used as reported for each collision, which were measured to the nearest centimeter. All data recorded within the NASS reports of each real-world collision event was used as reported with no interpretation or modifications. PTC® MathCAD Prime® 3.0 was used for the calculations, which completes all unit conversions internally so that the potential for unit conversion errors were eliminated[9].

The purpose of the final evaluation using the NASS-reported real-world collision data is to determine the accuracy and precision of the G-DaTAΔV™ System of Equations developed in this study as they relate to the data typically available or obtained during a real-world collision investigation. The capstone contribution of this study involves the incorporation of all of the contributions to the total velocity change produced by an oblique, offset, and non-central impact applied to the NASS real-world collisions involving SUVs and light trucks, which have minimal structural stiffness data for side and rear structures.

NASS G-DaTAΔV™ System of Equations Analysis Results

Due to NASS data collection practices and/or the lack of SUV and light trucks involved with downloadable EDRs capable of recording acceleration collision pulses, the year range of NASS-reported collision data that met the established criteria of this study was limited to the collision years of 2010 to 2013. Some NASS-reported collisions involved only one vehicle with a complete longitudinal and lateral Bosch CDR Tool report, while the other involved vehicle was limited to an earlier generation EDR that provided only one direction (lateral or longitudinal) of EDR recording. The condition when Bosch CDR Tool records contained only one direction of velocity change data (either longitudinal or lateral) is easily resolved by the following steps:

- Determine the principal direction of force (PDOF) acting upon the vehicle with a complete longitudinal and lateral Bosch CDR Tool report of the collision total velocity change vector.
- Position the vehicles together using a collision diagram as shown in **Figure 3**.
- Use trigonometric identities in determining the total velocity change for the collision of the vehicle having only a single reported velocity change vector and the PDOF acting upon the vehicle determined from the collision diagram.

Figure 4 summarizes the raw calculation results, and **Figure 5** provides the statistical analysis while determining the vehicle total velocity change of the NASS data utilizing the G-DaTAΔV™ System of Equations**.** The data is also plotted for linearity in **Figure 6** regarding the piecewise damage profile analysis and **Figure 7** for the weighted average damage profile analysis methodological approaches.

NASS #	ΔV CDR mph	PIECEWISE ΔVtotal mph	Difference (Calc-Test) mph	Percent Difference (Calc-Test)	WEIGHTED AVERAGE ΔVtotal mph	Difference (Calc-Test) mph	Percent Difference (Calc-Test)	Collision Description
2010-08-037 Veh 1	19.1	19.7	0.5	2.8%	19.0	-0.2	-0.9%	09 Toyota Tacoma PU into LR of 09 Pontiac G6 1 CDR
2010-12-154 Veh 1	19.3	20.5	1.3	6.5%	20.3	1.0	5.4%	09 Pontiac G6 frontal 1 CDR
2010-12-154 Veh 2	7.7	8.6	0.8	10.7%	8.5	0.7	9.6%	2010 Ford F150 RT side 2 CDR
2011-04-127 Veh 1	13.6	13.6	0.0	-0.4%	13.5	-0.1	-0.6%	05 Equinox strikes side of 02 Explorer 1 CDR
2011-08-107 Veh 1	10.2	10.4	0.1	1.2%	10.5	0.2	2.3%	01 Buick LeSabre frontal 1 CDR
2011-08-107 Veh 2	9.1	8.9	-0.2	-2.4%	9.0	-0.1	-1.3%	08 Chrysler Aspen side 2 CDR
2011-08-112 Veh 1	10.5	10.4	-0.1	-1.1%	10.1	-0.4	-3.7%	05 Chevrolet Equinox frontal 1 CDR
2011-08-112 Veh 2	11.8	11.5	-0.3	-2.6%	11.2	-0.6	-5.2%	06 Chevrolet Impala LF side 2 CDR
2011-09-075 Veh 1	13.1	14.5	1.4	10.7%	14.4	1.3	10.2%	10 Buick Lucrosse into LR side 08 Honda Ridgeline 1 CDR
2011-09-091 Veh 1	31.0	31.8	0.8	2.4%	31.2	0.2	0.8%	03 GMC 2500 into LF side 07 Acura MDX CDR 1
2011-11-085 Veh 2	13.9	14.1	0.2	1.5%	13.8	-0.1	-0.8%	04 Hyundai Sonata into LF side of 11 Ford Escape CDR1
2011-12-049 Veh 1	20.7	19.5	-1.2	-5.9%	18.9	-1.8	-8.7%	07 Chev Equinox into RF of 07 GMC 1500 CDR 1
2011-12-046 Veh 2	13.1	13.0	-0.1	-0.7%	12.7	-0.5	-3.7%	07 GMC 1500 RF struck by 07 Chev Equinox CDR 2
2011-12-183 Veh 1	10.1	10.6	0.5	5.1%	10.5	0.4	4.1%	11 Chev Equinox LF into RT side 06 Chev Impala CDR 1
2011-12-183 Veh 2	11.8	11.2	-0.6	-4.9%	11.1	-0.7	-5.8%	06 Chev Impala RT side struck LF 11 Chev Equinox CDR 2
2012-08-064 Veh 1	14.7	14.5	-0.2	-1.4%	14.2	-0.6	-3.9%	09 Cadillac Escalade LF into LF corner 98 Honda Accord CDR
2012-08-080 Veh 1	7.6	8.0	0.4	5.5%	8.1	0.5	6.2%	10 GMC Yukon LF corner sideswipe LT side 12 Toyota 4Run CDR1
2012-08-080 Veh 2	7.7	8.3	0.6	7.8%	8.3	0.6	8.4%	12 Toy 4Run LT sideswipe by LF corner 10 GMC Yukon CDR 2
2012-12-016 Veh 1	13.2	13.6	0.5	3.5%	13.4	0.2	1.7%	08 Cadillac CTS into side of 08 Chevrolet Trailblazer CDR 1
2012-12-016 Veh 2	13.8	15.3	1.5	10.6%	15.0	1.2	8.7%	08 Chevrolet Trailblazer side struck by 08 Cadillac CTS front CDR 2
2012-41-024 Veh 1	32.8	34.2	1.4	4.2%	32.8	0.0	-0.1%	05 Toyota Camry LF into 2010 Toyota Tundra RF CDR 1
2012-41-024 Veh 2	22.2	20.5	-1.6	-7.4%	19.7	-2.5	-11.3%	2010 Toyota Tundra RF into 05 Toyota Camry LF CDR 2
2012-43-014 Veh 1	30.8	33.5	2.7	8.7%	31.8	1.0	3.4%	2011 Jeep Liberty into side of 2011 Ford F250 CDR 1
2012-43-014 Veh 2	19.2	19.9	0.7	3.3%	18.9	-0.2	-1.3%	2011 Ford F250 struck on RT by 2011 Jeep Liberty CDR 2
2012-43-026 Veh 1	22.7	20.6	-2.0	-9.0%	20.4	-2.3	-10.0%	2003 Lexus RX350 strikes LF of 2005 Toyota Camry CDR 1
2012-43-026 Veh 2	24.1	26.0	1.9	8.0%	25.7	1.6	6.8%	2005 Toyota Camry LF struck by front of 2003 Lexus RX350 CDR 2
2012-43-106 Veh 1	25.4	27.5	2.1	8.4%	26.9	1.5	6.0%	2001 Lincoln Navigator strikes LT 2011 Dodge Durango CDR 1
2012-43-106 Veh 2	20.3	18.8	-1.5	-7.6%	18.3	-2.0	-9.6%	2011 Dodge Durango LT struck by 2001 Lincoln Navigator CDR 2
2012-48-106 Veh 1	13.0	13.4	0.4	3.0%	13.2	0.2	1.3%	2007 Toyota FJ Cruiser into LT 2007 Toyota RAV4 CDR 1
2012-48-106 Veh 2	13.3	13.3	0.0	0.1%	13.1	-0.2	-1.5%	2007 Toyota RAV4 LT struck by 2007 Toyota FJ Cruiser CDR 2
2013-12-059 Veh 1	8.7	9.9	1.3	14.4%	9.5	0.9	10.0%	2006 Chevrolet K1500 into LT 2005 Chevrolet Malibu CDR1
2013-12-059 Veh 2	17.1	17.3	0.3	1.7%	18.6	1.5	9.0%	2005 Chevrolet Malibu LT struck by 2006 Chevrolet K1500 CDR 2
2013-12-106 Veh 1	25.9	27.4	1.6	6.1%	27.1	1.3	5.0%	2012 Chevrolet Equinox into RT 2008 GMC C2500 wtrailer CDR 1
2013-12-106 Veh 2	10.3	9.7	-0.6	-5.7%	9.6	-0.7	-6.7%	2008 GMC C2500 wtrailer RT struck by 2012 Chevrolet Equinox CDR 2
2013-12-112 Veh 1	26.9	27.0	0.2	0.6%	26.3	-0.6	-2.1%	2004 Chevrolet Venture into RT 2012 Chevrolet Equinox CDR1
2013-12-112 Veh 2	17.9	16.8	-1.1	-6.2%	16.4	-1.6	-8.7%	2012 Chevrolet Equinox RT struck by 2004 Chevrolet Venture CDR 2
2013-43-152 Veh 1	14.0	13.1	-0.8	-6.0%	12.5	-1.5	-10.4%	1997 Chevrolet C1500 into LT 2011 Ford Ranger CDR 1
2013-43-152 Veh 2	14.2	13.4	-0.9	-6.2%	12.7	-1.5	-10.6%	2011 Ford Ranger LT struck by 1997 Chevrolet C1500 CDR 2
2013-76-094 Veh 1	19.1	16.7	-2.5	-12.9%	16.7	-2.4	-12.8%	2010 Dodge Journey into RT 2007 Pontiac Torrent CDR 1
2013-76-094 Veh 2	15.2	15.8	0.5	3.5%	15.8	0.5	3.6%	2007 Pontiac Torrent RT struck by 2010 Dodge Journey CDR 2
2013-76-165 Veh 1	21.8	22.6	0.8	3.8%	22.3	0.5	2.4%	2013 Ford F150 into LT side of 2013 Ford F150 CDR 1
2013-76-165 Veh 2	15.8	16.8	1.1	6.7%	16.6	0.8	5.2%	2013 Ford F150 LT struck by 2013 Ford F150 CDR 2
2013-79-139 Veh 1	32.0	32.4	0.4	1.4%	30.3	-1.7	-5.2%	2004 Toyota Prius head-on offset with 2007 Toyota Highlander CDR 1
2013-79-139 Veh 2	27.6	29.7	2.1	7.6%	27.7	0.1	0.5%	2007 Toyota Highlander head-on offset with 2004 Toyota Prius CDR 2
Absolute Averages	17.3	17.6	0.9	5.2%	17.2	0.9	5.4%	

Figure 4
NASS-reported Bosch CDR Tool data versus G-DaTAΔV™ analysis.

Piecewise Matching Method			Weighted Average Method		
χ2 Test of fit	2.92	standard deviation of error	χ2 Test of fit	2.98	standard deviation of error
χ2 critical => (α = 0.99)	24.43 (n=43)	±1.1 mph	χ2 critical => (α = 0.99)	24.43 (n=43)	±1.1 mph
R^2 =>	0.979	±6.3%	R^2 =>	0.975	±6.7%
T-test => (p=0.9129)	0.11		T-test => (p=0.6478)	0.46	
critical=> (α = 0.05)	2.017		critical=> (α = 0.05)	2.017	
F-test =>	0.75		F-test =>	0.99	
critical=> (α = 0.05)	3.209		critical=> (α = 0.05)	3.209	

Figure 5
Summary of statistics.

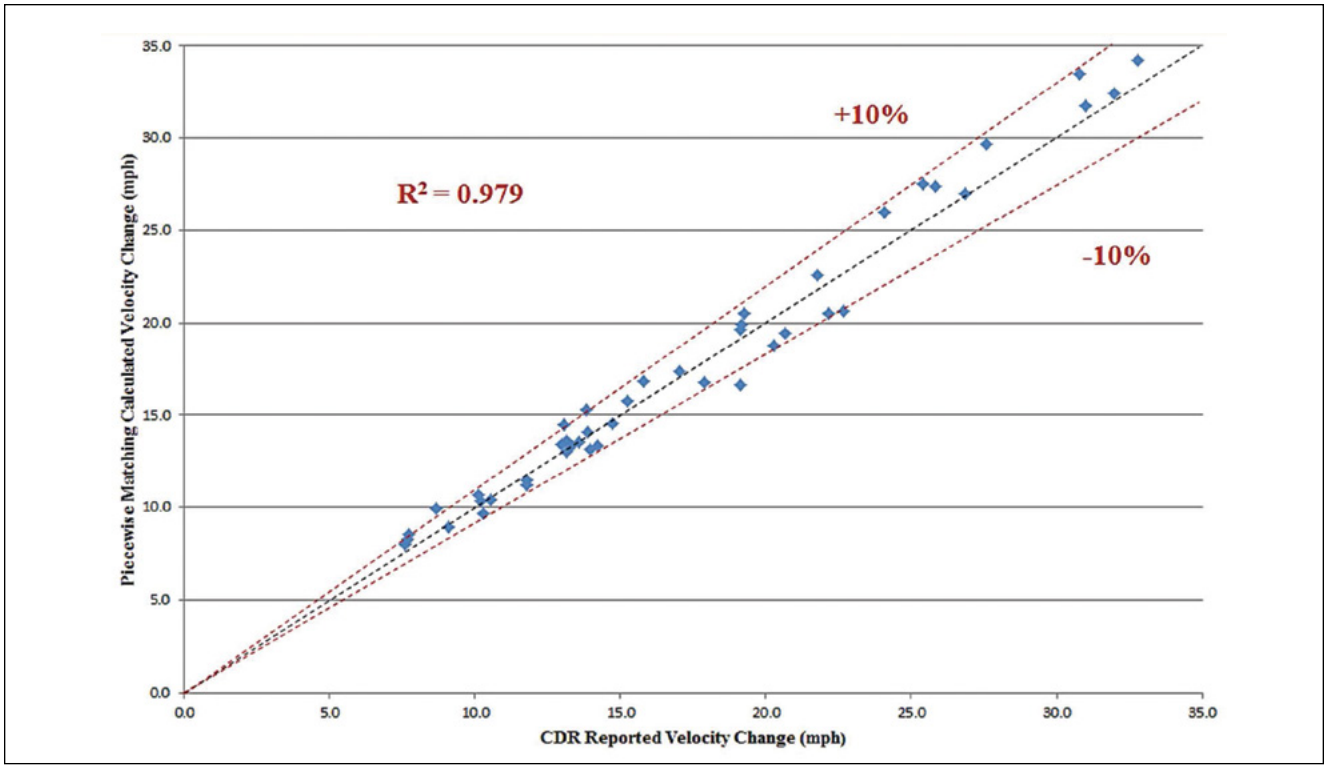

Figure 6
G-DaTAΔV™ piecewise damage match versus NASS Bosch CDR data.

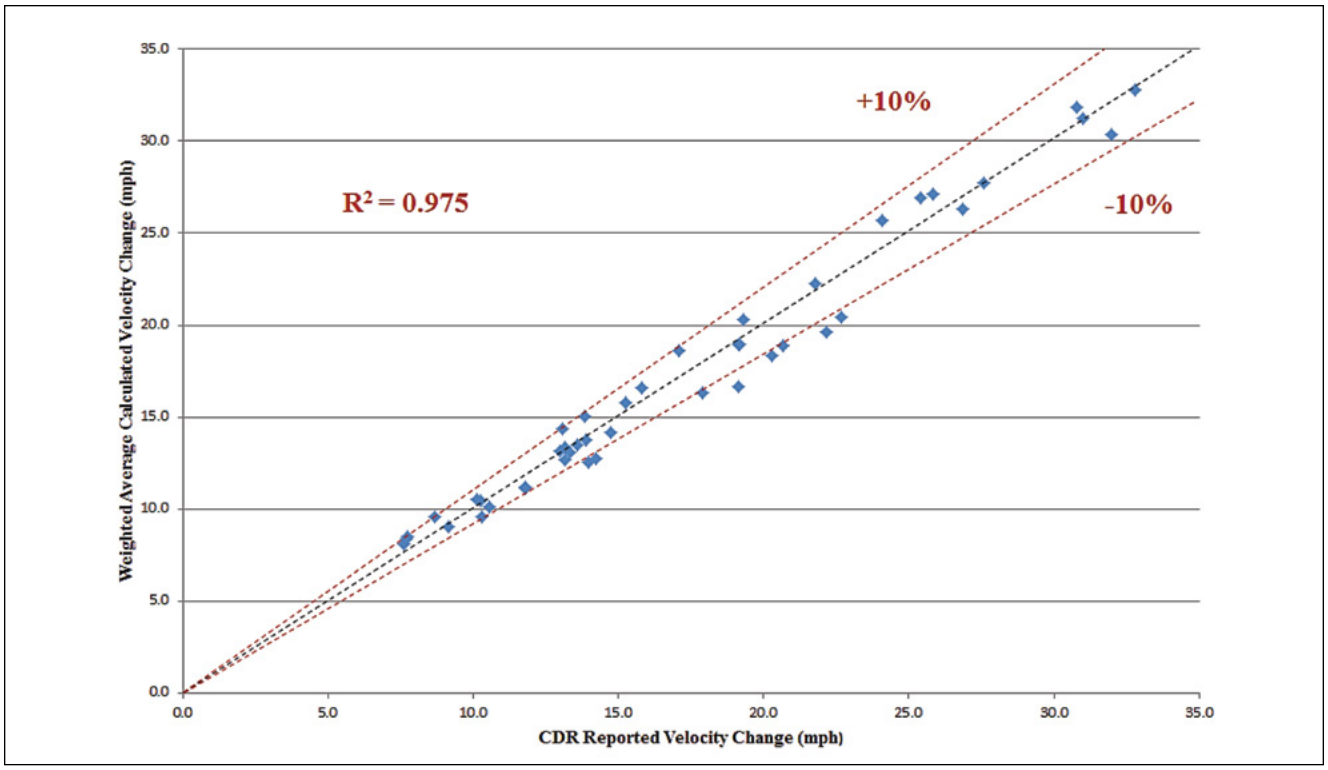

Figure 7
G-DaTAΔV™ weighted average damage versus NASS Bosch CDR data.

The G-DaTAΔV™ System of Equations showed excellent correlation to the NASS total velocity change Bosch CDR Tool reported data with an $R^2 = 0.979$ for piecewise damage profile analysis and an $R^2 = 0.975$ for the weighted average damage profile analysis. The $\chi^2 = 2.92$ for the piecewise and $\chi^2 = 2.98$ for the weighted average damage profile analysis methodologies ($\alpha = 0.99$, $n = 43$) indicate that the difference between the total velocity changes for the NASS Bosch CDR Tool reported real-world collisions and calculated values using either G-DaTAΔV™ System of Equations methodological approach is not statistically significant.

The overall precision of the results varies by ±6.3% (±1.1 mph) for the piecewise method and ±6.7% (±1.1 mph) for the weighted average damage profile methods for errors within one standard deviation of the mean. With respect to the piecewise damage profile method, the greatest percentage differences between the calculated and NASS real-world collision results varied between -12.89% (-2.46 mph difference) for vehicle 1 of NASS 2013-76-094 to +14.4% (1.25 mph difference) for vehicle 1 of NASS 2013-12-059. The precision utilizing the weighted average damage profile method improved to -12.81% (-2.45 mph difference) for vehicle 1 of NASS 2013-76-094 to +10.0% (0.87 mph difference) for vehicle 1 of NASS 2013-12-059. The fact that the outliers for both methods involved the same vehicles from the same reported collisions could be random, but is probably due to a systematic error in the data reported within the particular NASS files.

The relative high degree of correlation between the NASS-reported total velocity changes (from the vehicle EDR data as imaged within their respective Bosch CDR Tool reports), as compared to the results when utilizing the G-DaTAΔV™ System of Equations, indicates that the suite of equations produced reasonable precision and accuracy for determining the *total velocity change* resulting from these real-world collision events. Additionally, the evaluation results from utilizing the G-DaTAΔV™ System of Equations indicates the NASS training of investigators regarding vehicle deformation documentation appears adequate for reducing random and/or systematic errors between investigators.

Application Examples of the G-DaTAΔV™ System of Equations

The following example application of the G-DaTAΔV™ System of Equations is from NASS-reported collision 2010-08-037 involving a large amount of inter-vehicular friction due to the oblique-offset impact configuration of the collision event between a 2009 Toyota Tacoma and a 2009 Pontiac

G6[10]. The following **Figures 8** and **9** from the NASS report detail the damages to the vehicles from the impact. Measurements of damage profiles as well as CDR downloads were also part of the NASS report.

In accordance with steps 1 through 10 of the analysis procedures established for the application of the G-DaTAΔV™ System of Equations, the vehicles were placed together at maximum engagement for the determination of the *total velocity change* of each vehicle resulting from the impact. The collision diagram shown as **Figure 10** and subsequent MathCAD Prime 3.0 worksheets detail the analysis approach, as well as the mathematical results as compared to the *total velocity change* levels imaged in the vehicle CDR report.

Figure 8
Pontiac G6 damage diagram and sample photographs.

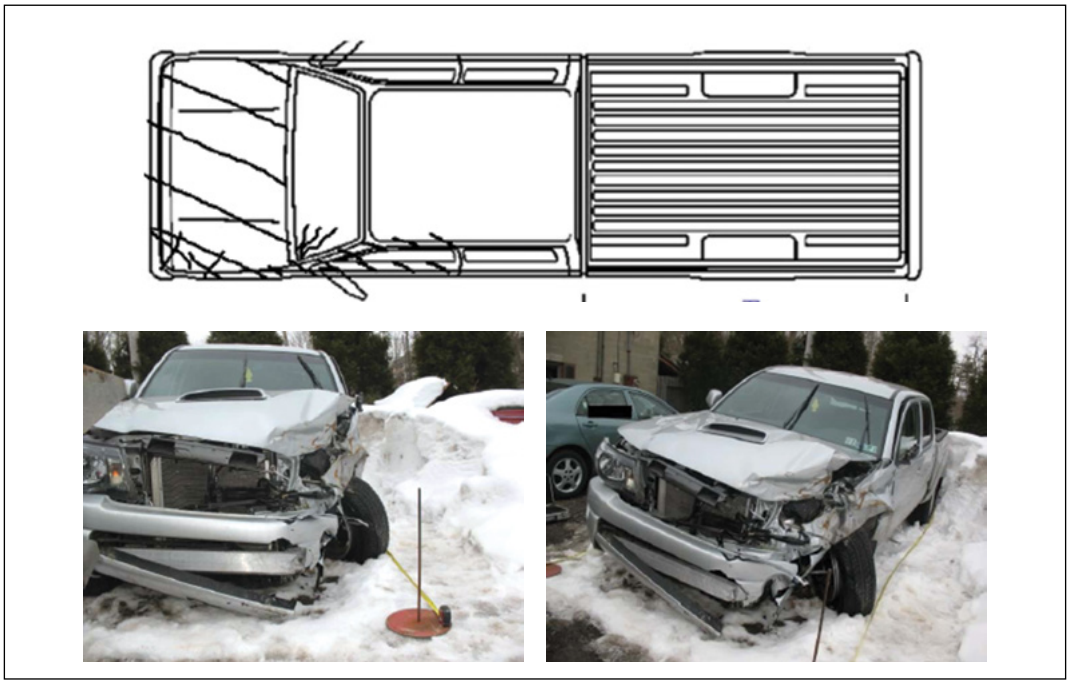

Figure 9
Toyota Tacoma damage diagram and sample photographs.

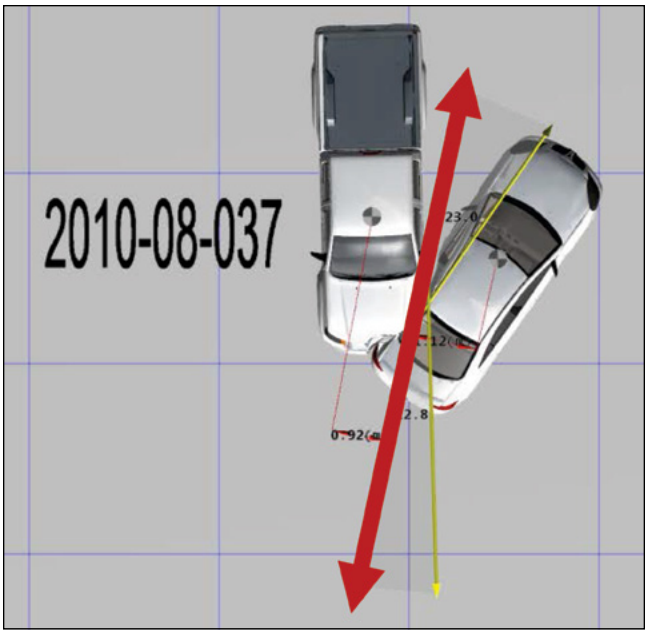

Figure 10
Maximum engagement diagram with moment arms and PDOF of applied force.

$$C1 := \begin{bmatrix} 25 \\ 18 \\ 16 \\ 14 \\ 12 \\ 10 \\ 0.0 \end{bmatrix} \cdot cm \qquad W1 := \begin{bmatrix} 0 \\ 17 \\ 34 \\ 51 \\ 68 \\ 85 \\ 102 \end{bmatrix} \cdot cm$$

$m_1 := \frac{(4259) \cdot lb}{g} = 132.4 \ \frac{lb \cdot s^2}{ft}$ 2009 Toyota Tacoma

$I1_{zz} := 2313.50 \cdot lb \cdot ft \cdot sec^2$ From 4N6Xpert Autostats

$A1 := 296 \cdot \frac{lb}{in}$ $B1 := 100 \cdot \frac{lb}{in^2}$ Neptune 04-05 Tacoma frontal

$\Pi_{PDOF1} := (-12.8) \cdot deg$ $h_1 := 0.9 \cdot m$ $\gamma_1 := \frac{I1_{zz}}{I1_{zz} + m_1 \cdot h_1^2}$

$$C2 := \begin{bmatrix} 18 \\ 37 \\ 45 \\ 33 \\ 9.0 \\ 0.0 \\ 0.0 \end{bmatrix} \cdot cm \qquad W2 := \begin{bmatrix} 0.0 \\ 36 \\ 72 \\ 108 \\ 144 \\ 180 \\ 216 \end{bmatrix} \cdot cm$$

$m_2 := \frac{(3543) \cdot lb}{g} = 110.1 \ \frac{lb \cdot s^2}{ft}$ 09 Pontiac G6

$I2_{zz} := 2318.66 \cdot lb \cdot ft \cdot sec^2$ From 4N6Xpert Autostats

$h_2 := 1.1 \cdot m$

$\gamma_2 := \frac{I2_{zz}}{I2_{zz} + m_2 \cdot h_2^2}$ $e := 0.0$ $i := 0 \ldots 5$

$CDRlong2 := -7.46 \ mph$

$CDRlat2 := 17.62 \cdot mph$

$CDRtotal2 := \sqrt{CDRlong2^2 + CDRlat2^2} = 19.1 \ mph$

$\Pi_{PDOF2} := \operatorname{atan}\left(\frac{CDRlong2}{CDRlat2}\right) = -22.9 \ deg$

$$C2\_bar := \frac{\sum_{i=0}^{5}\left(W2_{i+1} - W2_{i}\right)\cdot\left(\frac{C2_{i}+C2_{i+1}}{2}\right)}{W2_{6}} = 8.7\ in$$ weighted average deformation

$\Delta W_{scrape} := W2_{6} - W1_{6} = 44.9\ in$ scraping distance on vehicle 2

$\mu_k := 0.5$ scraping friction coefficient

$\mu_r := 0.80$ surface friction coefficient asphalt

$n_2 := 75\%$ brake efficiency (broadside rear rotate)

$$F1 := \sum_{i=0}^{5}\left(A1 + B1\cdot\left(\frac{C1_{i}+C1_{i+1}}{2}\right)\right)\cdot\left(W1_{(i+1)} - W1_{(i)}\right)\cdot\left(\frac{1}{\cos\left(\Pi_{PDOF1}\right)}\right) = \left(3.4\cdot 10^{4}\right)\ lb$$

Matched Segment Piecewise Analysis:

$$E1 := \left(\sum_{i=0}^{5}\left(A1\cdot C1_{i} + \frac{B1}{2}\cdot\left(\frac{C1_{i}+C1_{i+1}}{2}\right)^{2} + \frac{A1^{2}}{2\cdot B1}\right)\cdot\left(W1_{i+1} - W1_{i}\right)\cdot\left(1+\tan\left(\Pi_{PDOF1}\right)^{2}\right)\right) = \left(1.4\cdot 10^{4}\right)\ lb\cdot ft$$

$$E2 := \sum_{i=0}^{5} F_{i}\cdot\left(\frac{C2_{i}+C2_{i+1}}{2}\right)\cdot\left(1+\tan\left(\Pi_{PDOF2}\right)^{2}\right) = \left(3.3\cdot 10^{4}\right)\ lb\cdot ft$$

$$E1_{friction} := m_1\cdot g\cdot\mu_k\cdot\left(\frac{m_2}{m_1+m_2}\right)\cdot W1_{6} = \left(3.2\cdot 10^{3}\right)\ lb\cdot ft$$

$$E2_{friction} := m_2\cdot g\cdot\mu_k\cdot\left(\frac{m_1}{m_1+m_2}\right)\cdot\Delta W_{scrape} = \left(3.6\cdot 10^{3}\right)\ lb\cdot ft$$

$$E1_{Gen} := E1 + E1_{friction} = \left(1.7\cdot 10^{4}\right)\ lb\cdot ft$$

$$E2_{Gen} := E2 + E2_{friction} = \left(3.7\cdot 10^{4}\right)\ lb\cdot ft$$

$$\Delta tpeak := \sqrt{\left(\frac{2\cdot m_1\cdot\gamma_1\cdot m_2\cdot\gamma_2}{m_1\cdot\gamma_1 + m_2\cdot\gamma_2}\right)\cdot\frac{E1_{Gen}+E2_{Gen}}{F1^{2}}} \qquad \Delta tpeak = 0.06\ s$$

$$\Delta v1 := (1+e)\cdot\sqrt[2]{\left(\frac{2\cdot m_2\cdot\gamma_2\cdot\left(E1_{Gen}+E2_{Gen}\right)}{m_1\cdot\gamma_1\cdot\left(m_1\cdot\gamma_1+m_2\cdot\gamma_2\right)}\right)} - \frac{m_2\cdot\left(g\cdot\mu_r\cdot n_2\right)\cdot\Delta tpeak}{m_1} = 15.1\ mph$$

$$\Delta v2 := (1+e)\cdot\sqrt[2]{\left(\frac{2\cdot m_1\cdot\gamma_1\cdot\left(E1_{Gen}+E2_{Gen}\right)}{m_2\cdot\gamma_2\cdot\left(m_1\cdot\gamma_1+m_2\cdot\gamma_2\right)}\right)} - \left(g\cdot\mu_r\cdot n_2\right)\cdot\Delta tpeak = 19.7\ mph$$

CDR = 19.1 mph

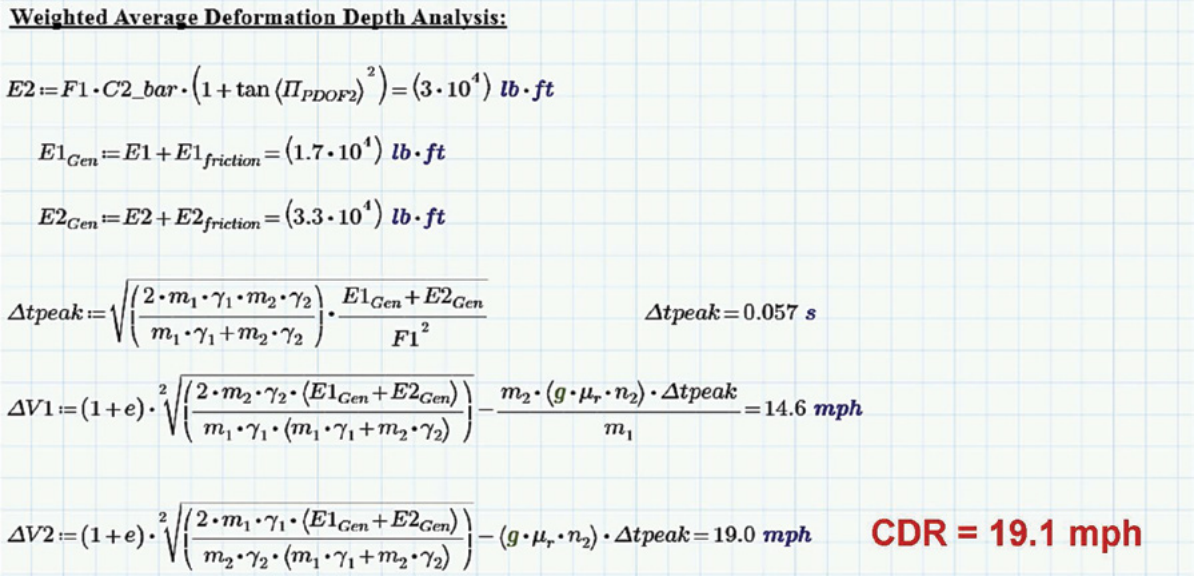

This example application to a real-world collision event demonstrates the G-DaTAΔV™ System of Equations accurately determines the *total velocity change* even for a collision with significant inter-vehicular friction due to scraping, which would have been difficult to reconstruct reliably with previous vehicle deformation analysis methods.

G-DaTAΔV™ System of Equations Limitations

Every model developed and intended to evaluate the behavior of a mechanical or physical condition is an approximation no matter how precise, detailed, or descriptive. Therefore, it is important to evaluate such models for accuracy through application comparisons with applicable testing. The RICSAC and NASS evaluations of the G-DaTAΔV™ System of Equations provide the comparative assessment of the accuracy, precision, and efficacy of the approximations of *total velocity change* for non-central impacts — when analyzing vehicle deformation profiles utilizing the derived algorithms[1]. Regardless of the relative degree of accuracy, it is equally important to determine where variable sensitivities to the accuracy of the approximations may exist. As a result of analyzing the RICSAC and NASS data, general observations regarding variable sensitivity while applying the G-DaTAΔV™ System of Equations are as follows[11]:

- The G-DaTAΔV™ System of Equations is not sensitive to reasonable random and/or systematic differences between collision deformation measurements obtained by different, properly trained investigators. Differences in deformation depth measurements of ±10% generally resulted in no more than a ±2% difference in the *total velocity change* results for all RICSAC tests combined. The greatest deviation for a systematic increase or decrease in deformation depth measurements for both involved vehicles of ±10% was a difference in *total velocity change* of ±8.6% (greatest deviation in RICSAC 2).

- The G-DaTAΔV™ System of Equations is not sensitive to the inertial properties approximated by using commercially available data in the absence of directly measured vehicle weights and weight distributions. Varying vehicle masses by ±10% resulted in approximately a ±3.1% difference in *total velocity change* results across the board for all RICSAC tests.

- The G-DaTAΔV™ System of Equations is not sensitive to the choice of A and B stiffness coefficients obtained through the NEI database[7], as long as they are for the appropriate impacted surface (i.e., front, rear, or side), and the test is for sister vehicles that are within the manufacture year range for the same vehicle or its corporate clones. Varying A/B stiffness values by ±10% resulted in approximately a ±3.1% difference in *total velocity change* results across the board for all RICSAC tests.

- The G-DaTAΔV™ System of Equations is not sensitive to the effects of inter-vehicular friction, since the majority of the work/energy contributions from this effect are quite small as compared to the work done by the impact impulse. Varying inter-vehicular friction values

by ±20% from a default m_k = 0.5 g produced no more than a ±1.1% difference in *total velocity change* results (greatest deviation in RICSAC 2). However, ignoring inter-vehicular friction for collisions with scraping of 0.75 m (30 inches) or more resulted in an under-approximation of *total velocity change* by as much as -9.4% (greatest deviation in RICSAC 6).

- The G-DaTAΔV™ System of Equations is not sensitive to the choice of drag factor for the roadway as long as the chosen drag factor is within reason for the particular roadway surface; i.e., asphalt, concrete, dry, wet, etc. Varying roadway friction or braking efficiency values by ±20% generally resulted in no more than a ±1.5% difference in total velocity change calculations (greatest deviation in RICSAC 1). Ignoring braking effects for broadside offset and oblique impacts resulted in errors in *total velocity change* up to approximately ±6.1% (greatest deviation in RICSAC 1).

The most critical elements of the G-DaTAΔV™ System of Equations having the greatest potential for affecting the accuracy of the *total velocity change* approximations lay in the determination of the restitution coefficient, the PDOF acting upon each vehicle during the impact, and the resultant moment arm about the vehicle mass centers. The PDOF angle contribution affects the total deformation depth and, therefore, the total work due to impact forces. Additionally, the direction and location of the application of the PDOF determines the moment arm created by an applied force offset from the vehicle mass center and thus the rotational contributions to the *total velocity change* resulting from a non-central impact condition[11].

- Neglecting restitution may produce as much as a -19.8% under-approximation of the *total velocity change* for the vehicle of the least mass with respect to collisions involving impacts with wheels, tires, and axles where the coefficient of restitution ranges from e = 0.2 to 0.4 (greatest deviation in RICSAC 3).

- Ignoring the principal direction of force correction to the deformation depth produced as much as an -33.0% effect upon the determination of *total velocity change* (greatest deviation in RICSAC 2).

- Ignoring the dynamic mass ratio rotational effects can result in as much as a -24.4% effect (greatest deviation in RICSAC 8) upon the *total velocity change* determination, with the most significant influence associated with oblique impacts with a moment arm approaching 1 m.

- As demonstrated in the original CRASH analysis of the RICSAC data[1,11], errors as high as 79.2% (greatest deviation in RICSAC 7) resulted when the PDOF adjustment, dynamic mass ratio for rotation, restitution, inter-vehicular friction, and tire/ground force contributions were neglected.

If a collision event results in a non-central configuration, the following steps should significantly reduce systematic errors introduced into the G-DaTAΔV™ System of Equations[11]:

- Produce scaled diagrams of the vehicles and damage profiles resulting from the impact, including contact and induced damages.

- Position colliding vehicles together at either initial contact or at maximum engagement for determining the location and direction of the PDOF application upon each vehicle, as demonstrated by **Figure 3**.

- Unless accurately and precisely determined, range the measured values for the PDOF angle and the moment arm for determining the effective rotational (dynamic) mass ratio, *g*, for both vehicles.

- Unless directly measured, range the effective roadway net drag factor when tire/ground impulse contributions should be considered.

Following these simple procedures when determining the *total velocity changes* and time to peak force application (used for determining peak accelerations), random and/or systematic errors should be significantly reduced, providing the forensic engineer with reasonable confidence in the accuracy and precision of the G-DaTAΔV™ System of Equations.

Application of the G-DaTAΔV™ System of Equations with respect to the RICSAC and NASS data also revealed the following observations regarding collision restitution considerations[11]:

- For high-speed collisions producing deformation depths averaging 0.3 m (12 inches) or more over the deformation width, ranging restitution between $0 \le e \le 0.10$ will provide accurate consideration of restitution effects.

- For impacts into the front or rear wheels/axles of at least one vehicle, even when deformation is significantly greater than 0.3 m, a restitution range between $0.2 \le e \le 0.40$ will provide accurate consideration of restitution effects.

- Low velocity impacts where the total velocity change is within the range $0 < Dv^{Total} \le 4.5$ m/sec (approximately 10 mph), the restitution will vary between $e = 0.6$ at very low velocities to $e = 0.3$ at the upper levels of the low velocity range. Selection of an appropriate restitution value is often an iterative process, but ranging the restitution is expected to provide greater assurance of an accurate consideration of restitution effects.

In all of the RICSAC and NASS collisions analyzed, an inter-vehicular friction of $m_{scrape}=0.5$ was used and did not vary between analyses. However, if evidence of snagging between the sliding surfaces is present, such as body panels pulled in the direction of sliding between vehicles, then consideration of higher inter-vehicular friction values may be appropriate. Again, ranging inter-vehicular friction for snagging conditions is likely to produce greater accuracy, but less precision in the analysis results. However, the contribution of inter-vehicular friction is the least significant of all other energy sinks or impulse and rotational contributions to *total velocity change*.

The damage analysis methods in existence previous to those developed by this engineer required knowledge of structural stiffness data for both vehicles involved in a given collision event, which limited their application with regard to many real-world collision events. However, the elimination of the need for the A and B stiffness data for one of the involved vehicles in a collision event allows for a much broader application to include collisions involving vehicle classifications with limited or no structural stiffness data. The major limitation of the G-DaTAΔV™ System of Equations is that it remains reliant upon full-scale impact testing for determining the A and B structural stiffness values for one of the involved vehicles. The continued reliance upon structural stiffness values requires continued full-scaled impact testing, and may require testing of non-conventional vehicles or impact conditions when structural stiffness data for at least one of the vehicles is not available.

Additional limitations to the applications of the G-DaTAΔV™ System of Equations result when vehicle deformation profiles cannot be reasonably measured directly or indirectly through photographic evidence — or when the analyst has limited training or understanding regarding proper deformation profile measurements. However, even though the G-DaTAΔV™ System of Equations are not particularly sensitive to minor deformation profile measurement fluctuations, unrealistic approximations of deformation width and/or depth will have an effect upon the accuracy of the model. Damage profile width and depth determination is quite intuitive, and is also the subject of collision investigation training courses. The NASS data analysis demonstrates that random differences in measurement of deformation profiles between properly trained investigators, outside of those individuals that are intentionally biasing measurements, do not produce significant random errors that tangibly affect the analysis of *total velocity change* when using the G-DaTAΔV™ System of Equations.

If critical variables are unknown or cannot be reasonably approximated, the use of the G-DaTAΔV™ System of Equations may be limited or unreliable. Proper engineering judgement should be exercised when applying these algorithms or any other form of analysis to a real-world or staged collision event, if the determination of critical variables is complicated by other factors or if there is uncertainty in their reliability.

Conclusions

Correlation and descriptive statistics, as well as the raw analysis results, indicate that a reliable and significantly improved degree of precision and accuracy was achieved when the G-DaTAΔV™ System of Equations were applied to both the RICSAC-staged collision tests presented in an earlier paper[1] and the NASS real-world collision data (when determining the total velocity changes for oblique and offset non-central impacts). Unlike the 12 RICSAC tests, the NASS real-world collisions were not carefully staged and instrumented, nor were the many variables input into the G-DaTAΔV™ System of Equations documented to the precision of the RICSAC tests. Additionally, the RICSAC testing documentation was completed by the

same team of researchers at one test facility, while each NASS real-world collision occurred at varying locations across the United States over a three-year span, and were each documented by different NASS-trained investigators. The NASS real-world collision data set represents a realistic comparison to field-collected data that a collision investigator could encounter when tasked with reconstructing an actual collision event. Stark and pronounced differences between the results of applying the G-DaTAΔV™ System of Equations to the controlled RICSAC staged testing (versus the random NASS documented real-world collisions) should have been present if the algorithms developed within this study had systematic errors, violations in the physics of oblique and offset non-central impacts, or significant sensitivity to analysis variable inputs. Instead, the results of the RICSAC and NASS evaluations using the G-DaTAΔV™ System of Equations demonstrate an expectation of a reasonable degree of data correlation, accuracy, precision, and efficacy when applied to real-world collision events.

G-DaTAΔV™ System of Equations provides an accurate and reliable tool for the forensic engineer to determine the *total velocity change* levels produced by real-world collision events. The presented methods have been applied by this author to the following impacts where vehicle and surface specific structural stiffness characteristics were either scarce or non-existent:

- Broadside or oblique side impacts.
- Rear end impacts.
- Impacts involving light trucks, vans, and sport utility vehicles where vehicle and surface-specific structural stiffness values are scarce.
- Impacts involving heavy vehicles, buses, RVs, motorcycles, and other similar vehicles with few vehicle and surface-specific data.
- Impacts with non-vehicular objects, or unique vehicles such as trailers or heavy equipment that deform when struck, but have no known structural stiffness data.

Future research should include further validation when applying the G-DaTAΔV™ System of Equations to commercial vehicles, motorcycles, and trailers.

References

1. Ogden J. Generalized deformation and total velocity change analysis with missing vehicle stiffness coefficients; G-DaTAΔV™. Journal of the National Academy of Forensic Engineers; 2015; 32(1):15-34.
2. National Automotive Sampling System (NASS). United States Department of Transportation. www.nhtsa.gov/NASS, 2010 to 2013.
3. Garrott R. Measured vehicle inertial parameters – NHTSA's data through September 1992. SAE Technical Paper 930897. Warrendale PA: Society of Automotive Engineers International; 1993.
4. Ogden J. Forensic engineering analysis of damage and restitution in low velocity impacts. Journal of the National Academy of Forensic Engineers; 1999;16(2):11-34.
5. Ogden J. Methods of investigating and reconstructing minor damage low velocity motor vehicle accidents. Master of Science Thesis. University of Colorado Denver. October 1995.
6. Neptune Engineering, Inc. NEI Database. www.neptuneeng.com.
7. Expert Autostats, Inc. 4N6XPRT Systems. Version 5.5. 2015.
8. Faro Reality version 1.1.1502.10. ARAS 360 Technologies, Inc.; 2014.
9. PTC® MathCAD Prime 3.0. Parametric Technology Corporation; 2013.
10. National Automotive Sampling System (NASS). United States Department of Transportation. 2010-08-037, rel. v. 1.0.112008.
11. Ogden J. Generalized deformation and total velocity change analysis system of equations (G-DaTAΔV™). Doctor of Philosophy dissertation. University of Colorado; College of Engineering and Applied Sciences. ProQuest No. 3739580. ProQuest LLC; 2015.